THE OTHER DARK MATTER: PYROGENIC ORGANIC MATTER CYCLING BY POST-FIRE SOIL MICROBES

by

Nayela Zeba

A dissertation submitted in partial fulfillment of

the requirements for the degree of

Doctor of Philosophy

(Soil Science)

at the

UNIVERSITY OF WISCONSIN-MADISON

2023

Date of final oral examination: 05/08/2023

The dissertation is approved by the following members of the Final Oral Committee:

Thea Whitman, Associate Professor, Soil Science
Karthik Anantharaman, Assistant Professor, Bacteriology
Katherine A. McCulloh, Associate Professor, Botany
Matthew Ginder-Vogel, Associate Professor, Civil and Environmental Engineering

DEDICATION

I dedicate this thesis to the remarkable women in my family. Their courage, tireless efforts, and perseverance have continuously inspired and motivated me throughout my academic journey.

ACKNOWLEDGEMENTS

First and foremost, I would like to express my gratitude to Dr. Thea Whitman for being the best PI and mentor I could have asked for. My professional relationship with Thea has been one of the most significant ones of my life so far. She has helped me grow both as a scientist and a person. Thank you, Thea, for being such an inspiration, and for doing so with kindness and grace.

I would also like to thank my dissertation committee members, Dr. Karthik Anantharaman, Dr. Kate McCulloh, Dr. Matthew Ginder-Vogel, and the late Dr. Joel Pedersen, for their generous time, knowledge and guidance.

I owe a debt of gratitude to my colleagues and friends, Tim, Jamie, Kelsey, Dana and Mengmeng, for their support and assistance during the numerous experiments we ran. I would also like to thank the entire Whitman Lab for their input over the years that has helped shape my research work.

I am grateful to the Department of Energy for funding my research, and to Kim Sparks at the Cornell Stable Isotope Laboratory for analyzing all our PyOM samples. I also extend my thanks to project collaborators for their valuable feedback. A special thanks to Matt Traxler and Monika Fischer at UC-Berkeley.

I am also grateful to the Soil Science Department for their support during my time at UW-Madison and for funding my conference travels. The soil science graduate student community has made my time at UW-Madison memorable.

I could not have undertaken this journey without the support of my family and friends. To my parents and my brother, thank you for everything. To Ankita, Anthony, Emily, Taylor and Gautham, who helped me navigate through the tough times, I cannot thank you enough.

Finally, I want to express my immense gratitude to my partner, Om, for his unwavering support, patience, and encouragement throughout this journey. Your belief in me has been a constant source of inspiration.

ABSTRACT

Pyrogenic organic matter (PyOM), formed during the incomplete combustion of organic matter, is a carbon-rich substance with potential for long-term carbon storage. This thesis investigates the impact of PyOM, also known as “biochar”, on carbon cycling in post-fire soils over different timeframes. The influence of PyOM properties, such as ageing and pyrolysis temperature, on carbon dynamics and microbial responses is examined. In a series of laboratory experiments, biochar produced from pine wood at 350 and 550 °C was studied. The first investigation focused on ageing effects on biochar carbon mineralization, aiming to understand the changes in surface and bulk chemical properties that influence microbial mineralization. Short-term differences in carbon mineralization between water-extractable and non-water-extractable PyOM fractions were then examined. High-resolution flux monitoring of burned soils, amended with ^{13}C-labeled PyOM, provided insights into the partitioning of carbon fluxes between PyOM fractions and soil organic carbon (SOC). The study also explored the influence of water-extractable fraction proportions in 350 °C vs. 550 °C PyOM on SOC mineralization (priming). Bacterial and fungal community dynamics were tracked concurrently to identify taxa responding to PyOM addition. Furthermore, a quantitative stable isotope probing (qSIP) study using highly enriched ^{13}C-labeled PyOM at 350 °C was conducted to identify bacteria actively incorporating non-water-extractable PyOM carbon. Overall, this research seeks to understand how PyOM heterogeneity and ageing influence carbon cycling in post-fire soils by investigating the response of soil microbial communities and identifying microbial taxa involved in PyOM degradation. The findings have implications for short and long-term carbon cycling estimates in post-fire soils and contribute to the understanding of functional changes in soil microbiomes post-fire.

TABLE OF CONTENTS

LIST OF TABLES

LIST OF FIGURES

LIST OF PICTURES

CHAPTER ONE: INTRODUCTION

Pyrogenic organic matter (PyOM) is a carbon (C)-rich substance, produced due to incomplete combustion of organic matter during fires (Santín et al., 2016; Schmidt & Noack, 2000). Its high content of aromatic structures makes it relatively resistant to microbial degradation (McBeath & Smernik, 2009; Singh et al., 2012), offering potential for long-term C storage (Lehmann & Joseph, 2012). Over time, ageing or weathering processes can alter the bulk and surface properties of PyOM, impacting its carbon cycling in soils (Wang et al., 2020). When produced under controlled, low-oxygen environments, PyOM is commonly referred to as "biochar" and is used as a soil amendment for carbon management (Lehmann & Joseph, 2012). However, a small portion of the carbon in PyOM may be readily used by microbes (Bird et al., 2015; Whitman et al., 2014), and factors such as pyrolysis temperature can influence both the total carbon content and the proportion of easily degradable carbon in PyOM (Bruun et al., 2011; Zimmerman et al., 2011).

As the frequency and severity of wildfires increases due to climate change (Abatzoglou & Williams, 2016; Westerling, 2016), it becomes crucial to investigate the cycling of PyOM-C in post-fire soils over short and long timeframes (Bird et al., 2015; Santín et al., 2016). Additionally, understanding the impact of PyOM on soil organic carbon (SOC) cycling and its potential role in net carbon storage is essential (Maestrini et al., 2015; J. Wang et al., 2016; Whitman et al., 2015). Although PyOM is known to affect microbial communities, the precise mechanisms through which microbes respond to PyOM remain unclear (Lehmann et al., 2011; Whitman et al., 2016; Woolet & Whitman, 2020). Gaining insight into these mechanisms is important for understanding how shifts in microbial communities will influence carbon cycling

in soils affected by fires. In my dissertation, I conducted a series of laboratory experiments with PyOM produced from pine wood at 350 and 550 °C to address these challenges.

First, I investigated the impact of ageing on biochar C mineralization by a putative biochar-decomposing *Streptomyces* isolate to gain insights into biochar C cycling in soils over longer timescales. My specific goal here was to determine whether ageing related changes in surface and bulk chemical properties would make the C in biochar more mineralizable by microbes. To achieve this, we simulated biochar ageing in lab using three different treatments - physical, chemical, and biological, and measured changes in biochar C mineralization, bulk chemistry, and surface properties in comparison with the unaged biochar.

Next, I aimed to identify short-term differences in C mineralization between two different fractions within PyOM – the predominantly aliphatic water-extractable and highly aromatic non-water-extractable PyOM fractions. To achieve this, we employed high-resolution flux monitoring of burned soils amended with ^{13}C-labeled PyOM over a month-long incubation and partitioned fluxes between the PyOM fractions and SOC. We also examined if differences in the proportion of water-extractable fraction in 350 °C vs. 550 °C PyOM would affect SOC mineralization (priming). During the same period, we tracked bacterial and fungal communities to identify taxa that increased in relative abundance in response to PyOM addition.

Lastly, I conducted a similar incubation with highly enriched ^{13}C-labeled 350 °C PyOM and used quantitative stable isotope probing (qSIP) of DNA (Hungate et al., 2015), to identify bacteria that actively incorporate the non-water-extractable PyOM-C. Besides documented PyOM responders like *Noviherbaspirillum* sp. (Woolet & Whitman, 2020), we expected that incorporators would include fire responsive bacteria that are capable of exploiting post fire aromatic C containing PyOM such as *Arthrobacter* sp. (Whitman et al., 2019).

Overall, my research aims to understand how PyOM-C heterogeneity and ageing influence C cycling in post-fire soils by investigating the response of soil microbial communities to PyOM addition and identifying microbial taxa that actively degrade it. The findings of this study have implications for both short and long-term C cycling estimates in post-fire soils and can contribute to our understanding of functional changes in soil microbiomes post-fire.

References

Abatzoglou, J. T., & Williams, A. P. (2016). Impact of anthropogenic climate change on wildfire across western US forests. Proceedings of the National Academy of Sciences, 113(42), 11770–11775.

Bird, M. I., Wynn, J. G., Saiz, G., Wurster, C. M., & McBeath, A. (2015). The pyrogenic carbon cycle. Annual Review of Earth and Planetary Sciences, 43, 273–298.

Bruun, E. W., Hauggaard-Nielsen, H., Ibrahim, N., Egsgaard, H., Ambus, P., Jensen, P. A., & Dam-Johansen, K. (2011). Influence of fast pyrolysis temperature on biochar labile fraction and short-term carbon loss in a loamy soil. Biomass and Bioenergy, 35(3), 1182–1189.

Hungate, B. A., Mau, R. L., Schwartz, E., Caporaso, J. G., Dijkstra, P., van Gestel, N., Koch, B. J., Liu, C. M., McHugh, T. A., Marks, J. C., Morrissey, E. M., & Price, L. B. (2015). Quantitative Microbial Ecology through Stable Isotope Probing. Applied and Environmental Microbiology, 81(21), 7570–7581.

Lehmann, J., & Joseph, S. (2012). Biochar for environmental management: An introduction. In Biochar for Environmental Management: Science and Technology.

Lehmann, J., Rillig, M. C., Thies, J., Masiello, C. A., Hockaday, W. C., & Crowley, D. (2011). Biochar effects on soil biota—A review. Soil Biology and Biochemistry, 43(9), 1812–1836.

Maestrini, B., Nannipieri, P., & Abiven, S. (2015). A meta-analysis on pyrogenic organic matter induced priming effect. GCB Bioenergy, 7(4), 577–590.

McBeath, A. V., & Smernik, R. J. (2009). Variation in the degree of aromatic condensation of chars. Organic Geochemistry, 40(12), 1161–1168.

Santín, C., Doerr, S. H., Kane, E. S., Masiello, C. A., Ohlson, M., de la Rosa, J. M., Preston, C. M., & Dittmar, T. (2016). Towards a global assessment of pyrogenic carbon from vegetation fires. Global Change Biology, 22(1), 76–91.

Schmidt, M. W. I., & Noack, A. G. (2000). Black carbon in soils and sediments: Analysis, distribution, implications, and current challenges. Global Biogeochemical Cycles, 14(3), 777–793.

Singh, B. P., Cowie, A. L., & Smernik, R. J. (2012). Biochar carbon stability in a clayey soil as a function of feedstock and pyrolysis temperature. Environmental Science and Technology, 46(21), 11770–11778.

Wang, J., Xiong, Z., & Kuzyakov, Y. (2016). Biochar stability in soil: Meta-analysis of decomposition and priming effects. GCB Bioenergy, 8(3), 512–523.

Wang, L., O'Connor, D., Rinklebe, J., Ok, Y. S., Tsang, D. C. W., Shen, Z., & Hou, D. (2020). Biochar Aging: Mechanisms, Physicochemical Changes, Assessment, And Implications for Field Applications. Environmental Science & Technology, 54(23), 14797–14814.

Westerling, A. L. (2016). Increasing western US forest wildfire activity: Sensitivity to changes in the timing of spring. Philosophical Transactions of the Royal Society B: Biological Sciences, 371(1696), 20150178.

Whitman, T., Enders, A., & Lehmann, J. (2014). Pyrogenic carbon additions to soil counteract positive priming of soil carbon mineralization by plants. Soil Biology and Biochemistry, 73, 33–41.

Whitman, T., Pepe-Ranney, C., Enders, A., Koechli, C., Campbell, A., Buckley, D. H., & Lehmann, J. (2016). Dynamics of microbial community composition and soil organic carbon mineralization in soil following addition of pyrogenic and fresh organic matter. ISME Journal, 10(12), 2918–2930.

Whitman, T., Singh, B. P., & Zimmerman, A. (2015). Priming effects in biochar-amended soils: Implications of biochar-soil organic matter interactions for carbon storage. Biochar for Environmental Management, 453–486.

Whitman, T., Whitman, E., Woolet, J., Flannigan, M. D., Thompson, D. K., & Parisien, M. A. (2019). Soil bacterial and fungal response to wildfires in the Canadian boreal forest across a burn severity gradient. Soil Biology and Biochemistry, 138(April), 107571.

Woolet, J., & Whitman, T. (2020). Pyrogenic organic matter effects on soil bacterial community composition. Soil Biology and Biochemistry, 141, 107678.

Zimmerman, A. R., Gao, B., & Ahn, M.-Y. (2011). Soil Biology & Biochemistry Positive and negative carbon mineralization priming effects among a variety of biochar-amended soils. Soil Biology and Biochemistry, 43, 1169–1179.

CHAPTER TWO: EFFECTS OF PHYSICAL, CHEMICAL, AND BIOLOGICAL AGEING ON THE MINERALIZATION OF PINE WOOD BIOCHAR BY A STREPTOMYCES ISOLATE

Nayela Zeba[1], Timothy D. Berry[1], Kevin Panke-Buisse[2], and Thea Whitman[1]

[1] Department of Soil Science, University of Wisconsin-Madison

[2] Dairy Forage Research Center, University of Wisconsin-Madison

This chapter is a slightly modified version of the research article titled "Effects of physical, chemical, and biological ageing on the mineralization of pine wood biochar by a *Streptomyces* isolate" published in PLoS ONE. https://doi.org/10.1371/journal.pone.0265663

Abstract

If biochar is to be used for carbon (C) management, we must understand how weathering or ageing affects biochar C mineralization. Here, we incubated aged and unaged eastern white pine wood biochar produced at 350 and 550 °C with a *Streptomyces* isolate, a putative biochar-decomposing microbe. Ageing was accelerated via three different processes, namely, (a) physical ageing – subjecting biochar to alternating freeze-thaw and wet-dry cycles, (b) chemical ageing – treating biochar with concentrated hydrogen peroxide and (c) biological ageing – incubating biochar in the presence of nutrients and microorganisms. Elemental composition and surface chemistry (Fourier Transform Infrared spectroscopy) of biochar samples were compared before and after ageing. Biochar C mineralization between ageing treatments was significantly different in the case of 350 °C biochar (p value = 0.03). Among the 350 °C biochars, physical ageing resulted in the greatest increase (by 103%) in biochar C mineralization (p value = 0.05). However, in the case of 550 °C biochar, ageing did not result in a significant change in biochar C mineralization (p value = 0.40). Biochar C mineralization was positively correlated with an increase in O/C ratio post-ageing (r_s = 0.86, p value = 0.01). In the case of 350 °C biochar, surface oxidation during ageing enhanced biochar degradation by the isolate. For 550 °C biochar, however, ageing did not significantly increase biochar C mineralization, likely due to high condensed aromatic C content and lower surface oxidation during ageing. The results from our study suggest that low temperature aged biochar is more susceptible to biological degradation by soil microbes. These findings have implications for the use of biochar for long term C storage in soils.

Introduction

Biochar is the carbon-rich solid product of pyrolysis, the process of heating biomass under oxygen limited conditions [1]. Biochar has the potential to be used as a soil amendment for agricultural management (*e.g.*, to increase water holding capacity and enhance nutrient management) and as a carbon (C) management strategy to help mitigate greenhouse gas emissions [2]. Converting waste biomass into biochar can potentially be an effective way to sequester C, since the C contained in biochar is generally more resistant to mineralization compared to the C in the parent biomass [2,3]. However, the net C effects of biochar application in soil depend heavily on system-specific parameters, particularly what would have happened to the parent biomass had it not been used to produce biochar (*e.g.*, would it have decomposed rapidly, or would it have continued to grow and fix C) [4–7].

The persistence of biochar C in soil can be attributed to its high proportion of condensed aromatic C [2,8,9], which has been shown to be resistant to mineralization by both abiotic and biotic processes [10,11]. Further, biochar, while being rich in C, tends to have a low oxygen (O) and hydrogen (H) content, and low O/C and H/C ratios in biochar have been shown to correlate with biochar persistence in soil [12,13]. The chemical and physical properties of biochar that affect its persistence are initially determined by the production conditions, such as feedstock and production temperature [14]. But once the biochar is deposited in soil, these properties change over time in a process known as weathering or ageing [15–18]. Natural ageing of biochar in soil is a complex process with multiple relevant mechanisms [15]. We focus on three of these dominant mechanisms over the course of this paper:

Physical ageing - physical breakdown of biochar, primarily by freeze-thaw cycles and changes in temperature and moisture [15,19–21]

Chemical ageing - degradation of biochar through abiotic oxidation upon exposure to various oxidizing agents [22–24]

Biological ageing - biotic degradation and corresponding physical and chemical modifications of biochar by microbes and other soil organisms [25–29]

Commonly reported effects of biochar ageing include a drop in pH, an increase in O content, and an increase in O-containing functional groups on the surface of aged biochar compared to unaged biochar [18,30]. This suggests that ageing of biochar, both naturally and artificially, causes changes to its elemental composition and surface chemistry. Furthermore, these changes have been shown to affect properties of biochar such as sorption [19,31] and cation exchange capacity [32,33]. However, there is limited information on how these changes will alter the mineralizability of biochar itself. Spokas [34] reported an increase in total C mineralization upon incubation of soil amended with 3 year aged woody biochar, primarily due to chemical oxidation of biochar surfaces. On the other hand, Liu et al. [35] observed lower total C mineralization in soil incubations amended with 6 year aged wheat straw biochar due to loss of easily mineralizable C during ageing. Notably, these studies primarily looked at changes in total C mineralization after addition of aged biochar to soil, while the effect of ageing specifically on the mineralizability of the aged biochar itself by soil microbes has not been fully explored.

Investigating the relationship between physicochemical changes due to ageing and biochar mineralizability is one of the primary tranches of this work. Specifically, the aim of this study is to examine the mineralizability of aged biochar by a specific biochar-degrading microbe from a genus that is common to soils worldwide – a *Streptomyces* isolate [36]. We predicted that the change in mineralization with ageing will depend on whether

(i) the ageing process results in loss of easily mineralizable C (as indicated by aliphatic chemical groups), which would lead to lower mineralization, or

(ii) an increase in the O content (as indicated by the O/C ratios), which would lead to higher mineralization

Materials and Methods

Production of biochar

Biochar was produced from eastern white pine wood chips (*Pinus strobus* (L.)) at highest treatment temperatures (HTT) of 350 and 550 °C in a modified Fischer Scientific Lindberg/Blue M Moldatherm box furnace (Thermo Fisher Scientific, Waltham, MA, USA) under continuous argon flow (1 L min^{-1}) and a peak temperature residence time of 30 min [37]. We chose 350 and 550 °C HTTs as they fall within the range of temperatures recorded for naturally produced pyrogenic organic matter (PyOM) during wildfires in addition to being common HTTs for biochar production [38,39]. Including biochar produced at two different temperatures also allowed us to observe the effect that increasing C content and aromaticity has on the mineralizability of aged biochar [11]. Biochar was ground using a ball mill and sieved to a particle size of <45 μm. We used finely ground biochar to maximize the surface area available for both the ageing process and mineralization of biochar C by the *Streptomyces* isolate during incubation. The full details of biochar production can be found in Appendix S2.

Ageing of biochar

Biochar produced at 350 and 550 °C was subjected to one of three different ageing processes - physical, chemical and biological. We performed all ageing treatments on single batches of biochar to give us a final set of physically, chemically and biologically aged chars produced at 350 °C (350PHY, 350CHEM and 350BIO) and 550 °C (550PHY, 550CHEM and

550BIO). A batch each of 350 °C unaged biochar (350UN) and 550 °C unaged biochar (550UN) acted as controls in our study.

Physical ageing

For physical ageing, we subjected biochar samples to 20 freeze-thaw-wet-dry cycles between -80 °C and 100 °C using pint-sized Mason jars (473.18 mL), building on the method reported by Hale et al. [19]. In addition to the freeze-thaw process used by Hale et al., we included a wet-dry cycle to further accelerate physical breakdown of biochar. Wet-dry cycles at different moisture levels have been used in previous studies to artificially age biochar [18]. While our freezing temperature was close to that used by Hale et. al, we chose to dry our samples at 100 °C to ensure that the biochar rapidly and completely dried out between cycles. Quartz sand (Sargent Welch, Buffalo Grove, IL, USA) was used to simulate an inactive soil matrix (80 g with a 5% weight biochar amendment) due to its inability to retain water or nutrients. Ultrapure water was added to the jars containing 4 g of biochar to achieve 40% water holding capacity (WHC). During each cycle, the jars were frozen at -80 °C for a median time of 7 hours (min 5 h – max 48 h), thawed for a period of 1-2 hours, following which they were dried in the oven at 100 °C for a median time of 18 hours (min 14 h – max 54 h) and cooled to room temperature for a period of 1-2 hours. After each drying period, masses of the jars were measured, and ultrapure water was added to reach 40% WHC. After 20 cycles, biochar particles were separated from the sand by wet sieving using a US mesh size no. 270 sieve that allowed the biochar particles less than 45 μm in size to pass through while retaining the sand particles.

Chemical ageing

For chemical ageing, we treated biochar samples with H_2O_2 based on the method reported by Huff and Lee [22]. We used a high concentration of H_2O_2 based on findings from previous

studies that reported maximum changes in surface chemistry of biochar upon treatment with 30% w/w H_2O_2 solution [22,40]. Briefly, 30% w/w H_2O_2 solution was added to 5 g of biochar at a ratio of 1 g biochar: 20 mL solution and shaken inside a chemical fume hood for 2 hours at 100 rpm. After 2 hours of shaking, we filtered the biochar samples through sterile Whatman glass microfiber filters (Grade 934-AH Circles – 1.5 μm particle retention) and rinsed with 100 mL aliquots of ultrapure water to remove any residual H_2O_2.

Biological ageing

For biological ageing, we exposed the biochar samples to a microbial community in a nutrient solution supplemented with glucose (40 μg glucose mg^{-1} biochar C), building on the method reported by Hale et al. [19]. We added glucose to stimulate microbial activity and, with it, the decomposition of biochar. We chose a microbial community expected to be enriched in microbes that could degrade biochar to further accelerate the biological ageing treatment. We derived the microbial inoculum from soil samples collected at the Blodgett Forest Research Station at University of California, Berkeley, which has been used to conduct multiple prescribed burn studies [41]. The soil samples for the inoculum were collected from 0-10 cm depth at the center of a slash pile burn after removing the ash layers. To extract the inoculum, we mixed the field-moist soil samples with Millipore water in sterile 50 mL centrifuge tubes and vortexed the tubes for 2 hours at high speed. After vortexing, the tubes were allowed to stand for 5 minutes, and the soil suspensions were filtered through sterile 2.7 μm Whatman membrane filters into sterile centrifuge tubes. For the biological ageing process, nutrient solution was prepared from autoclave-sterilized basal salt solution (500 mL L^{-1} final biochar nutrient media), modified from Stevenson et al. [42], filter-sterilized vitamin B12 solution (200 μL L^{-1} final biochar nutrient media), filter-sterilized vitamin mixture (200 μL L^{-1} final biochar nutrient media) and a filter-

sterilized trace elements solution (1 mL L^{-1} final biochar nutrient media) [43]. We combined 5 g of biochar and glucose supplement (40 μg mg^{-1} biochar carbon) with 250 mL ultrapure water and autoclave-sterilized the mixture. After autoclaving, the biochar mixture was transferred to a quart-sized (946.35 mL) Mason jar and combined with 250 mL of the nutrient solution. Note that the pH of the basal salt solution, which is a part of the nutrient solution was adjusted to 7 to obtain pH neutral final biochar nutrient media. The detailed composition of the nutrient solution along with the steps for preparation of the final biochar nutrient media are provided as supplementary material accompanying this work (S2 Appendix). To the resulting biochar and glucose supplemented nutrient media, we added 8 mL of the filtered inoculum and incubated the jars at 30 °C in a shaker incubator set to 100 rpm for a period of 2 weeks to allow for biological ageing to take place.

Incubation

We performed the incubations with all the aged biochar (PHY, CHEM and BIO) as well as unaged biochar (UN) produced at both 350 and 550 °C as solid agar biochar media, inoculated with a bacterial isolate known to grow on biochar at room temperature, while tracing CO_2 emissions from each replicate.

The bacterial isolate we used was a *Streptomyces* that was isolated on media with eastern white pine wood biochar produced at 500 °C as the sole C source. We confirmed that the isolate was a *Streptomyces* by Sanger sequencing the full length 16S ribosomal RNA gene and BLASTing the sequences against the GenBank database. The primary motivation for selecting this specific isolate is that it was able to grow on biochar media during trial lab incubations. Further, there is evidence that indicates that bacterial genera that respond positively to biochar addition in soils include members that have the potential to break down polycyclic aromatic hydrocarbons

(PAHs) [44], a constituent of biochar, particularly high-temperature ones. We recovered the isolate from glycerol stocks by streaking onto a biochar (produced from pine wood at 350 °C) nutrient media agar plate (as described in S2 Appendix) and incubating for 5 days at 37 °C. A single colony from the biochar media plate was inoculated into 30 g L^{-1} tryptic soy broth (Neogen Culture Media, Lansing, MI, USA) and incubated at 30 °C in a shaking incubator until growth was visible, characterized by turbidity in the media.

We performed incubations in quarter-pint sized Mason jars (118.29 mL). The final biochar nutrient media that was used for the study was prepared by combining the nutrient solution with a biochar agar suspension. The nutrient solution was prepared as described earlier under "biological ageing" section. A suspension of biochar (1 g L^{-1} final biochar nutrient media) and noble agar (30 g L^{-1} final biochar nutrient media) was sterilized by autoclaving and combined with the nutrient solution to obtain a pH neutral final biochar nutrient media (S2 Appendix). For each sample, we poured 40 mL of the final biochar nutrient media into sterile Mason jars. This volume was estimated from previous incubations, where we confirmed that it was sufficient to ensure that the final media did not dry out during incubation. After the agar solidified, the plates were inoculated with 20 μL of the bacterial suspension in malt extract broth and plated onto the agar surface using the spread plate technique [45]. All our treatment jars received the same volume of the bacterial suspension during inoculation.

We performed the incubations in replicates of three for each treatment (five each for 350BIO and 550BIO) and included uninoculated controls for each treatment. The uninoculated controls were included to account for CO_2 that may accumulate due to abiotic degradation of biochar. In addition, we included two empty jars as gas flux blanks for the experiment. After plating and inoculation, the jars were capped and sealed with sterile, gas-tight lids with fittings for CO_2 gas

measurements and attached to randomly selected positions on the distribution manifolds (multiplexer) using polyurethane tubing [46]. We incubated the jars at room temperature and measured the concentration of CO_2 respired in the headspace of each jar at intervals of 3-4 days using a Picarro G2131i cavity ringdown spectrometer attached to the multiplexer over a period of one month. After each measurement, we flushed the jars with a 400 ppm CO_2-air gas mixture to ensure aerobic conditions inside the jar. The precise concentration after flushing each jar was measured and subtracted from the next time point reading to determine the respired CO_2 in the jar. From previous biochar incubation trials with the isolate, we confirmed that sampling over a 3-4-day interval did not lead to oxygen depletion inside the jars.

The raw CO_2 readings measured using the multiplexer-Picarro system were processed in R to calculate biochar C mineralized over the period of incubation using the following packages: 'tidyverse' [47], 'zoo' [48], 'RColorBrewer' [49] and 'broom' [50]. Briefly, we calculated the cumulative biochar C mineralized for each replicate at each time point. We calculated the biological cumulative biochar C mineralized values for all replicates by subtracting the corresponding mean C mineralized of uninoculated replicates within each treatment. The biological cumulative biochar C mineralized values were normalized by the mean biochar C content within each treatment and a time series was plotted comparing the biochar C mineralization trends between the aged and unaged biochar samples.

After the incubation period, we disconnected the jars and analyzed images of the agar surfaces using the software *ImageJ* [51]. The percentage area occupied by the growth of bacterial colonies was determined for each incubation jar and used as a rough proxy to compare microbial growth between jars (Fig. S2.1).

Chemical analyses

Total C and N were determined for aged and unaged biochar samples using a Thermo Scientific Flash EA 1112 Flash Combustion Analyzer (Thermo Fisher Scientific, Waltham, MA, USA) at the Department of Agronomy, UW- Madison, WI, USA. Total H was determined using a Thermo Delta V isotope ratio mass spectrometer interfaced to a Temperature Conversion Elemental Analyzer (Thermo Fisher Scientific, Waltham, MA, USA) at the Cornell Isotope Laboratory, NY, USA. Total O was calculated by subtraction as per Enders et al. [14], after determining ash content of aged and unaged biochar samples using the method prescribed by ASTM D1762-84 Standard Test Method for Chemical Analysis of Wood Charcoal (See further details in Appendix S2).

The pH of aged and unaged biochar samples was measured in deionized water at a 1:20 solid: solution ratio using an Inlab Micro Combination pH electrode (Mettler Toledo, Columbus, OH, USA) connected to a Thermo Scientific Orion Star A111 benchtop pH meter (Thermo Fisher Scientific, Waltham, MA, USA). Further details of this procedure can be found in the S2 Appendix.

The FT-IR measurements were performed at the U.S. Dairy Forage Research Center, Madison, WI, USA with a Shimadzu IRPrestige-21 FT-IR spectrometer (Shimadzu, Kyoto, Japan) on the ATR (Attenuated Total Reflection) absorbance mode. Briefly, 5-10 mg of the biochar sample was placed on the Zn-Se sample trough and scanned. For each sample, we obtained 256 scans per sample in the range from 4000 to 650 cm^{-1} with a resolution of 1 cm^{-1} (550UN, 350PHY and 550PHY) and 2 cm^{-1} (350CHEM, 550CHEM, 350BIO, 550BIO and 350UN). Background corrections were performed between each sample measurement. We assigned wavenumbers for selected functional groups based on previous studies (S2.1 Table) and quantified the peak heights

of selected functional groups after spectrum normalization using the Shimadzu IR Solution FT-IR software. Fractional signal heights for each of the FT-IR peaks were calculated by dividing the signal height of each of the peaks by the sum total of signal heights of all peaks of interest to determine the contribution of the signal generated by a particular species to the full spectra. Peaks for OH and CO_2 stretching at 3370 cm^{-1} and 2350 cm^{-1}, respectively, are identified in figures but were not expected to reflect meaningful differences in PyOM chemistry, and hence were not included in our fractional signal heights calculations. Further details of this procedure can be found in the Appendix S2.

Statistical analyses

We performed most calculations in R. Figures were made using the 'ggplot2' [52] and 'wesanderson' [53] packages. All code used for analyses and figures in this paper is available at github.com/nayelazeba/biochar-ageing.

We used the Shapiro-Wilk test to check for normality of data. Since the data did not follow a normal distribution, non-parametric tests were used to compare significant differences between cumulative biochar C mineralized. The Kruskal–Wallis one-way analysis of variance (ANOVA) and a nonparametric multiple comparison Dunn's test were used to investigate significant differences in cumulative biochar C mineralized between groups of temperature and ageing treatments. In order to determine significant correlations between cumulative biochar C mineralized and molar O/C ratios, we used the Spearman's rank correlation analysis. The above-mentioned tests were all performed using the 'stats' package in R.

To compare the full FT-IR spectra of biochar samples across temperatures and different ageing treatments, we used a multivariate dendrogram technique. We used the continuous normalized spectral data for these analyses, excluding the region from 4000 cm^{-1}- 3100 cm^{-1} wavenumber to

remove signals from water sorbed to the biochar surface. We used the 'dendextend' [54] package in R to construct a dendrogram. Euclidean distances between biochar samples were calculated using the dist() function, and the hclust() function with the complete linkage method used for hierarchical clustering, where the two most similar samples are clustered together, one after another, forming an ordered hierarchical tree/ dendrogram.

Results and Discussion

Effect of ageing on biochar C mineralization

The biochar C mineralization trends for all treatments show a similar pattern overall, with an initial period of steep increase in C mineralization, followed by the onset of a period of lower C mineralization (about 350 hours after the start of incubation, Fig. 2.1 and S2.1 Fig.). The mean cumulative C mineralized in uninoculated replicates at the end of the incubation period was 0.04 mg CO_2-C g^{-1} biochar-C for 350 °C biochar and 0.03 mg CO_2-C g^{-1} biochar-C for 550 °C biochar. Mean cumulative biochar C mineralized at the end of the incubation was significantly higher by 39% for 350 °C biochars compared to 550 °C biochars (Kruskal-Wallis$_{ANOVA}$, p value = 0.01). The difference in cumulative C mineralization between 350 °C and 550 °C biochars is further discussed in Appendix S2.

Amongst the 350 °C chars, the mean cumulative biochar C mineralized for aged biochars was higher than that for unaged biochar through the entire incubation period (Fig. 2.1). At the end of the incubation period, the mean cumulative biochar C mineralized was significantly different between the ageing treatments (Kruskal-Wallis$_{ANOVA}$, p value = 0.03). The greatest increase was measured for 350PHY which showed 103% higher C mineralization compared to unaged biochar, although we did not identify a statistically significant difference using the Dunn's test (p_{adj} value = 0.05). The rate of C mineralization was highest for 350PHY at the onset of the

incubation and remained higher than the C mineralization rate of unaged biochar throughout the incubation period (S2.1 Fig.). 350PHY treatments also showed 87% higher surface growth of the isolate compared to unaged biochar at the end of the incubation period (S2.2 ..), consistent with the cumulative biochar C mineralized data. The mean cumulative biochar C mineralization was 22% higher for 350BIO compared to the unaged treatment (Dunn's test, p_{adj} value = 0.29), while the increase for 350CHEM was negligible.

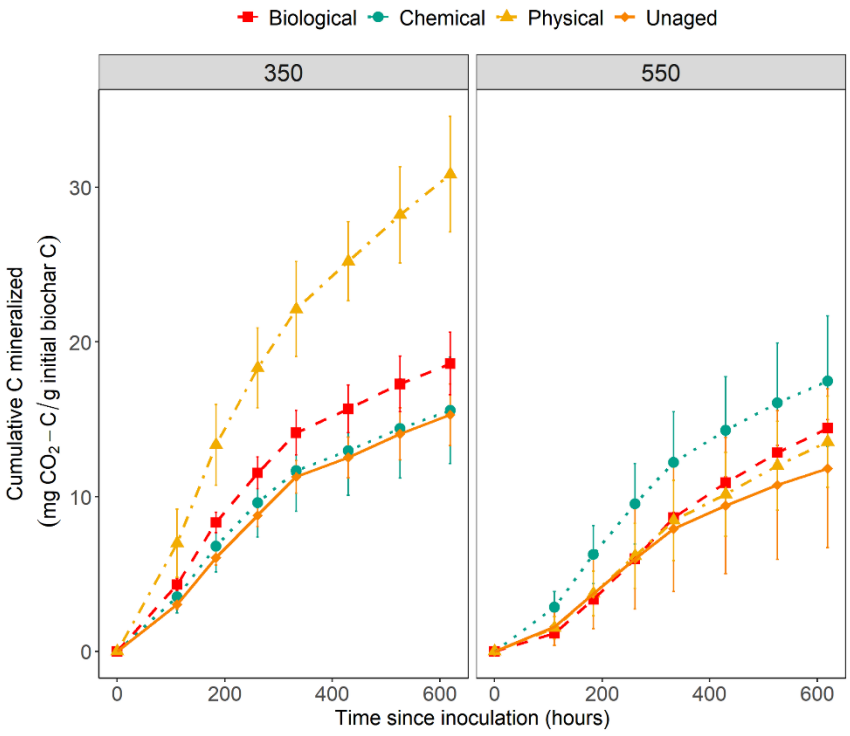

Figure 2.1. Cumulative biochar C mineralization over time.
Data represent mean cumulative C mineralized from unaged and physically, chemically and biologically aged biochar samples over time, with uninoculated blanks subtracted and normalized with mean biochar-C. n = 3 for physical, chemical and unaged, n = 5 for biological. Error bars represent 95% confidence intervals. The left panel shows biochar produced at 350 °C and the right panel shows biochar produced at 550 °C.

Amongst the 550 °C biochar, there were not large differences between mean cumulative biochar C mineralization in aged versus unaged biochar. We observed an increase in biochar C

mineralized for 550CHEM compared to unaged biochar through the incubation period and a slight increase in 550PHY and 550BIO after about 400 hours after the start of incubation (Fig. 2.1). The mean cumulative biochar C mineralized at the end of the incubation period was 47% higher for 550CHEM compared to unaged biochar and higher by 15% and 22% for 550PHY and 550BIO respectively, but the differences in means were not significant (Kruskal-Wallis$_{ANOVA}$, p value = 0.40). These observations were consistent with trends in growth measurements of the isolate on 550 °C biochar agar surfaces, where the mean surface growth was 43.4% greater for 550CHEM compared to 550UN but no difference in growth was observed for 550BIO and 550PHY treatments (S2.2 Fig.).

Changes in elemental composition during ageing

Aged biochars produced at both 350 °C and 550 °C had lower mean total C and higher mean total O contents than unaged biochar, except in the case of 350CHEM, where we did not observe similar trends (Table 2.1). The molar O/C ratio increased for 350BIO (0.26) and 350PHY (0.39). The O/C ratio for the control 350UN was 0.20. In the case of 550 °C chars, the O/C ratio increased for 550BIO (0.18), 550PHY (0.15) and was highest for 550CHEM (0.26) compared to 550UN (0.11). This is consistent with previous studies that have shown an increase in O/C ratio following natural as well as artificial ageing of biochar through abiotic and biotic processes [15,20,21,32,55]. The relative decrease in C with ageing is likely due in part to leaching of C-rich dissolved organic matter [20]. Additionally, abiotic oxidation of C to carbon dioxide and utilization of C as a substrate by microbes in the case of biologically aged biochars is likely to result in relatively greater loss of C than O [10,25,32,56]. The higher O content in aged biochars indicates an increase in O-containing functional groups that is likely due to both abiotic oxidation of C in the case of chemically and physically aged biochars [15,32] as well as

microbially mediated oxidation in the case of biologically aged biochar [55]. The effects of pyrolysis temperature on the elemental composition of biochar are discussed in Appendix S2.

Table 2.1. Elemental composition, elemental ratio, and pH of the unaged and physically, chemically and biologically aged biochar samples

HTT (°C)	Ageing treatment	Total C	Total N	Total H	Ash	Derived total O	O/C	H/C	pH in solution
		(wt %)							
350	Unaged	75	0.3	3.9	0.6	20.4	0.20	0.62	6.1
	Physical	61	0.3	2.7	4.3	31.8	0.39	0.53	3.3†
	Chemical	80 ± 4.6*	0.3	2.5	1.6	15.6	0.15	0.38	4.3
	Biological	70	0.3	3.5	1.8	24.4	0.26	0.60	4.8
550	Unaged	85 ± 1.2*	0.2	2.4	0.8	11.9	0.11	0.34	6.9
	Physical	79	0.4	2.2	3.1	15.8	0.15	0.34	6.5†
	Chemical	71	0.3	3.8	0.7	24.4	0.26	0.63	5.0
	Biological	77	0.3	2.5	2.4	18.2	0.18	0.39	4.8

Note: Data shown represent the mean of all lab replicates unless specified otherwise.
*Mean ± standard deviation is shown for data where the standard deviation of lab replicates (n = 4) is > 1
†No replicate measurements were included due to sample limitation

Changes in surface chemistry during ageing

Amongst the ageing treatments, the surface chemistry of physically aged biochar was altered the most when compared against the control, as indicated by their spectra being most dissimilar from the unaged biochar's (Fig. 2.2.b). While chemical and biological ageing also led to changes in surface chemistry, we see these samples cluster together more by production temperature than treatment method – *i.e.*, production temperature was a more important determinant of biochar chemistry than ageing treatment. An important factor distinguishing 350 °C and 550 °C biochars is the increase in aromatic carbon content and decrease in H and O-containing functional groups

on the surface of biochar with increasing pyrolysis temperatures [10,11,39] (See Appendix S2 for further discussion on effects of pyrolysis temperature on surface chemistry). It is interesting to note that the two PHY samples are more similar to each other than to other samples produced at the same pyrolysis temperatures. This suggests that the surface chemistry in PHY samples was more strongly affected by the ageing treatment than the production temperature. It is possible that subjecting biochar to repeated freeze-thaw-wet-dry cycles during physical ageing altered the particle structure, thereby causing an increase in the surface area over which these modifications would take place, although we did not investigate changes in surface area during ageing.

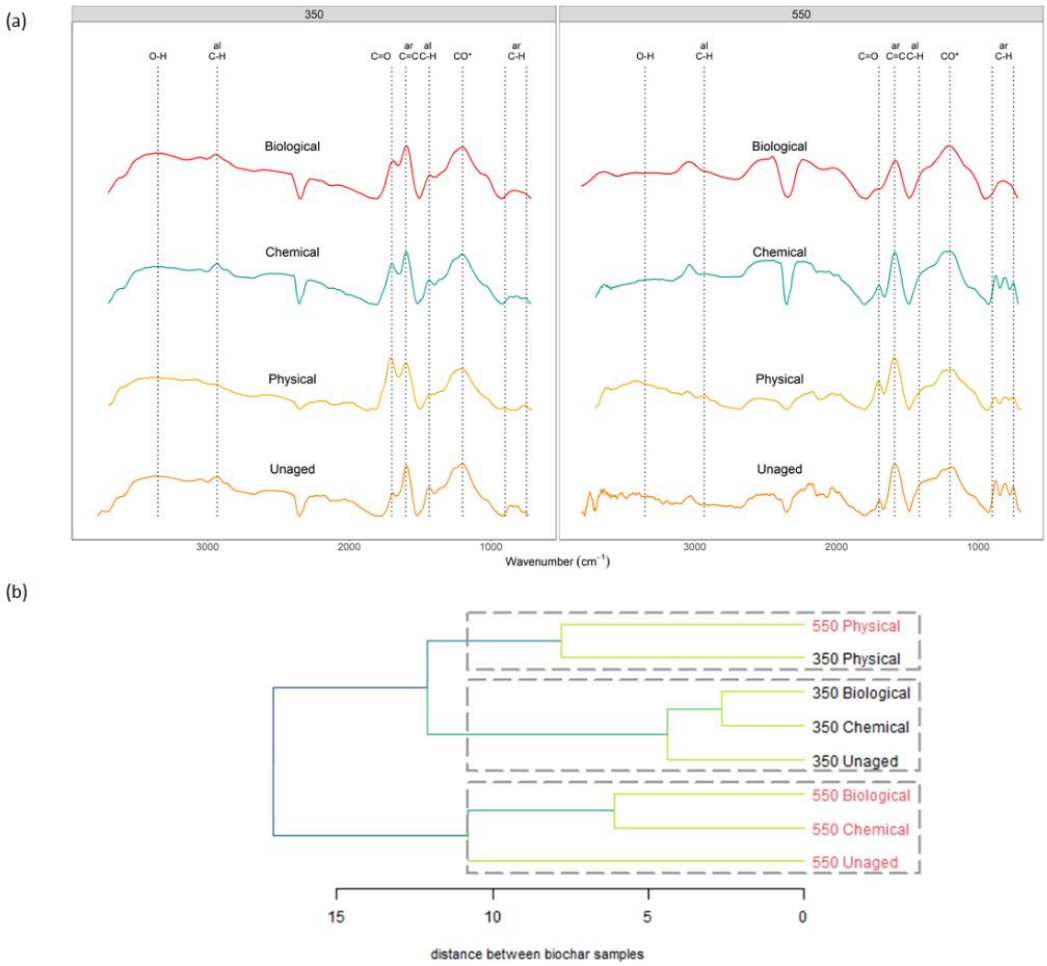

Figure 2.2. Changes in surface chemistry during ageing inferred using FTIR spectroscopy. ***(a)*** *FT-IR spectra of unaged and physically, chemically and biologically aged biochar samples produced at 350 °C (left panel) and 550 °C (right panel). Labels on top indicate the peak names assigned to different functional groups as described in detail in supplementary information (O-H: O–H stretching in carboxylic acids, phenols, alcohols at 3370 cm-1; al CH: aliphatic C-H stretch in CH_3 and CH_2 at ~2932 cm^{-1} and C-H bending of CH_3 and CH_2 at 1413 cm^{-1}; CO_2: CO_2 asymmetric stretching at 2350 cm^{-1}; C=O: C=O stretch in carboxylic acids and ketones at ~1701 cm^{-1}; ar C=C: aromatic C=C vibrations and stretching of quinones at ~1593 cm^{-1}; CO*: C–O stretching and O–H bending of COOH and/or C–OH stretching of polysaccharides at ~1200 cm^{-1}; ar C-H: aromatic C-H out of plane deformation at 810 cm^{-1}.* ***(b)*** *The clustering of biochar FT-IR spectra based on Ward's hierarchical clustering method represented as a dendrogram. The distance of the link between any two clusters (or samples) is a measure of the relative dissimilarity between them.*

An important feature that stood out when comparing the FTIR spectra of unaged and aged biochars was the increase in O-containing carboxylic groups, measured by changes in the relative peak height of the C=O stretch at 1701 cm^{-1} wavenumber (Fig. 2.2.a and S2.2 Table). PHY samples across pyrolysis temperatures showed the maximum values for C=O stretch, indicating that the surfaces of physically aged biochar were the most oxidized and rich in carboxylic groups. We also measured a slight increase in carboxylic groups for both 350CHEM and 550CHEM compared to unaged chars. The increase in surface oxygenation and O-containing functional groups after ageing is consistent with the findings of previous studies that investigated changes in surface chemistry using methods analogous to the physical and chemical treatments used in this study [15,20–23]. For biological ageing, we observed a relative increase in carboxylic groups only in the case of 350BIO. This suggests that abiotic oxidation through physical and chemical ageing methods used in the study resulted in more surface oxidation and carboxylic groups compared to biotic oxidation through biological ageing. This agrees with the finding of Cheng et al. [32], where they noted that abiotic processes were more important than biotic processes for the initial surface oxidation of fresh biochar.

Amongst the surface aromatic and aliphatic groups, we consistently observed a decrease in relative peak height in the 1413 cm^{-1} aliphatic C-H stretch, 810 cm^{-1} aromatic C-H stretch and 1593 cm^{-1} C=C aromatic stretch regions after ageing in 350 °C biochar. The maximum decrease in peak values was consistently observed for 350PHY. Additionally, in the case of 350PHY, we measured a considerable decrease in relative peak height for the aliphatic C-H stretch at 2932 cm^{-1} after ageing. In the case of 550 °C char, we observed a considerable decrease in the relative peak height for the aromatic C-H stretch and a slight decrease in the 1413 cm^{-1} aliphatic C-H

stretch after ageing but the same was not observed in the case of the C=C aromatic stretch. These changes indicate a relative loss or transformation of both surface aliphatic and aromatic carbon groups during ageing. As discussed earlier, the loss in C could be due to leaching or abiotic oxidation of C during ageing. Further, in the case of biological ageing, the relative loss in aliphatic C group at 1413 cm^{-1} and 2932 cm^{-1} (for 350°C chars) could be a result of decomposition of aliphatic C by soil microbes [25,26,57]. While it may not be possible to conclusively determine whether oxidized functional groups were previously associated with aromatic vs. aliphatic compounds, the drop in relative heights in the aromatic regions (810 and 1593 cm^{-1} wavenumbers) accompanied by a relative increase in signal for carboxyl (1701 cm^{-1}) group suggests that the oxidation of aromatic C results in the development of carboxylic groups. It has been previously suggested that oxidation on the edges of the aromatic backbone of biochar, taking place over a long period of time, could lead to the formation of negatively charged carboxyl groups [56,58,59]. A loss in aromatic functional groups was documented during physical ageing of peanut straw biochar [21] and during chemical ageing of pine wood biochar [22]. More recently, Yi et al. [60] measured loss and transformation of condensed aromatic C after nine years of field ageing of high temperature bamboo and rice straw biochar. It is expected that these changes would appear more slowly in studies that rely on natural ageing compared to our study where simulated ageing was more intense than natural weathering. These previous findings support the inference that the ageing methods used in this study could have caused the disruption of aromatic carbon to form carboxylic groups.

It is important to note that FTIR spectra as produced and analyzed in this study are only semi-quantitative – *i.e.*, a doubling in peak height does not necessarily represent twice as much of the bond associated with that wavenumber. Furthermore, since replicates for ageing treatments and

FTIR measurements were not included, we cannot determine whether these differences are statistically significant. However, the spectra represent an average of 265 scans on pooled and homogenized samples, and consistent responses to ageing at the two different temperatures as well as consistent temperature effects across different ageing treatments both help give us confidence in the trends observed here.

Relationship between biochar C mineralization and chemical composition

There is a significant positive correlation between biochar C mineralization across temperature and ageing treatments and the molar O/C ratio (Spearman's correlation test, $r_s = 0.87$, p value = 0.01; Fig. 2.3). While this indicates that the ageing treatments where we observed a relative increase in the O/C ratio tended to have increased biochar C mineralizability, pyrolysis temperature is also an important factor here: we see a stronger impact of ageing on biochar C mineralization in low temperature chars. Specifically, we saw the greatest increase in cumulative and rate of biochar C mineralization compared to unaged biochar during physical ageing (Fig. 2.1 and S2.1 Fig.), and 350PHY was also the treatment for which the O/C ratio is the greatest and the FTIR data shows the highest increase in carboxyl groups (Fig. 2.2.a and S2.2 Table). We also observed a positive correlation between biochar C mineralization and the molar H/C ratio across all temperature and ageing treatments, although, the correlation was not statistically significant (Spearman's correlation test, $r_s = 0.67$, p value = 0.08; S2.3 Fig.). An increase in the carboxylic groups, molar O/C and molar H/C ratio of biochar during ageing could make it less stable, more hydrophilic and more likely to be mineralized by microbes [12,61,62]. This surface-oxidized biochar is easier to break down and could potentially facilitate the microbial metabolism of ring structures that would ordinarily be highly recalcitrant [15,18,56].

Additionally, in the case of 350 °C biochars, we see a drop in surface aromatic groups due to ageing, with maximum drop observed in the case of 350PHY (Fig. 2.2.a and S2.2 Table). Oxidative transformation of aromatic C to linear alkyl-C and O-alkyl-C could decrease ring condensation and make carbon more susceptible to microbial breakdown [60]. This is observed during the incubation, after 350 hours, wherein we observed higher rate of biochar C mineralization for 350PHY than unaged biochar (S2.1 Fig.). During this period, we would expect to see an increase in the breakdown of more complex, aromatic C by the isolate, as the easily mineralizable C is more likely to be consumed early on. Further, studies have documented breakdown and release of aromatic moieties in biochar to low molecular-weight organic acids during ageing [63,64]. The surface oxidation of aromatic C groups has important implications for C management and cycling for both low temperature biochars and naturally produced wildfire pyrogenic organic matter (PyOM). It has been suggested that the chemical stability of PyOM produced at high temperatures during natural wildfires is more comparable to low temperature biochars produced in the lab. This is because natural PyOM was found to consist of small clusters of aromatic C units and not highly condensed polyaromatic structures [38,65,66]. Based on our findings, the carbon in these PyOM materials could be more susceptible to surface oxidation and C loss during ageing which could lead to increased mineralizability and thus decreased C storage potential.

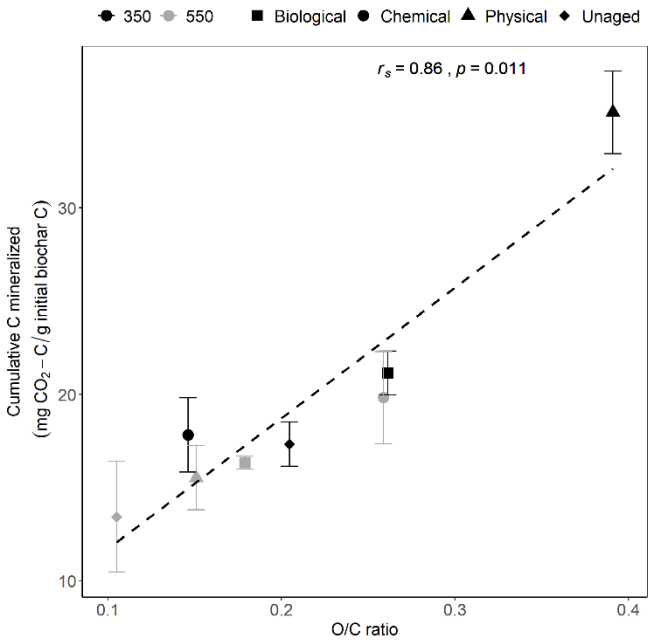

Figure 2.3. Relationship between mean cumulative biochar-C mineralized and molar O/C ratio.
n=3 for physical, chemical and unaged, n=5 for biological treatments. Error bars represent standard error of the mean. Shapes indicate unaged, physically, chemically and biologically aged biochar samples produced at 350 °C (black) and 550 °C (gray).

For the 550 °C chars, we did not observe a significant increase in biochar C mineralization despite seeing an increase in the O/C and H/C ratio during ageing. This is perhaps because even though increases in surface oxidation and loss of some surface aromatic and aliphatic C groups were observed during ageing, 550 °C aged chars still retained more aromatic C and were less oxidized than 350 °C aged chars, as observed in FTIR spectra (Fig. 2.2.a and S2.2 Table). As a result, there is likely to be less easily mineralizable C present in 550 °C biochars even after ageing. This is in line with other studies that have documented an inverse relationship between mineralization and aromatic fraction in biochars [56,67]. This effect is potentially the primary reason we did not observe a significant increase in biochar C mineralized for 550 °C chars during ageing despite observing changes in the surface oxidation (Fig. 2.1 & Fig. 2.2.a).

Ageing considerations and future directions

The primary goal of this study is to examine the effect that long-term ageing-related changes in surface chemistry and elemental composition have on mineralizability of biochar C. To this effect, all three ageing treatments used in this study were designed to simulate extreme degrees of real-world processes that occur naturally to biochar in soil. However, it is not feasible to develop a scale to quantify the relative severity of the treatments compared to their expected severity in nature, or even measure the relative severity of the treatments. It is possible that further increasing the severity of the biological and chemical ageing processes could lead to increased C mineralization for those treatments as well. For instance, increasing the duration of biological ageing may result in a continued increase in biochar surface oxidation and O/C ratio. Despite the lack of quantitative comparison, this study highlights the increased susceptibility of biochar to microbial degradation with increase in surface oxidation. In particular, it demonstrates the ability of abiotic processes such as freeze-thaw-wet-dry cycles in accelerating surface oxidation. The precise mechanism by which oxidation of biochar takes place during physical ageing remains unknown and warrants further research [30].

It is important to note that ageing and incubation of biochar was performed in the absence of soil. However, we note that in soil systems, biochar-clay interactions, biochar-soil organic matter interactions, as well as physical protection of biochar through aggregate formation are likely to affect both ageing of biochar and its interactions with microbes [68–70]. Further investigation into changes in bulk and surface properties associated with long term ageing of biochar in biochar amended soils could help in verification of laboratory biochar ageing and incubation studies as well as broaden our understanding of the potential of biochar as a C sink [30]. While this study focusses on changes in surface chemistry and elemental composition, we note that

other effects of ageing such as changes in specific surface area, cation exchange capacity and solubility will affect how microbes interact with biochar in soil, in terms of accessibility to the biochar as well as its mineralizability.

We note that despite this *Streptomyces* isolate being a known degrader of unaged PyOM, we still observed a trend of increase in biochar C mineralization after ageing, particularly in the case of physical ageing. For other soil microbes that do not share this capability of decomposing aromatic C in PyOM, we would predict ageing could potentially have a larger impact on their ability to break down PyOM. This would be interesting to test directly, as it could have implications in how post fire C is cycled by microbes based on their affinity for metabolizing PyOM. It would also be interesting to perform future experiments on PyOM degradation using consortia of microbes, in addition to single isolates.

In conclusion, this study provides evidence that higher O/C ratio and surface oxidation during ageing is likely to accelerate biochar C mineralization by microbes. The greatest relative increase in surface carboxylic groups and O/C ratio was observed during physical ageing in low temperature char. As such, our lab experiments demonstrate that the C in low temperature biochar is more susceptible to oxidation and microbial mineralization. Further research is required to better understand how ageing due to both abiotic and microbial processes in soil will affect the C sequestration potential of biochar.

Acknowledgements

We thank Akio Enders for supplying the biochar that we used to isolate *Streptomyces* and for assistance with biochar production. We are thankful to Maggie Phillips at the Jackson Lab and Kim Sparks at the Cornell Stable Isotope Laboratory for assistance with chemical analyses. Thanks to Jamie Woolet for isolating *Streptomyces* on biochar and for all the technical assistance with the incubations. We also thank Monika Fischer and Neem Patel for supplying the soil samples that we used during biological ageing.

Author Contributions

The authors confirm contribution to the paper as follows: study conception and design: NZ, TLW; data collection: NZ, TDB, KPB; analysis and interpretation of results: NZ, TDB, KPB, TLW; draft manuscript preparation: NZ; manuscript review and editing: NZ, TDB, KPB, TLW. All authors have reviewed the results and have given approval to the final version of the manuscript.

References

1. International Biochar Initiative. Standardized product definition and product testing guidelines for biochar that is used in soil. 2015.
2. Lehmann J, Joseph S, editors. Biochar for environmental management: Science, technology and implementation. 2nd ed. London: Routledge; 2015.
3. Schmidt MWI, Noack AG. Black carbon in soils and sediments: analysis, distribution, implications, and current challenges. Global Biogeochem Cycles. 2000;14: 777–793.
4. Woolf D, Amonette JE, Street-Perrott FA, Lehmann J, Joseph S. Sustainable biochar to mitigate global climate change . Nat Commun. 2010;1: 56.
5. Whitman T, Scholz SM, Lehmann J. Biochar projects for mitigating climate change: an investigation of critical methodology issues for carbon accounting. Carbon Manag. 2010;1: 89–107.
6. Whitman T, Hanley K, Enders A, Lehmann J. Predicting pyrogenic organic matter mineralization from its initial properties and implications for carbon management. Org Geochem. 2013;64: 76–83.

7. Campbell JL, Sessions J, Smith D, Trippe K. Potential carbon storage in biochar made from logging residue: basic principles and southern Oregon case studies. PLoS One. 2018;13: e0203475.

8. Baldock J, Smernik R. Chemical composition and bioavailability of thermally altered Pinus resinosa (Red pine) wood. Org Geochem. 2002;33: 1093–1109.

9. Preston CM, Schmidt MWI. Black (pyrogenic) carbon: a synthesis of current knowledge and uncertainties with special consideration of boreal regions. Biogeosciences. 2006;3: 397–420.

10. Nguyen BT, Lehmann J, Hockaday WC, Joseph S, Masiello CA. Temperature sensitivity of black carbon decomposition and oxidation. Environ Sci Technol. 2010;44: 3324–3331.

11. Keiluweit M, Nico PS, Johnson MG, Kleber M. Dynamic molecular structure of plant biomass-derived black carbon (biochar). Environ Sci Technol. 2010;44: 1247–1253.

12. Spokas KA. Review of the stability of biochar in soils: predictability of O:C molar ratios. Carbon Manag. 2010;1: 289–303.

13. Crombie K, Mašek O, Sohi SP, Brownsort P, Cross A. The effect of pyrolysis conditions on biochar stability as determined by three methods. GCB Bioenergy. 2013;5: 122–131.

14. Enders A, Hanley K, Whitman T, Joseph S, Lehmann J. Characterization of biochars to evaluate recalcitrance and agronomic performance. Bioresour Technol. 2012;114: 644–653.

15. Cheng C-H, Lehmann J. Ageing of black carbon along a temperature gradient. Chemosphere. 2009;75: 1021–1027.

16. Mukherjee A, Zimmerman AR, Hamdan R, Cooper WT. Physicochemical changes in pyrogenic organic matter (biochar) after 15 months of field aging. Solid Earth. 2014;5: 693–704.

17. Singh B, Fang Y, Johnston CT. A Fourier-Transform Infrared study of biochar aging in soils. Soil Sci Soc Am J. 2016;80: 613–622.

18. Mia S, Dijkstra FA, Singh B. Chapter one - Long-term aging of biochar: a molecular understanding with agricultural and environmental implications. Advances in Agronomy. Amsterdam: Elsevier; 2017. pp. 1–51.

19. Hale SE, Hanley K, Lehmann J, Zimmerman AR, Cornelissen G. Effects of chemical, biological, and physical aging as well as soil addition on the sorption of pyrene to activated carbon and biochar. Environ Sci Technol. 2012;46: 2479–2480.

20. Xu Z, Xu X, Tsang DCW, Cao X. Contrasting impacts of pre- and post-application aging of biochar on the immobilization of Cd in contaminated soils. Environ Pollut. 2018;242: 1362–1370.

21. Cao Y, Jing Y, Hao H, Wang X. Changes in the physicochemical characteristics of peanut straw biochar after freeze-thaw and dry-wet aging treatments of the biomass. BioResources. 2019;14: 4329–4343.

22. Huff MD, Lee JW. Biochar-surface oxygenation with hydrogen peroxide. J Environ Manage. 2016;165: 17–21.

23. Gámiz B, Hall K, Spokas KA, Cox L. Understanding activation effects on low-temperature biochar for optimization of herbicide sorption. Agronomy. 2019;9: 588.

24. Cross A, Sohi SP. A method for screening the relative long-term stability of biochar. GCB Bioenergy. 2013;5: 215–220.

25. Kuzyakov Y, Subbotina I, Chen H, Bogomolova I, Xu X. Black carbon decomposition and incorporation into soil microbial biomass estimated by 14C labeling. Soil Biol Biochem. 2009;41: 210–219.

26. Kuzyakov Y, Bogomolova I, Glaser B. Biochar stability in soil: decomposition during eight years and transformation as assessed by compound-specific 14C analysis. Soil Biol Biochem. 2014;70: 229–236.

27. Santos F, Torn MS, Bird JA. Biological degradation of pyrogenic organic matter in temperate forest soils. Soil Biol Biochem. 2012;51: 115–124.

28. Farrell M, Kuhn TK, Macdonald LM, Maddern TM, Murphy D V, Hall PA, et al. Microbial utilisation of biochar-derived carbon. Sci Total Environ. 2013;465: 288–297.

29. Whitman T, Zhu Z, Lehmann J. Carbon mineralizability determines interactive effects on mineralization of pyrogenic organic matter and soil organic carbon. Environ Sci Technol. 2014;48: 13727–13734.

30. Wang L, O'Connor D, Rinklebe J, Ok YS, Tsang DCW, Shen Z, et al. Biochar aging: mechanisms, physicochemical changes, assessment, and implications for field applications. Environ Sci Technol. 2020;54: 14797–14814.

31. Jones DL, Edwards-Jones G, Murphy D V. Biochar mediated alterations in herbicide breakdown and leaching in soil. Soil Biol Biochem. 2011;43: 804–813.

32. Cheng C-H, Lehmann J, Thies JE, Burton SD, Engelhard MH. Oxidation of black carbon by biotic and abiotic processes. Org Geochem. 2006;37: 1477–1488.

33. Liu Z, Demisie W, Zhang M. Simulated degradation of biochar and its potential environmental implications. Environ Pollut. 2013;179: 146–152.

34. Spokas KA. Impact of biochar field aging on laboratory greenhouse gas production potentials. GCB Bioenergy. 2013;5: 165–176.

35. Liu Z, Zhu M, Wang J, Liu X, Guo W, Zheng J, et al. The responses of soil organic carbon mineralization and microbial communities to fresh and aged biochar soil amendments. GCB Bioenergy. 2019;11: 1408–1420.

36. Schlatter DC, Kinkel LL. Global biogeography of Streptomyces antibiotic inhibition, resistance, and resource use. FEMS Microbiol Ecol. 2014;88: 386–397.

37. Güereña DT, Lehmann J, Thies JE, Enders A, Karanja N, Neufeldt H. Partitioning the contributions of biochar properties to enhanced biological nitrogen fixation in common bean (Phaseolus vulgaris). Biol Fertil soils. 2015;51: 479–491.

38. Santín C, Doerr SH, Merino A, Bucheli TD, Bryant R, Ascough P, et al. Carbon sequestration potential and physicochemical properties differ between wildfire charcoals and slow-pyrolysis biochars. Sci Rep. 2017;7: 11233.

39. Tomczyk A, Sokołowska Z, Boguta P. Biochar physicochemical properties: pyrolysis temperature and feedstock kind effects. Rev Environ Sci Bio/Technology. 2020;19: 191–215.

40. Han L, Ro K, Wang Y, Sun K, Sun H, Libra J, et al. Oxidation resistance of biochars as a function of feedstock and pyrolysis condition. Sci Total Environ. 2017;616–617: 335–344.

41. Blodgett Forest Research Station | Berkeley Forests. [cited 3 Jun 2021].

42. Stevenson BS, Eichorst SA, Wertz JT, Schmidt TM, Breznak JA. New strategies for cultivation and detection of previously uncultured microbes. Appl Environ Microbiol. 2004;70: 4748–4755.

43. Widdel F, Bak F. Gram-negative mesophilic sulfate-reducing bacteria. In: Balows A, Trüper HG, Dworkin M, Harder W, Schleifer K-H, editors. The Prokaryotes. New York, NY: Springer New York; 1992. pp. 3352–3378.

44. Woolet J, Whitman T. Pyrogenic organic matter effects on soil bacterial community composition. Soil Biol Biochem. 2020;141: 107678.

45. Hartman D. Perfecting your spread plate technique. J Microbiol Biol Educ. 2011;12: 204–205.

46. Berry TD, Creelman C, Nickerson N, Enders A, Whitman T. An open-source, automated, gas sampling peripheral for laboratory incubation experiments using cavity ring-down spectroscopy. HardwareX. 2021;10: e00208.

47. Wickham H, Averick M, Bryan J, Chang W, McGowan LD, Francois R, et al. Welcome to the tidyverse. J Open Source Softw. 2019;4: 1686.

48. Zeileis A, Grothendieck G. zoo: S3 infrastructure for regular and irregular time series. J Stat Softw. 2005;14: 1–27.

49. Neuwirth E. RColorBrewer: ColorBrewer palettes. 2014.

50. Robinson D, Hayes A. broom: convert statistical analysis objects into tidy tibbles. 2020.

51. Schneider CA, Rasband WS, Eliceiri KW. NIH Image to ImageJ: 25 years of image analysis. Nat Methods. 2012;9: 671–675.

52. Wickham H. ggplot2: elegant graphics for data analysis. Springer-Verlag New York; 2016.

53. Ram K, Wickham H. wesanderson: a Wes Anderson palette generator. 2018. Available:

54. Galili T. dendextend: an R package for visualizing, adjusting, and comparing trees of hierarchical clustering. Bioinformatics. 2015.

55. Quan G, Fan Q, Zimmerman AR, Sun J, Cui L, Wang H, et al. Effects of laboratory biotic aging on the characteristics of biochar and its water-soluble organic products. J Hazard Mater. 2020;382: 121071.

56. Bruun E, Hauggaard-Nielsen H, Ibrahim N, Egsgaard H, Ambus P, Jensen P, et al. Influence of fast pyrolysis temperature on biochar labile fraction and short-term carbon loss in a loamy soil. Biomass Bioenergy. 2011;35: 1182–1189.

57. Zimmerman AR, Ouyang L. Priming of pyrogenic C (biochar) mineralization by dissolved organic matter and vice versa. Soil Biol Biochem. 2019;130: 105–112.

58. Glaser B, Lehmann J, Zech W. Ameliorating physical and chemical properties of highly weathered soils in the tropics with charcoal – a review. Biol Fertil Soils. 2002;35: 219–230.

59. Liang B, Lehmann J, Solomon D, Kinyangi J, Grossman J, O'Neill B, et al. Black carbon increases cation exchange capacity in soils. Soil Sci Soc Am J. 2006;70: 1719–1730.

60. Yi Q, Liang B, Nan Q, Wang H, Zhang W, Wu W. Temporal physicochemical changes and transformation of biochar in a rice paddy: insights from a 9-year field experiment. Sci Total Environ. 2020;721: 137670.

61. Zimmerman AR. Abiotic and microbial oxidation of laboratory-produced black carbon (biochar). Environ Sci Technol. 2010;44: 1295–1301.

62. Harvey OR, Kuo L-J, Zimmerman AR, Louchouarn P, Amonette JE, Herbert BE. An nndex-based approach to assessing recalcitrance and soil carbon sequestration potential of engineered black carbons (biochars). Environ Sci Technol. 2012;46: 1415–1421.

63. Yao FX, Arbestain MC, Virgel S, Blanco F, Arostegui J, Maciá-Agulló JA, et al. Simulated geochemical weathering of a mineral ash-rich biochar in a modified soxhlet reactor. Chemosphere. 2010;80: 724–732.

64. Hammes K, Smernik RJ, Skjemstad JO, Schmidt MWI. Characterisation and evaluation of reference materials for black carbon analysis using elemental composition, colour, BET surface area and 13C NMR spectroscopy. Appl Geochemistry. 2008;23: 2113–2122.

65. Knicker H, Hilscher A, González-Vila FJ, Almendros G. A new conceptual model for the structural properties of char produced during vegetation fires. Org Geochem. 2008;39: 935–939.

66. Schneider MPW, Pyle LA, Clark KL, Hockaday WC, Masiello CA, Schmidt MWI. Toward a "molecular thermometer" to estimate the charring temperature of wildland charcoals derived from different biomass sources. Environ Sci Technol. 2013;47: 11490–11495.

67. Dai Z, Barberán A, Li Y, Brookes PC, Xu J. Bacterial community composition associated with pyrogenic organic matter (biochar) varies with pyrolysis temperature and colonization environment. mSphere. 2017;2: e00085-17.

68. Cheng C-H, Lehmann J, Engelhard MH. Natural oxidation of black carbon in soils: Changes in molecular form and surface charge along a climosequence. Geochim Cosmochim Acta. 2008;72: 1598–1610.

69. Singh BP, Cowie AL, Smernik RJ. Biochar carbon stability in a clayey soil as a function of feedstock and pyrolysis temperature. Environ Sci Technol. 2012;46: 11770–11778.

70. Wang J, Xiong Z, Kuzyakov Y. Biochar stability in soil: meta-analysis of decomposition and priming effects. GCB Bioenergy. 2016;8: 512–523.

Supporting Information

Table S2.1. FT-IR functional group peak assignment for biochar

Functional group	Wavenumber (cm^{-1})
O–H stretching of carboxylic acids, phenols, alcohols	3370 [1,2]
Aliphatic C-H stretching	2932 [1–3]
CO_2 asymmetrical stretching	2350 [4]
Carboxyl and carbonyl C=O stretching	1701 [1–3]
Aromatic C=C vibrations	1593 [1–3]
Aliphatic C-H deformation	1413 [5,6]
*C–O stretching and O–H deformation of carboxylic groups and/or C–OH stretching of polysaccharides	1200 [3,5]
Aromatic C-H out of plane deformation	810 [7,8]

*The peak at wavenumber 1200 cm^{-1} detected could be a combination of peaks observed in the region 1260-1200 cm^{-1}: C–O stretching and O–H bending of COOH and 1170-950 cm^{-1}: C–OH stretching of polysaccharides.

Table S2.2. FTIR spectra relative peak heights of the unaged and physically, chemically and biologically aged biochar samples

HTT (°C)	Ageing treatment	aromatic out of plane C-H stretch	C-O stretch and O-H bend in carboxylic acids*	aliphatic C-H stretch in CH_3 and CH_2	aromatic C=C stretch in quinones	C=O stretch in carboxylic acids/ ketones	aliphatic C-H stretch in CH_3 and CH_2
		810 cm^{-1}	1200 cm^{-1}	1413 cm^{-1}	1593 cm^{-1}	1701 cm^{-1}	2932 cm^{-1}
350	Unaged	0.09	0.29	0.12	0.36	0.08	0.07
	Physical	0.05	0.32	0.00	0.28	0.35	0.00
	Chemical	0.06	0.28	0.10	0.30	0.18	0.08
	Biological	0.07	0.32	0.09	0.31	0.13	0.07
550	Unaged	0.28	0.19	0.02	0.41	0.09	0.01
	Physical	0.12	0.23	0.00	0.42	0.17	0.05
	Chemical	0.25	0.18	0.00	0.43	0.12	0.01
	Biological	0.20	0.30	0.00	0.41	0.09	0.00

*The peak at wavenumber 1200 cm^{-1} detected could be a combination of peaks observed in the region 1260-1200 cm^{-1}: C–O stretching and O–H bending in carboxylic acids and 1170-950 cm^{-1}: C–OH stretching in polysaccharides.

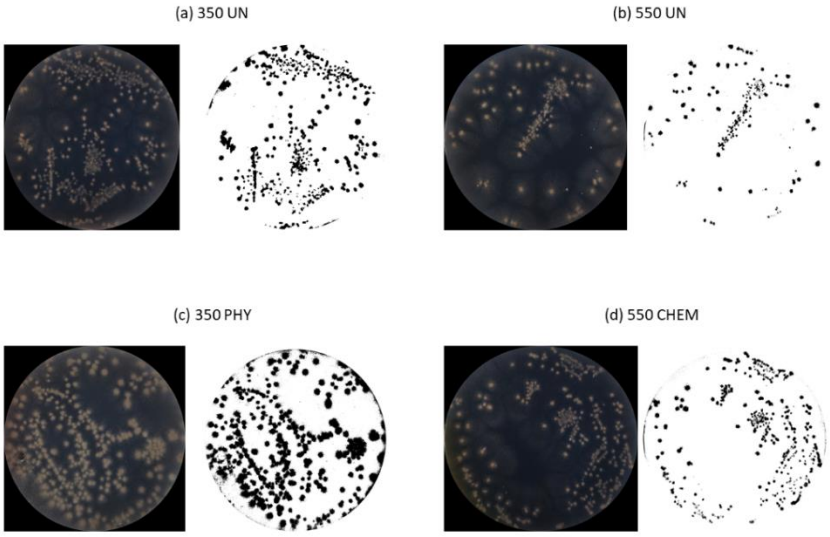

Picture S2.1. Images of Streptomyces isolate growth on biochar- raw and processed using ImageJ.

(Left) Images of Streptomyces isolate growth on the surface of biochar nutrient agar media at the end of the incubation period for a replicate of (a) 350 °C unaged biochar (b) 550 °C unaged biochar (c) 350 °C physically aged biochar (d) 550 °C chemically aged biochar. (Right) Processed images of Streptomyces isolate growth on the surface of the biochar sample shown on the left using the ImageJ software.

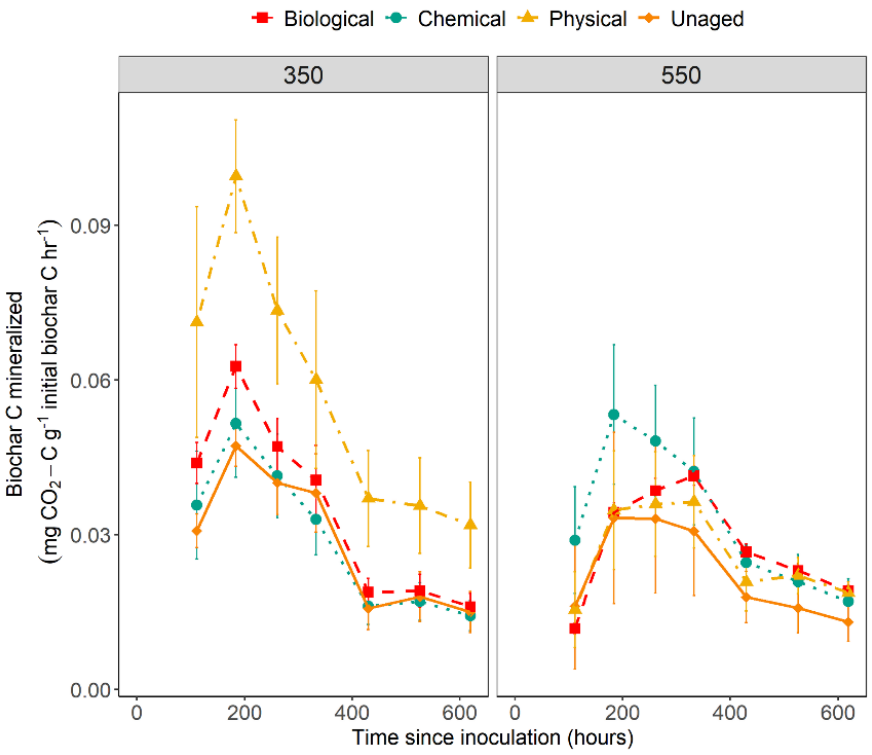

Figure S2.1. Rate of biochar C mineralization over time.
Data show mean C mineralization rate of unaged and physically, chemically and biologically aged biochar samples over time, with uninoculated blanks subtracted and normalized with mean biochar-C. n=3 for physical, chemical and unaged, n=5 for biological. Error bars represent 95% confidence intervals. The left panel shows biochar produced at 350 °C and the right panel shows biochar produced at 550 °C.

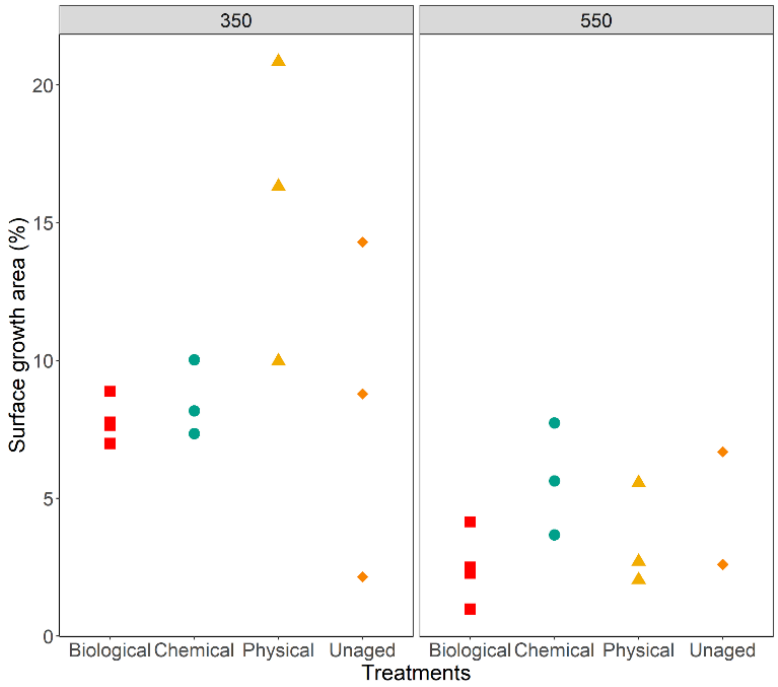

Figure S2.2. Comparison of Streptomyces isolate growth on aged and unaged biochar nutrient agar media.

Growth of Streptomyces isolate on biologically, chemically, and physically, aged biochar and unaged biochar agar media over the incubation period. n=3 for physical, chemical and unaged, n=5 for biological. The left panel shows biochars produced at 350 °C and the right panel shows biochars produced at 550 °C.

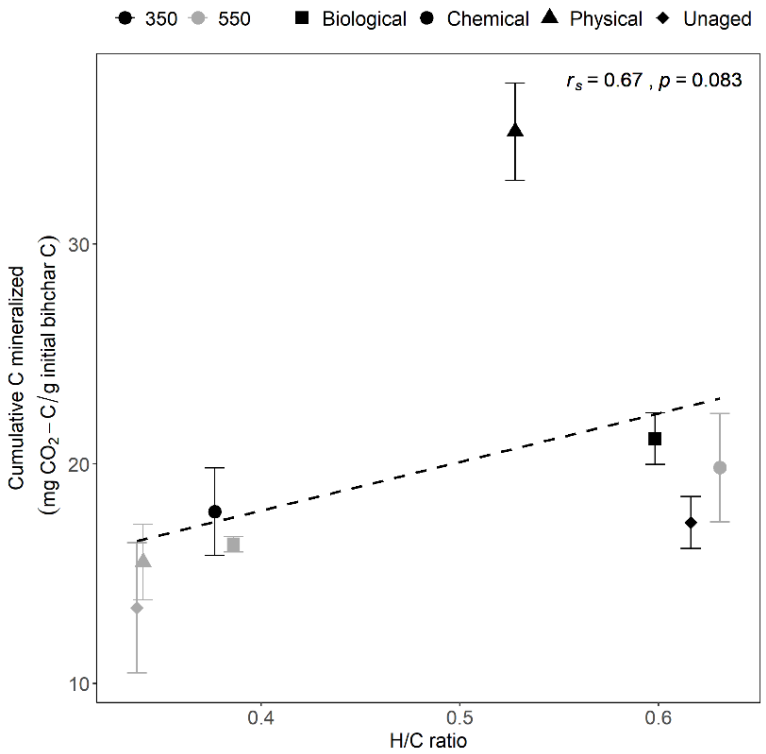

Figure S2.3. Relationship between mean cumulative biochar-C mineralized and molar H/C ratio.
n=3 for physical, chemical and unaged, n=5 for biological treatments. Error bars represent standard error of the mean. Shapes indicate unaged, physically, chemically and biologically aged biochar samples produced at 350 °C (black) and 550 °C (gray).

Appendix S2

Materials and Methods

Production of biochar

Biochar was produced from eastern white pine wood chips (*Pinus strobus* (L.)) at 350 and 550 °C in a modified Fischer Scientific Lindberg/Blue M Moldatherm box furnace (Thermo Fisher Scientific, Waltham, MA, USA) fitted with an Omega CN9600 SERIES Autotune Temperature Controller (Omega Engineering Inc., Norwalk, CT, USA) [9]. The feedstock was placed in a steel cylinder inside the furnace chamber and subjected to a continuous argon gas

supply at a rate of 1 L min^{-1} to maintain anaerobic conditions during pyrolysis. The heating rate for production of biochar was kept constant at 5 °C min^{-1} and mixing of the feedstock inside the steel cylinder via mechanical paddles started once temperatures hit 250 °C. We held the temperature constant for 30 minutes once the highest treatment temperature was reached (350 and 550 °C), after which the product was rapidly cooled by circulating cold water in stainless steel tubes wrapped around the steel cylinder. Pyrolyzed material was ground using a ball mill and sieved to collect biochar with particle size < 45 µm.

Chemical Analyses

Elemental analysis: Total C and N were determined for aged and unaged biochar samples using a Thermo Scientific Flash EA 1112 Flash Combustion Analyzer (Thermo Fisher Scientific, Waltham, MA, USA) at the Department of Agronomy, UW- Madison, WI, USA. Total H was determined using a Thermo Delta V isotope ratio mass spectrometer interfaced to a Temperature Conversion Elemental Analyzer (Thermo Fisher Scientific, Waltham, MA, USA) at the Cornell Isotope Laboratory, NY, USA. In order to estimate total O by subtraction, we determined ash content of aged and unaged biochar samples using the method prescribed by ASTM D1762-84.

Replicates were included for all samples for the CHN elemental analysis and ash measurements. Total O was calculated by subtraction as per Enders et al. [10] as follows:

O (%w/w) = 100 - C (%w/w) - N (%w/w) - H (%w/w) - ash (%w/w)

pH: The pH of aged and unaged biochar samples was measured in deionized water at a 1:20 solid:solution ratio using an Inlab Micro Combination pH electrode (Mettler Toledo, Columbus, OH, USA) connected to a Thermo Scientific Orion Star A111 benchtop pH meter (Thermo Fisher Scientific, Waltham, MA, USA). Briefly, we added 0.15 g of biochar to 3 mL of

deionized water in 5 mL centrifuge tubes and vortexed for 1 hour at low speed. After vortexing, the tubes were centrifuged at 15000 X g for 2 min to sediment the biochar particles. We aliquoted 200 μL of the clear suspension into microtubes and measured the pH. All pH measurements were performed in replicates except in the case of 350PHY and 550PHY where we had limited material.

Fourier-transform infrared (FT-IR) spectroscopy: We quantified the heights of selected functional groups using the Shimadzu IR Solution FT-IR software. The spectra were attenuated total reflection (ATR) corrected to approximate a transmission spectrum and smoothed to reduce the background noise. Spectra baselines were drawn in the following regions using a quartic fitting function: 3800-2300 cm^{-1}, 2300-1820 cm^{-1}, 1820-1500 cm^{-1}, 1500-925 cm^{-1} and 925-700 cm^{-1}. Wavenumbers were assigned for selected functional groups based on studies as described in Table S1. Peaks were manually detected around specific wavenumbers by identifying peak maxima, upper and lower baselines for each of the functional groups. Baselines for selected peaks were drawn as follows: 3006-2783 cm^{-1} for aliphatic C-H stretch, 1808-1645 cm^{-1} for C=O stretch, 1670-1483 cm^{-1} for C=C vibrations and stretch, 1501-1307 cm^{-1} for C-H bending of CH_2 and CH_3, 1334-919 cm^{-1} for C–O stretching, O–H bending of COOH and/or C–OH stretching of polysaccharides and 934-713 cm^{-1} for aromatic C-H deformation.

Biochar nutrient media preparation

The final biochar nutrient media used for biochar incubations is a combination of the following components:

1. Nutrient solution which consists of

a. Basal salt solution (described in detail below)
b. Trace elements solution (described in detail below)
c. Vitamin mixture (described in detail below)
d. Vitamin B12

2. Agar and biochar suspension

The same media recipe was used throughout the study to (i) isolate and recover the *Streptomyces* sp. on biochar (ii) perform the biological ageing treatment of biochar with a microbial community and (iii) perform the incubation study of the *Streptomyces* isolate with aged and unaged biochar. For the biological ageing treatment, we used the biochar suspension without addition of agar.

<u>To prepare the final biochar nutrient media agar plates (per 1 L):</u>

Agar and biochar suspension = 500 mL

Basal salt solution = 500 mL

Vitamin B12 = 200 uL of 250 mg L-1 solution* , **

Vitamin mix = 200 uL* , **

Trace elements solution = 1 mL* , **

*To be added after autoclaving

**Filter sterilize with 0.2 micron filter

<u>To prepare the biochar agar suspension (per 1 L):</u>

Nobel agar = 60 g

Ground biochar = 2 g

<u>To prepare the basal salt solution (per 1 L):</u>

KH_2PO_4 = 0.4 g

NH_4Cl = 0.5 g

KCl = 1.0 g

$CaCl_2$. $2H_2O$ = 0.3 g

NaCl = 2 g

$MgCl_2$. $6H_2O$ = 1.24 g

$NaSO_4$ = 5.86 g

Note: This solution will end up being acidic with a pH of ~6, The pH was adjusted to 7 by addition of NaoH and buffered by adding 1 g of MES (2-(N-Morpholino) ethane sulfonic acid) (VWR International, Radnor, PA, USA) before autoclaving.

To prepare the trace elements solution (aka SL-10, per 1 L):

HCl 25% (v/v) = 10 mL

$FeCl_2$. $4H_20$ = 1.5 g

$CoCl_2$. $6H_20$ = 190 mg

$MnCl_2$. $4H_20$ = 100 mg

$ZnCl_2$ = 70 mg

H_3BO_3 = 6 mg

Na_2MoO_4. $2H_2O$ = 36 mg

$NiCl_2$. $6H_2O$ = 24 mg

$CuCl_2$. $2H_2O$ = 2 mg

To prepare the vitamin mixture (per 1L):

4-aminobenzoic acid (Vitamin B9 precursor) = 40 mg

D(+)-biotin (Vitamin B7) = 10 mg

Nicotinamide (Vitaman B3) = 100 mg

D(+)-pantothetic acid hemicalcium (Vitamin B5) = 50 mg

Pyridoxamine dihydrocloride (Vitamin B6) = 100 mg

Thiamine dihydrochloride (Vitamin B1) = 100 mg

Effect of pyrolysis temperature on biochar C mineralization of unaged biochar

Mean cumulative biochar C mineralized at the end of the incubation was significantly higher by 39% for 350 °C biochars compared to 550 °C biochars (Kruskal-Wallis$_{ANOVA}$, p value = 0.01). This is consistent with previous studies that have noted higher microbial activity and respiration in incubations with low temperature chars [15–18], since biochar produced at high pyrolysis temperature contains a larger fraction of condensed aromatic C, which is more difficult for microorganisms to oxidize [19–23]. Mean colony growth on agar surfaces over the month-long incubation, as measured by percentage of total surface area, was 166% higher for 350 °C biochar treatments as compared to their 550 °C counterparts (Fig.S2.3). This corresponds to trends observed in the cumulative biochar C mineralized over the incubation period, indicating that the *Streptomyces* strain more effectively colonizes and grows on agar surfaces containing biochar particles produced at 350 °C.

Effect of pyrolysis temperature on the elemental composition and surface chemistry of unaged biochar

Elemental analysis

For unaged biochar, the total C in 550UN was higher (mean = 84.7%) than that in 350UN (mean = 74.8%), while the total O and H contents were lower in 550UN (mean O = 11.9%; mean H = 2.4%) compared to 350UN (mean O = 20.4%; mean H = 3.9%; Table 2.1). This is consistent with previous studies that have reported an increase in the total carbon content of biochars with

increasing pyrolysis temperature, due to increased carbonization and greater relative loss of H and O [10,12].

FTIR

While comparing the individual FTIR peaks between 350UN and 550UN, we observed changes in regions associated with aliphatic and aromatic C groups (Fig. 2.2a). There was, however, no notable change in relative height for the C=O stretch peak in carboxylic acids from 350UN (0.08) to 550UN (0.09). For the aromatic C functional groups, we observed an increase in the relative peak height with increasing pyrolysis temperatures (Fig. 2.2a and Table S2.2). The greatest increase appeared in the 810 cm^{-1} aromatic C-H out of plane deformation (0.09 to 0.28) and a slight increase was seen in the 1593 cm^{-1} C=C aromatic stretch (0.36 to 0.41). In contrast, the relative peak heights of groups indicative of aliphatic and lignin/cellulose-derived transformation products that are present in low temperature biochar decreased with increasing pyrolysis temperature. We observed a slight decrease in the relative peak height from 350UN to 550UN for 2932 cm^{-1} aliphatic C-H stretch of CH_3 and CH_2 (0.07 to 0.01), 1413 cm^{-1} C-H bending of CH_3 and CH_2 (0.12 to 0.02) and 1200 cm^{-1} C–O stretching of phenols/ COOH/ polysaccharides (0.29 to 0.19). With the exception of the C=O carboxyl stretch, these broad trends in surface chemistry with increasing pyrolysis temperature are consistent with previous studies that investigated the effect of pyrolysis temperature on the chemical properties of biochar [19,24,25].

Supplementary References

1. Guo Y, Bustin RM. FTIR spectroscopy and reflectance of modern charcoals and fungal decayed woods: implications for studies of inertinite in coals. Int J Coal Geol. 1998;37: 29–53.

2. Cheng C-H, Lehmann J, Thies JE, Burton SD, Engelhard MH. Oxidation of black carbon by biotic and abiotic processes. Org Geochem. 2006;37: 1477–1488.

3. Chen J, Gu B, Leboeuf EJ, Pan H, Dai S. Spectroscopic characterization of the structural and functional properties of natural organic matter fractions. Chemosphere. 2002;48: 59–68.

4. Chatterjee R, Sajjadi B, Chen W-Y, Mattern DL, Hammer N, Raman V, et al. Effect of Pyrolysis Temperature on PhysicoChemical Properties and Acoustic-Based Amination of Biochar for Efficient CO2 Adsorption. Front Energy Res. 2020;8: 85.

5. Solomon D, Lehmann J, Kinyangi J, Liang B, Schäfer T. Carbon K-Edge NEXAFS and FTIR-ATR spectroscopic investigation of organic carbon speciation in soils. Soil Sci Soc Am J. 2005;69: 107–119.

6. Stevenson FJ. Humus Chemistry: Genesis, Composition, Reactions. 2nd ed. New York: John Wiley & Sons Inc.; 1994.

7. Politou AS, Morterra C, Low MJD. Infrared studies of carbons. XII The formation of chars from a polycarbonate. Carbon N Y. 1990;28: 529–538.

8. Dutta S, Brocke R, Hartkopf-Fröder C, Littke R, Wilkes H, Mann U. Highly aromatic character of biogeomacromolecules in Chitinozoa: A spectroscopic and pyrolytic study. Org Geochem. 2007;38: 1625–1642.

9. Güereña DT, Lehmann J, Thies JE, Enders A, Karanja N, Neufeldt H. Partitioning the contributions of biochar properties to enhanced biological nitrogen fixation in common bean (Phaseolus vulgaris). Biol Fertil soils. 2015;51: 479–491.

10. Enders A, Hanley K, Whitman T, Joseph S, Lehmann J. Characterization of biochars to evaluate recalcitrance and agronomic performance. Bioresour Technol. 2012;114: 644–653.

11. Mukherjee A, Zimmerman AR, Harris W. Surface chemistry variations among a series of laboratory-produced biochars. Geoderma. 2011;163: 247–255.

12. Ronsse F, van Hecke S, Dickinson D, Prins W. Production and characterization of slow pyrolysis biochar: influence of feedstock type and pyrolysis conditions. GCB Bioenergy. 2013;5: 104–115.

13. Huff MD, Lee JW. Biochar-surface oxygenation with hydrogen peroxide. J Environ Manage. 2016;165: 17–21.

14. Mukherjee A, Zimmerman AR, Hamdan R, Cooper WT. Physicochemical changes in pyrogenic organic matter (biochar) after 15 months of field aging. Solid Earth. 2014;5: 693–704.

15. Dai Z, Barberán A, Li Y, Brookes PC, Xu J. Bacterial community composition associated with pyrogenic organic matter (biochar) varies with pyrolysis temperature and colonization environment. mSphere. 2017;2: e00085-17.

16. Zimmerman AR, Gao B, Ahn M-Y. Positive and negative carbon mineralization priming effects among a variety of biochar-amended soils. Soil Biol Biochem. 2011;43: 1169–1179.

17. Luo Y, Durenkamp M, De Nobili M, Lin Q, Brookes PC. Short term soil priming effects and the mineralisation of biochar following its incorporation to soils of different pH. Soil Biol Biochem. 2011;43: 2304–2314.

18. Bruun E, Hauggaard-Nielsen H, Ibrahim N, Egsgaard H, Ambus P, Jensen P, et al. Influence of fast pyrolysis temperature on biochar labile fraction and short-term carbon loss in a loamy soil. Biomass Bioenergy. 2011;35: 1182–1189.

19. Keiluweit M, Nico PS, Johnson MG, Kleber M. Dynamic molecular structure of plant biomass-derived black carbon (biochar). Environ Sci Technol. 2010;44: 1247–1253.

20. Wiedemeier DB, Abiven S, Hockaday WC, Keiluweit M, Kleber M, Masiello CA, et al. Aromaticity and degree of aromatic condensation of char. Org Geochem. 2015;78: 135–143.

21. Singh BP, Cowie AL, Smernik RJ. Biochar carbon stability in a clayey soil as a function of feedstock and pyrolysis temperature. Environ Sci Technol. 2012;46: 11770–11778.

22. Wang T, Camps Arbestain M, Hedley M. Predicting C aromaticity of biochars based on their elemental composition. Org Geochem. 2013;62: 1–6.

23. Harvey OR, Kuo L-J, Zimmerman AR, Louchouarn P, Amonette JE, Herbert BE. An nndex-based approach to assessing recalcitrance and soil carbon sequestration potential of engineered black carbons (biochars). Environ Sci Technol. 2012;46: 1415–1421.

24. Nguyen BT, Lehmann J, Hockaday WC, Joseph S, Masiello CA. Temperature sensitivity of black carbon decomposition and oxidation. Environ Sci Technol. 2010;44: 3324–3331.

25. Singh B, Fang Y, Johnston CT. A Fourier-Transform Infrared study of biochar aging in soils. Soil Sci Soc Am J. 2016;80: 613–622.

CHAPTER THREE: SOIL CARBON MINERALIZATION AND MICROBIAL COMMUNITY DYNAMICS IN RESPONSE TO PYOM ADDITION

Nayela Zeba[1], Timothy D. Berry[1], Monika S. Fischer[2], Matthew F. Traxler[2], and Thea Whitman[1]

[1] Department of Soil Science, University of Wisconsin-Madison

[2] Department of Plant and Microbial Biology, The University of California, Berkeley

This chapter is prepared for submission to The ISME Journal.

Abstract

Wildfires can either negatively impact soil carbon (C) stocks through combustion or increase soil carbon stocks through the production of pyrogenic organic matter (PyOM), which is highly persistent and can affect non-pyrogenic soil organic carbon (SOC) mineralization rates. In this study, we used fine-resolution $^{13}CO_2$ flux tracing to investigate PyOM-C mineralization, soil priming effects, and their impacts on soil microbial communities in a Californian mixed conifer forest Xerumbrept soil burned in the 2014 King Fire. We added PyOM produced from pine biomass at 350 ℃ and 550 ℃ to the soil and separately traced the mineralization of ^{13}C-labeled water-extractable and non-water-extractable PyOM-C fractions in a short-term incubation.

Our results indicate that the water-extractable fraction is 10-50x more mineralizable in both 350°C and 550 °C PyOM treatments than the SOC or non-water-extractable PyOM fraction. 350 °C PyOM addition led to a short-term positive priming effect, likely due to co-metabolism of easily mineralizable PyOM-C and the SOC, whereas 550 °C PyOM addition induced negative priming, potentially due to physical protection of SOC through sorption to the PyOM surface. We observed significant shifts in bacterial community composition in response to both 350 ℃ and 550 °C PyOM, with positive PyOM responders belonging to the genera *Noviherbaspirillum*, *Pseudonocardia*, and *Gemmatimonas*. In contrast, fungal communities were less responsive to PyOM additions. Our findings expand our understanding of the post-fire cycling of PyOM and SOC, providing insights into the microbial mineralization of different PyOM-C fractions and their influence on soil C dynamics in fire-affected ecosystems.

Introduction

Since the mid-1970s, the number of forest wildfires in the western US and the percentage of area burned within them have increased due to a warming climate (Westerling, 2016). These fires can impact the biogeochemical cycling of nutrients like carbon (C) within an ecosystem. Increasing fire frequencies can have a negative impact on C storage in forest soils, predominantly due to combustion of wood and litter as well as organic matter in the upper soil layers, leading to direct C losses from the system. Furthermore, the combustion of biomass can also reduce C inputs to soil, which can contribute to the loss of C (Pellegrini et al., 2018). Simultaneously, fires can have an indirect positive effect on C storage via the production of pyrogenic organic matter (PyOM) (Santín et al., 2015). For example, during fires in pine-dominated forest systems, between 5-27% of the biomass C can be converted to PyOM, which is likely to persist in soils due to a high proportion of C that is resistant to degradation (DeLuca et al., 2020; Santín et al., 2015). PyOM is also produced intentionally as a soil amendment and as part of a C management strategy, in which case it is referred to as "biochar" (Lehmann & Joseph, 2012). The conditions under which the addition of PyOM/biochar to soils will have a net positive C impact is still not clearly understood and depends on many factors, including the chemical composition and mineralizability of PyOM itself and whether its presence in the soil affects the mineralizability of soil organic carbon (SOC) (Maestrini et al., 2015; Wang et al., 2016; Whitman et al., 2015). *A key step to addressing this problem is taking a mechanistic approach to understanding how soil microbes decompose different carbon fractions of PyOM in fire-affected soils and if PyOM addition increases the abundance of microbes with the capacity to degrade the different C fractions in PyOM.* This is the overarching goal of this study.

In recent years, through a combination of field studies and lab incubations, we have gained a better understanding of the factors that can affect the mineralization of PyOM by soil microbes. These factors primarily include PyOM properties like feedstock and pyrolysis temperature, PyOM chemical and physical properties, soil characteristics, and the duration of measurement (Wang et al., 2016; Zeba et al., 2022). These same factors also determine whether PyOM addition will affect the mineralization of the native SOM – *i.e.*, whether PyOM addition will induce a "priming" effect (DeCiucies et al., 2018; Maestrini et al., 2015; Wang et al., 2016; Whitman et al., 2015). However, a key challenge to making these predictions is that PyOM is not homogeneous, even within a given sample, and different PyOM fractions may play fundamentally different roles in determining its net effect on soil C stocks. For example, a relatively small fraction of PyOM-C, included in the water-extractable fraction, is more easily mineralizable by microbes and may drive the observed increases in SOC mineralization (Hamer et al., 2004; Keith et al., 2011; Santos et al., 2012; Whitman, Enders, et al., 2014). Differences in the relative abundance of this easily mineralizable fraction would be reflected in the degree to which PyOM stimulates microbial activity, thereby increasing the rate of SOC mineralization (*i.e.*, inducing a "positive priming effect") in the short term (Maestrini et al., 2015; Whitman, Zhu, et al., 2014). Simultaneously, sorption is often invoked as an explanation for decreased SOC mineralization with PyOM additions ("negative priming") (Maestrini et al., 2015; Whitman et al., 2015), and would be expected to be associated with the more persistent and water-insoluble (*i.e.*, non-water-extractable) PyOM fraction. However, it can be challenging to independently trace the cycling of these different PyOM fractions, as adding them to soil separately would undermine the objective of understanding how these fractions cycle upon bulk PyOM addition.

In this study, we aimed to determine if C fractions within PyOM are differentially mineralized by microbes and how this affects the mineralization of SOC. We addressed this question by tracking the mineralization of two ^{13}C labeled PyOM-C fractions – ^{13}C labeled water-extractable and non-water-extractable PyOM-C in our soil-^{13}C PyOM incubations and used this information to decipher the dominant priming mechanisms. We sought to isolate the short-term dynamics of the water-extractable vs. non-water-extractable PyOM fraction, given that positive priming effects usually occur over relatively short timescales. We produced PyOM at two different pyrolysis temperatures (350 and 550 °C) to capture the differences in both PyOM-C content and chemistry with increasing temperature, particularly the fraction of water-extractable PyOM-C. PyOM-C concentration increases with higher pyrolysis temperatures, retaining a relatively lower proportion of easily mineralizable PyOM-C structures (Bruun et al., 2011; Keiluweit, Nico, & Johnson, 2010; Zimmerman et al., 2011). We hypothesized that the water-extractable PyOM-C fraction would be more rapidly mineralized, since it primarily consists of aliphatic C compounds that are readily consumed by microbes, and that the mineralizability of this fraction would be a strong predictor of SOC priming.

While it is important to understand how PyOM chemistry affects its cycling by microbes, it is also critical to understand how PyOM affects the soil microbial communities. There are numerous ways in which PyOM addition can affect soil microbes in the short term, such as the availability of easily mineralizable C as a nutrient source (Whitman, Enders, et al., 2014), changes in soil properties such as water holding capacity and pH (Chen et al., 2017; Luo et al., 2011), and interactions with signaling molecules (Masiello et al., 2013). To date, a relatively small number of lab and field studies have looked at the effects of PyOM on soil bacterial communities (summarized in Woolet and Whitman, 2020). While individual studies often found

significant effects of PyOM on soil bacterial community composition, soil characteristics played a more important role than PyOM in predicting community composition across soil types (Woolet & Whitman, 2020). In addition to community-wide effects, numerous PyOM-responsive bacterial taxa, across phylogenetic levels have been identified in recent studies. However, only a few genera have been found to have a consistently positive response to PyOM across soil types – these genera include known fire responders, and many have members that are known PAH degraders, indicating a capacity to break down complex aromatic C fractions in PyOM (Woolet & Whitman, 2020). In addition to PyOM-responsive taxa identified via high throughput sequencing, specific bacteria (*e.g.*, *Streptomyces* sp.) readily grow on agar media containing PyOM-C as the sole carbon source (Zeba et al., 2022), while others (*e.g.*, *Pseudomonas* and *Pseudonocardiaceae* sp.) can colonize the PyOM surface (Dai et al., 2017; Tu et al., 2020).

Much of our understanding of the effects of PyOM on soil fungi comes from studying fungal responses to fire. Certain fungi, such as *Pholiota*, *Pyronema* and *Penicillium* sp. are known to thrive in post-fire environments (Fox et al., 2022). Their potential to exploit post-fire resources, such as PyOM, could contribute to their relative increase (Enright et al., 2022; Fischer et al., 2021; Whitman et al., 2019), along with other factors like heat tolerance (Bruns et al., 2020; Fox et al., 2022). A few studies examining the effects of PyOM application on fungi have observed changes in the fungal community structure, primarily driven by alterations in soil properties (Gao et al., 2021; Q. Yao et al., 2017). The aromatic C fraction in PyOM may also play an important role in shaping the fungal community composition (Li et al., 2019). For instance, dominant post-fire fungus, *Pyronema domesticum* has the capacity to break down complex aromatic C when grown on agar media containing PyOM-C (Fischer et al., 2021).

Despite these insights, the effect of PyOM addition on soil fungi, both in terms of whole communities and individual taxa remains relatively unexplored.

While the list of PyOM-responsive fungal and bacterial taxa is growing, the mechanisms by which both the community and individual taxa respond to PyOM are poorly understood. Specifically, with regard to the C heterogeneity of PyOM, it is possible that the relative abundance of some species increases in response to the easily mineralizable PyOM-C fractions, while others increase in response to the more aromatic PyOM-C fractions. Although methods like stable isotope probing would be required to conclusively demonstrate these different responses, this should result in a time-dependent response, with responders to the easily mineralizable PyOM-C fraction increasing early in the incubation period as this fraction is consumed early on, while responders to the aromatic C fractions emerge later. To investigate these dynamics, we performed parallel soil-PyOM incubations and destructively sampled the soils for microbial community profiling at key time points, informed by real-time isotopically partitioned PyOM-C mineralization data. This allowed us to track shifts in microbial community composition and identify PyOM-responsive taxa that increase in relative abundance at key time points during the incubation period. We also used LC-MS analysis to track changes in the soil C chemical profile during these select time points to characterize the nature of carbon compounds available to soil microbes during the incubation. We hypothesized that PyOM addition would result in shifts in both the bacterial and fungal communities within the first few days, tracking the consumption of the easily mineralizable water-extractable fraction. We expected PyOM responders to belong to known fire-responsive and PyOM-responsive genera. We predicted that early responders would mostly be bacteria, while late responders could include both bacteria and

fungi that have the ability to degrade complex aromatic C structures, such as *Sphingomonas*, *Gemmatimonadetes* and *Pyronema* sp.

Materials and Methods

Soil description

To increase the likelihood of finding PyOM-adapted taxa, we targeted a soil with known burn history. Soil was collected in the winter of 2020 from the El Dorado National Forest in California from a region that burned during the 2014 King Fire (38.86953, -120.61322). The soil belongs to the Pilliken series and is a coarse-loamy, mixed, mesic entic Xerumbrept. Topsoil (0-0.1 m) was collected after removing the O-horizon litter layer and stored at -20 °C until it was shipped to Madison, WI on dry ice, after which it was stored at -20 °C until the start of the incubation. We chose to focus on the top 10 cm of mineral soil as this horizon would be expected to have meaningful contact with surface-produced PyOM after a wildfire. Standard soil properties (Table 3.1) were analyzed at the UW Soil and Forage Lab with a sample that was thawed and sieved to < 2 mm.

Table 3.1. Properties of soil collected from the 2014 King fire affected region

Property (units)	
Sand (%)	55
Silt (%)	24
Clay (%)	20
Texture (USDA classification)	Sandy clay loam
Total C (%)	7.79
Total N (%)	0.46
Bulk $\delta^{13}C$ vs. VPDB (‰)	-27.07
NO_3-N (ppm)	28.8
NH_4-N (ppm)	4.9
P (ppm)	9
K (ppm)	84
pH (H_2O)	6.1

Biomass production

Two-year-old eastern white pine tree seedlings (*Pinus strobus* (L.)) from the Wisconsin Department of Natural Resources (DNR) were grown in an enriched $^{13}CO_2$ atmosphere custom growth chamber for one growing season. The trees were pulse labeled with 99% $^{13}CO_2$ at regular intervals over the course of their growth with the goal of producing evenly labeled trees. The labeled trees were watered with deionized water and Hoagland's solution.

A paired same-aged set of eastern white pine trees from the Wisconsin DNR, grown under ambient, non-enriched CO_2, was used as an unlabeled control for this study, keeping moisture, humidity, and light conditions equivalent (Labeled and unlabeled biomass properties are provided in Table S3.1).

PyOM production and analyses

We used the aboveground biomass of the eastern white pine trees to produce PyOM. For each set of labeled and unlabeled trees, we ground tree stems and needles and mixed them in 1:4 ratio to account for small differences in the labeled and unlabeled trees. We pyrolyzed both sets of trees at 350 °C (referred to as "350 PyOM") and 550 °C (referred to as "550 PyOM") in a modified Fischer Scientific Lindberg/Blue M Moldatherm box furnace (Thermo Fisher Scientific, Waltham, MA, United States) fitted with an Omega CN9600 SERIES Autotune Temperature Controller (Omega Engineering Inc., Norwalk, CT, United States). We modified the furnace and adapted the PyOM production design developed by Güereña et al. (2015). Briefly, the feedstock was placed in a steel cylinder inside the furnace chamber and subjected to a continuous argon gas supply at a rate of 1 L min^{-1} to maintain anaerobic conditions during pyrolysis. The heating rate for production of PyOM was kept constant at 5 °C min^{-1} and mixing of the feedstock inside the steel cylinder via mechanical paddles started once temperatures hit 250 °C. We held the temperature constant for 30 min once the target temperature was reached, after which the PyOM was rapidly cooled by circulating cold water in stainless steel tubes wrapped around the steel cylinder. The PyOM was ground using a mortar and pestle and sieved to collect PyOM with particle size < 45 µm.

Total C, nitrogen (N), bulk $\delta^{13}C$ and $\delta^{15}N$ were measured at the Cornell Stable Isotope Laboratory (COIL) using a Delta V Isotope Ratio Mass Spectrometer (Thermo Scientific, Germany) interfaced to a dry combustion analyzer (Carlo Erba NC2500 Elemental Analyzer, Italy). Total hydrogen (H), and oxygen (O) were also measured at COIL on a Delta V Isotope Ratio Mass Spectrometer interfaced to a Temperature Conversion Elemental Analyzer (Thermo Scientific, Germany). The pH was measured in deionized water at a 1:20 solid: solution ratio

using an Inlab Micro Combination pH electrode (Mettler Toledo, OH, USA) connected to a Thermo Scientific Orion Star A111 benchtop pH meter (Thermo Fisher Scientific, MA, USA). The properties of all PyOM materials are provided in Table 3.2.

Table 3.2. Properties of PyOM

Property (units)	^{13}C labeled		Unlabeled	
	350 °C	550 °C	350 °C	550 °C
pH (H_2O)	9.42	10.09	7.97	10.19
Total C (%)	64.75 ± 2.64	71.87 ± 1.35	72.87 ± 8.43	78.17 ± 1.81
Total N (%)	3.24 ± 0.15	2.91 ± 0.05	2.82 ± 0.31	2.47 ± 0.06
Total H (%)	3.52	1.75	3.78	1.93
Total O (%)	16.28	10.96	17.46	9.32
Bulk δ^{13}C vs. VPDB (‰)	1513.12 ± 9.47	1596.51 ± 8.32	-29.38 ± 0.05	-29.27 ± 0.08
Bulk δ^{15}N vs. atmospheric air (‰)	0.40 ± 0.21	0.46 ± 0.41	0.50 ± 0.05	0.74 ± 0.08
Total water extractable C (DOC) (mg g^{-1} PyOM)	2.11 ± 0.43	0.95 ± 0.65	1.24 ± 0.38	0.67 ± 0.47

The values presented for total C, total N, bulk δ^{13}C and bulk δ^{15}N are means of five replicates ± standard deviation. The values for total water-extractable C represent DOC in original PyOM before exchange. pH values of the original PyOM before adjustment are shown.

Water-extractable PyOM-C extraction and exchange

To isolate and compare the mineralization rates between water-extractable and non-water-extractable PyOM-C fractions, we removed and exchanged the water-extractable fraction from the ^{13}C labeled vs. unlabeled PyOM, at C-equivalent rates. This resulted in two PyOM treatments (Fig. 3.1): ^{13}C water-extractable PyOM (where the water-extractable fraction is ^{13}C-labeled) and ^{13}C non-water-extractable PyOM (where the non-water-extractable fraction is ^{13}C-labeled).

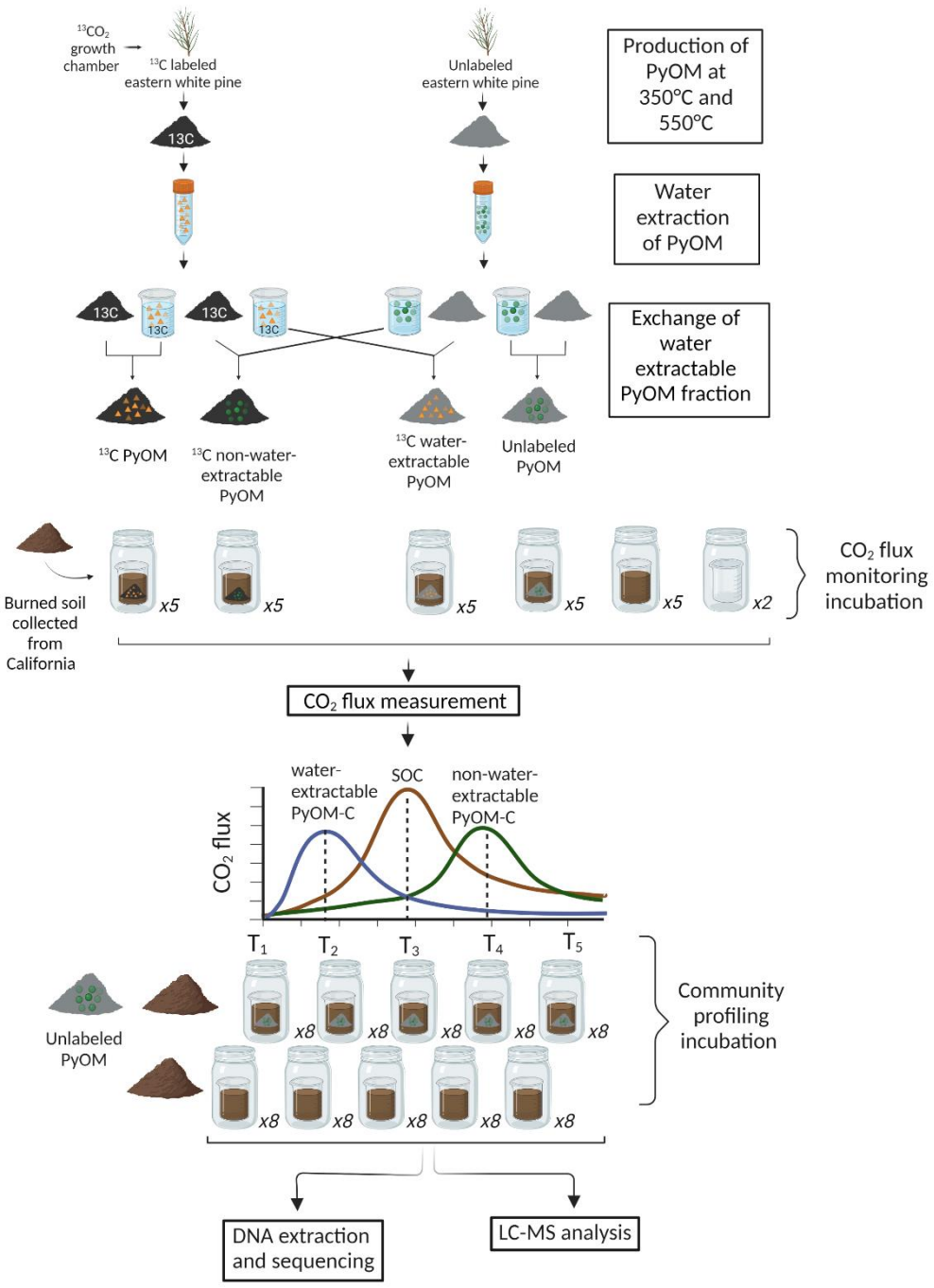

Figure 3.1. Experimental setup.

To separate the water-extractable PyOM-C, we used a series of five sequential extractions with ultrapure water, using the methods described in Smith et al. (2013) and Whitman, Zhu, et al.,

(2014). In each round of extraction, PyOM was shaken with ultrapure water (1:10 solid:water ratio) in a 15 mL Falcon conical centrifuge tube (Corning, NY, USA) for 15 min and then centrifuged at 2593 x g for 15 min at 4 °C. After centrifugation, the supernatant was syringe-filtered through a sterile 0.45 mm C-free glass microfiber filter (cat # 6902-2504, Cytiva, MA, USA). The resulting extracts were retained, with sequential extractions performed on the remaining PyOM and pooled in order to extract as much DOC as possible. The total dissolved organic carbon (DOC) content of the water-extractable PyOM-C fraction was measured at the Water Science and Engineering Laboratory, UW-Madison using a Sievers M5310C Total Organic Carbon Analyzer (GE Analytical Instruments Inc., CO, USA).

Before returning the water-extractable fraction (DOC) to the non-water-extractable PyOM, we dried the non-water-extractable PyOM at 70 °C and measured total C, N, bulk $\delta^{13}C$, $\delta^{15}N$ and pH as described above. We also measured the total organic carbon (TOC) content of the non-water-extractable PyOM, at the UW Soil and Forage Lab using the dry combustion technique (Table S3.2). We then returned the water-extractable PyOM to the non-water-extractable PyOM fractions (Fig. 3.1), adjusted the pH of all treatments to match that of the soil using HCl additions, and then dried the final materials at 70 °C. We also extracted water-extractable fraction for the control ^{13}C PyOM and unlabeled PyOM samples and returned it at the same rates. The ratios of water-extractable to non-water-extractable PyOM-C were selected to match the DOC content of the water-extracted PyOM for the ^{13}C labeled 350 and 550 PyOM treatments (Table 3.2). Thus, all 350 PyOM treatments had 2.1 mg water-extractable PyOM-C g^{-1} non-water-extractable PyOM-C, while all 550 PyOM treatments had 1 mg water-extractable PyOM-C g^{-1} non-water-extractable PyOM-C.

Incubation setup and monitoring

Before the incubation, soil was thawed, sieved to < 2 mm and maintained at room temperature and open to the air for two weeks. We used a sub-sample of the soil to determine field capacity for unamended and PyOM amended soils (350 and 550 PyOM) separately to ensure equivalent moisture levels with and without PyOM additions. Water holding capacity was determined as in Whitman et al. (2021). The moisture content of the thawed soils was determined one day before the start of the incubation to calculate the water required to reach target moisture levels of 65% field capacity for each treatment.

We ran two sets of parallel incubations – (i) a CO_2 flux monitoring incubation to partition C mineralization between different PyOM fractions and (ii) a community profiling incubation to analyze the effects of PyOM on microbial community composition at critical time points during the incubation. We analyzed data from the CO_2 flux monitoring incubation in real time, so we could dynamically select 4-5 timepoints that reflect initial conditions, peak PyOM-C mineralization, peak SOC mineralization and final conditions. At each of these selected timepoints, sample jars from the community profiling incubation were frozen for DNA sequencing. For the flux monitoring jars, we had five replicates for each PyOM temperature and each treatment (Fig. 3.1): (i) Soil + unlabeled PyOM (ii) Soil + ^{13}C PyOM (iii) Soil + ^{13}C water-extractable PyOM (iv) Soil + ^{13}C non-water-extractable PyOM (v) Unamended soil control. For the community sequencing jars, we were not performing ^{13}C partitioning, so we only had two treatments for each temperature, with eight replicates destructively sampled at each timepoint (Fig. 3.1): (i) Soil + unlabeled PyOM (including both fractions) (ii) Unamended soil control.

Incubations were performed in 60 mL glass jars placed inside pint-sized Mason jars (473 mL). Each 60 mL glass jar received 3.5 g soil on a dry mass basis and the soil-PyOM amended

jars received PyOM at a consistent rate of 18 mg TOC PyOM g^{-1} dry soil (*i.e.*, 3.1% dry mass addition for 350 PyOM and 2.8% dry mass addition for 550 PyOM). These addition rates were designed to represent locally high inputs of PyOM after a wildfire. We added water drop-wise to gradually bring up the moisture of each jar to the target moisture level of 65% field capacity.

CO_2 flux monitoring incubation

After moisture adjustment, we placed the 60 mL glass jars inside Mason jars containing 20 mL acidified deionized water (pH ~4) at the bottom to maintain humidity and prevent water loss. We capped and sealed the jars with sterile, gas-tight lids with fittings for CO_2 gas measurements and connected them to randomly selected positions on the distribution manifolds (multiplexer) using polyurethane tubing (Berry et al., 2021). The connected jars were immediately flushed with a 400 ppm CO_2-air gas mixture to reset the headspace CO_2 concentration in all jars at the initial timepoint. We incubated the jars at room temperature in the dark and measured the concentration of CO_2 emitted in the headspace of each jar at frequent intervals using a Picarro G2131i cavity ringdown spectrometer attached to the multiplexer over a period of one month. For 350 PyOM, we measured headspace CO_2 concentration at intervals of 6 h during the first 2 days, and gradually increased the intervals to 12 h during the first and second weeks, 24 h during the third week and 48 h during the last week of incubation. Similarly, for 550 PyOM, we measured headspace CO_2 concentration every 6-12 h during the first 3 days, 24 h during the first and second weeks and 48-72 h till the end of the incubation. After each measurement, we flushed the jars with the 400 ppm CO_2-air gas mixture to prevent oxygen depletion and excessive CO_2 accumulation inside the jars. The precise concentration after flushing each jar was measured and subtracted from the next timepoint reading to calculate the emitted CO_2 in the jar during that interval.

Community profiling incubation

For community profiling, after moisture adjustment, we placed the glass jars inside Mason jars containing 20 mL deionized water at the bottom and capped them with sterile regular lids. The jars were then incubated in the dark at room temperature. During the incubation, the jars were opened for 1-2 min every 48 hours to prevent oxygen depletion inside the Mason jars and to mirror the CO_2 flux incubations. We checked the mass of the jars once a week to determine moisture loss and water was added to return jars to target moisture levels. At each sampling timepoint, eight jars were destructively sampled and placed in sterile Whirl-Pak bags and stored at -80 °C until DNA extraction was performed. During the setup, eight unamended and PyOM amended soil samples were randomly selected and frozen to represent community profile on Day 0.

$^{13}CO_2$ partitioning and statistical analyses

We used R Studio (v4.2.2; R Core Team, 2022) with the 'tidyverse' (Wickham et al., 2019), 'zoo' (Zeileis & Grothendieck, 2005) and 'broom' (Robinson et al., 2022) packages to process raw CO_2 readings from the multiplexer-Picarro system. Stable isotope partitioning, as represented by Equation 1, was used to partition the CO_2 emissions from the flux monitoring treatments to determine the fraction of CO_2 emitted from water-extractable PyOM, non-water-extractable PyOM, and soil in the soil-PyOM amended incubations.

(1) $$f_A = (\delta_{Total} - \delta_B)/ (\delta_A - \delta_B)$$

Equation 1 calculates the fraction of CO_2 emitted from source A (f_A) using the ^{13}C isotopic composition of the total respired CO_2 (δ_{Total}), CO_2 respired from source A (δ_A), and source B (δ_B).

For example, we partitioned the total CO_2 emissions from the "Soil + ^{13}C water-extractable PyOM" treatments into two sources: CO_2 emitted from the ^{13}C labeled water-extractable PyOM source and CO_2 emitted from the unlabeled soil and non-water-extractable PyOM source. We calculated the fraction of total CO_2 emitted from the water-extractable PyOM source ($f_{water\text{-}extractable\ PyOM}$) using Equation 2:

(2) $$f_{water\text{-}extractable\ PyOM} = (\delta_{Total\ CO2} - \delta_{CO2\ soil+non\text{-}water\text{-}extractable\ PyOM}) / (\delta_{CO2\ water\text{-}extractable\ PyOM} - \delta_{CO2\ soil+non\text{-}water\text{-}extractable\ PyOM})$$

In this equation,

$\delta_{Total\ CO2}$ represents the isotopic composition of the total CO_2 emitted from the "Soil + ^{13}C water-extractable PyOM" treatments, $\delta_{CO2\ soil+non\text{-}water\text{-}extractable\ PyOM}$ represents the average isotopic composition of the CO_2 emitted from soil and non-water-extractable PyOM (determined from the "Soil + unlabeled PyOM" treatments), and $\delta_{CO2\ water\text{-}extractable\ PyOM}$ represents the isotopic composition of the CO_2 emitted from water-extractable PyOM, assumed to be the isotopic composition of the ^{13}C labeled PyOM.

Similarly, we determined the fraction of CO_2 emitted from non-water-extractable PyOM ($f_{non\text{-}water\text{-}extractable\ PyOM}$) and the fraction of CO_2 emitted from SOC (f_{SOC}) by partitioning the flux from other treatments (Appendix S3). We note that the isotopic composition of the labeled water-extractable and non-water-extractable PyOM-C fractions may differ slightly; however, small differences in isotopic composition of the bulk ^{13}C-labeled PyOM for CO_2 emitted from both fractions would not meaningfully impact our overall partitioning results.

We determined the mineralizability of each PyOM-C fraction by normalizing the amount of C mineralized with the quantity of each carbon source added to the jars. We assessed

normality and homogeneity of variance across treatment groups using the Shapiro and Bartlett test functions in the R 'stats' package. Welch's ANOVA was employed to test significant differences in mineralizability between the PyOM-C fractions and SOC, due to unequal variances. The Games-Howell post-hoc test function in the 'rstatix' package (Kassambara, 2022) was used to compare mineralizability between different treatment pairs. All code used for flux partitioning, analyses and figures in this chapter is available at https://github.com/nayelazeba/Chapter3.

Microbial community analyses

DNA extraction, amplification, and sequencing

We extracted DNA from each soil sample using the DNEasy PowerLyzer PowerSoil DNA extraction kit (QIAGEN, Germantown, MD), following the manufacturer's instructions. One blank extraction without soil was included for every 24 samples. We performed PCR in triplicate to amplify the extracted DNA, targeting the 16S rRNA gene v4 region with 515f and 806r primers (Walters et al., 2015), and targeting the ITS2 gene region with 5.8S-Fun and ITS4-Fun primers (Taylor et al., 2016) with barcodes and Illumina sequencing adapters added as per Kozich et al. (2013). During PCR, we included one negative control (PCR-grade water) and one positive control (known microbial community mix) for every 30 samples. The PCR amplicon triplicates were pooled, purified and normalized using a SequalPrep Normalization Plate (96) Kit (ThermoFisher Scientific, Waltham, MA). Samples, including blanks, were pooled and library cleanup was performed using a Wizard SV Gel and PCR Clean-Up System A9282 (Promega, Madison, WI) according to manufacturer's instructions. A detailed procedure for the DNA extraction and PCR amplification and purification is described in Whitman et al. (2019). We

submitted the pooled library to the UW Madison Biotechnology Center (UW-Madison, WI) for 2x300 paired end Illumina MiSeq sequencing for both 16S and ITS2 amplicons.

Sequence data processing and taxonomic assignments

We used the QIIME2 pipeline (QIIME2, v2020.6; Bolyen et al., 2019) to process the sequences following the steps described in Woolet & Whitman, (2020). The sequence processing steps were performed on the UW-Madison Centre for High Throughput Computing cluster (Madison, WI). Raw sequence data were demultiplexed and quality filtered followed by denoising with DADA2 (Callahan et al., 2016). The dada2 denoise-paired command as implemented within QIIME2 was used to determine OTUs. This resulted in a retention of a mean of 45,246 16S sequences and a mean of 27,358 ITS2 sequences per sample. For ITS2 reads, we then ran the sequences through ITSx (Bengtsson-Palme et al., 2013) to identify fungi and to remove plant and other eukaryotic sequences. Taxonomy was assigned to the 16S sequences using the Silva 138 database (Quast et al., 2013) at 99% similarity using the QIIME2 feature-classifier classify-sklearn. Pre-trained taxonomy classifiers specific to the primers used for 16S sequencing were used (Bokulich et al., 2018). For the IT2 reads, we assigned taxonomy using the UNITE "developer" database (v8.3) at 99% similarity (Abarenkov et al., 2021). UNITE taxonomy classifiers were trained on the full reference sequences using the QIIME2 feature-classifier fit-classifier-naive-bayes (Pedregosa et al., 2011). The ITS2 sequences were then classified using the trained UNITE classifier.

Statistical analysis

We worked in R Studio, primarily with the 'phyloseq' (McMurdie & Holmes, 2013) and 'vegan' packages (Oksanen et al., 2022), to compare microbial community composition between soil and PyOM amended soil samples. We removed 381 OTUs that belonged to "Chloroplast"

and “Mitochondria” in the 16S OTU table and removed samples with less than 6650 16S reads and 1560 ITS2 reads. We then calculated Bray-Curtis dissimilarity between samples (Bray & Curtis, 1957), normalized by relative abundance and represented them as NMDS ordinations. We tested for significant effects of PyOM addition after controlling for time using permutational multivariate ANOVA (PERMANOVA) on Bray-Curtis dissimilarities, implemented in vegan as the ‘adonis2’ function.

To identify PyOM-responsive taxa, we calculated $\log_2$-fold changes in taxon abundances in control vs. PyOM-amended soils using the ‘DESeq2’ R package which is used to analyze differential abundance between treatments (Love et al., 2014). To test for specific effects of PyOM addition on taxon abundance, we used a design formula that models differences in taxon abundance across samples on Day 0, over time and due to PyOM addition over time (Love et al., 2016). We then performed a likelihood ratio test with a reduced model without the PyOM addition effects over time to identify significant responder OTUs (Benjamini and Hochberg correction, adjusted p value < 0.05). This approach allowed us to identify only those taxa that at one or more time points after Day 0 showed a significant $\log_2$-fold change with PyOM addition.

The t-test function from the ‘stats’ R package was used to test for significant differences in relative abundances between PyOM-amended and unamended soils for PyOM-responsive genera identified using DESeq2.

LC-MS analysis

To acquire chemical profiles, we first prepared chemical extracts by combining 0.4 g of soil with 4 mL of LC/MS-grade methanol, sonicated for five minutes, and then shaken overnight (~16 hours) at 25 °C and 200 rpm. Blank extraction controls were prepared in parallel, in which empty tubes lacking any soil sample were subjected to the same chemical extraction protocol.

Solids were allowed to settle to the bottom for 30 minutes and then 3.5 mL was carefully collected from the top and immediately dried via SpeedVac (Savant SPD1010). To analyze these dried extracts via LC/MS, we resuspended them in 1 mL of 100 nM nonactin LC/MS-grade methanol solution, to a final concentration of approximately 1 mg extract / 1 mL of solvent. These resuspended samples were sonicated for 5 min to ensure that the extract dissolved into the solvent, and then centrifuged at 15,000 rpm to pellet any particulate, after which, 900 μL of solution was transferred to an HPLC vial. To create a pooled quality control (QC) sample we combined 10 μL of each sample. Samples were analyzed in a randomized order with a methanol blank and pooled QC analyzed after every 12 samples. Samples were analyzed with an ultra-high-pressure liquid chromatography (UHPLC) system (Dionex Ultimate 3000; Thermo Fisher, USA) coupled to a high-resolution mass spectrometer (HRMS; Thermo Q-Exactive QuadrupoleOrbitrap; Thermo Fisher, USA) using a heated electrospray ionization (HESI) source and a C18 column (Thermo Scientific Acclaim rapid-separation liquid chromatography [RSLC] system, 50 mm by 2.1 mm, 2.2 μm pore size). We used the following 20 min UHPLC method; 1 min 40% acetonitrile (ACN) plus 0.1% formic acid (FA), 1 min gradient from 40% to 65% ACN plus 0.1% FA, 11 min gradient from 65% to 99% ACN plus 0.1% FA, 3.5 min 99% ACN plus 0.1% FA, 0.5 min gradient from 99% to 40% ACN plus 0.1% FA, and 3 min re-equilibration in 40% ACN plus 0.1% FA; injection volume of 5 μl, flow rate of 0.4 mL/min, and column oven temperature of 35 °C. The full MS1 scan was performed in positive mode at a resolution of 35,000 FWHM (full width at half-maximum) with an automatic gain control (AGC) target of 1e6 ions and a maximum ion injection time (IT) of 100 ms with a mass range from m/z 200 to m/z 2000. Data were processed using MS-DIAL v4.9 (Tsugawa et al., 2015). We used R v4.1.3 to omit features with a peak height value greater than 100,000 in any negative control samples (*i.e.*,

methanol blanks and blank extraction controls) prior to ordination and statistical analyses as described above.

Results

PyOM-C and SOC flux dynamics

Over the 30-day incubation, the mineralizability of PyOM-C from the water-extractable fraction was significantly higher than that of the non-water-extractable PyOM-C fraction and soil organic carbon for both the 350 and 550 PyOM treatments ($p < 0.05$, Games-Howell post-hoc test; Fig. 3.2.A). The amount of C mineralized per gram of initial C from the water-extractable fraction was 10 and 50 times higher than the non-water-extractable PyOM-C in the 350 and 550 PyOM treatments, respectively. The C mineralizability of the 350 non-water-extractable PyOM-C fraction was higher than that of soil organic carbon. However, this pattern was not observed in the 550 PyOM treatment, where the C mineralizability of soil organic carbon was higher. Our focus in this study was to compare the relative mineralizability of the different PyOM-C fractions with soil organic carbon (*i.e.*, on a per carbon gram basis). Considering the total C mineralized, the cumulative mineralization from the water-extractable PyOM-C fractions was lower compared to the non-water-extractable PyOM-C and SOC due to the small fraction of total PyOM represented by water-extractable PyOM-C in the jars (Fig. S3.1).

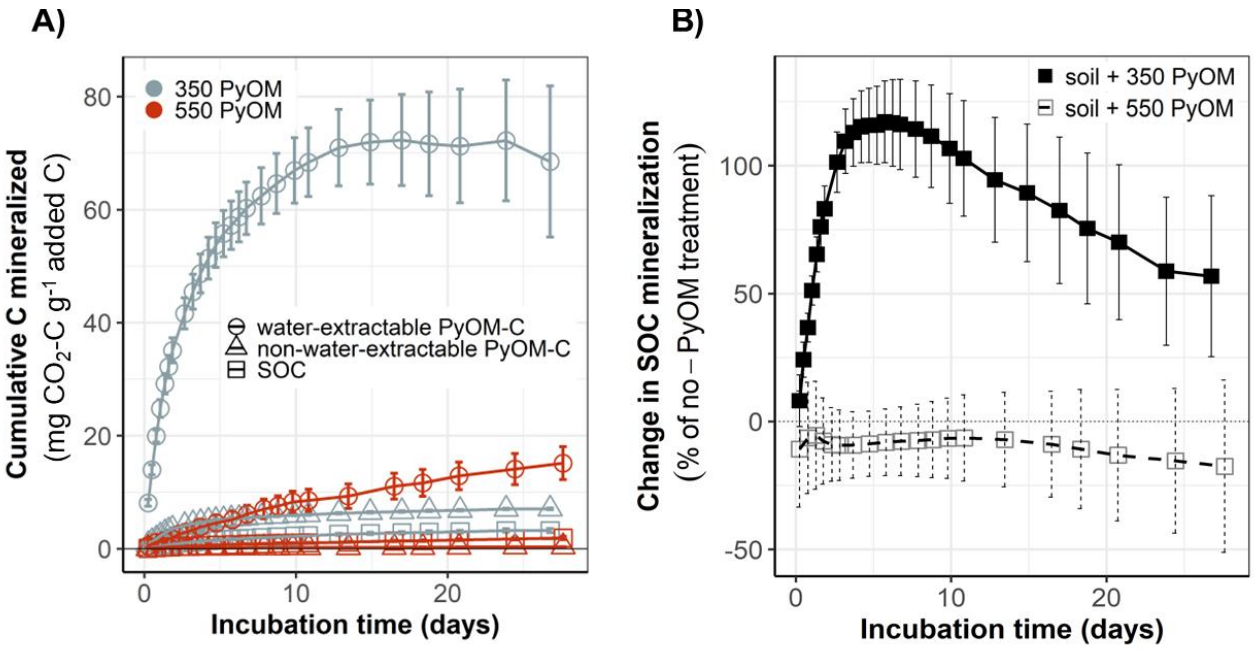

Figure 3.2. Mineralizability of PyOM fractions and effect of PyOM addition on SOC mineralizability

A) *Cumulative mean C mineralized per gram of added C for water-extractable PyOM-C, non-water-extractable PyOM-C and SOC. (n=4-5, error bars=SE).* ***B)*** *Cumulative mean SOC priming over time represented as % of mineralization in no-PyOM treatment. Priming calculated as: [[$SOC_{(PyOM)}$-$SOC_{(no-PyOM)}$] / $SOC_{(no-PyOM)}$] (n=4-5, error bars=SE).*

The addition of 350 PyOM resulted in a net 57% increase in cumulative SOC mineralization after 30 days of incubation, indicating a strong positive priming effect (Fig. 3.2.B). This effect was immediately apparent, with cumulative SOC mineralization in the 350 PyOM amended soils being over 100% higher than in the unamended soils after just 5 days of incubation. However, this strong positive priming effect diminished after 5 days, although the net effect remained positive for the duration of the study. In contrast, the addition of 550 PyOM resulted in a net 17% decrease in cumulative SOC mineralization, indicating a negative priming effect. This negative priming was also observed immediately upon the start of the incubation, with the cumulative amount of SOC mineralized in the 550 PyOM amended soils being on

average 8% lower than in the unamended control soil treatments during the first 10 days of incubation.

Microbial community composition

We observed significant shifts in the bacterial community composition over time (PERMANOVA, $p_{time} < 0.01$) and in response to the addition of 350 PyOM (PERMANOVA, $p_{350PyOM} = 0.01$, $R^2_{350PyOM} = 0.03$, Fig. 3.3.A) and 550 PyOM (PERMANOVA, $p_{550PyOM} < 0.01$, $R^2_{550PyOM} = 0.04$, Fig. 3.3.C). The impact of PyOM on bacterial communities was evident within a few days of incubation – the communities in both the 350 and 550 PyOM amended soils were distinct from the unamended soils by Day 2 and Day 4, respectively. In contrast, we only detected significant shifts in the fungal community composition over time (PERMANOVA, $p_{time} < 0.01$) and not in response to PyOM addition (Fig. 3.3.B and 3.3.D). Time had the most explanatory power for variations in both the bacterial and fungal communities (R^2 values between 0.08 and 0.25).

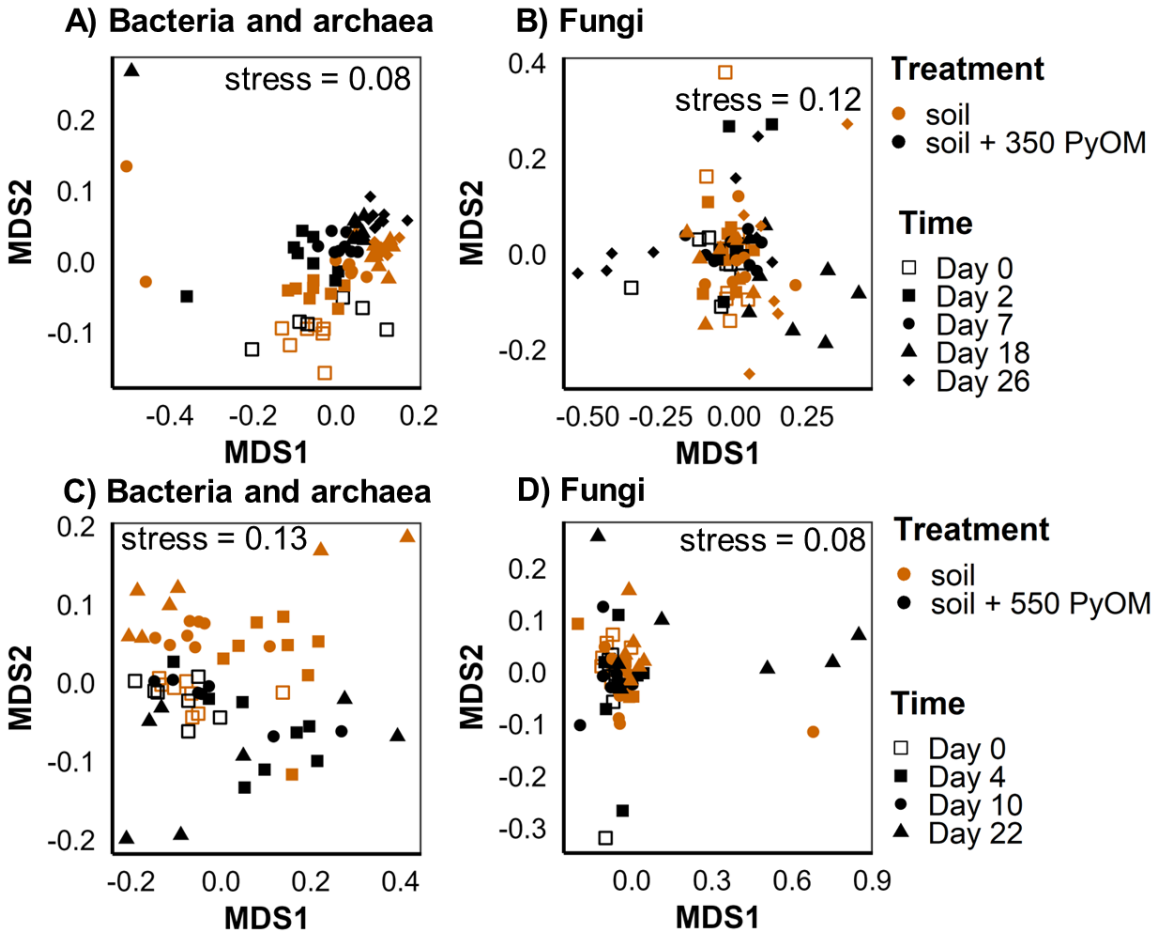

Figure 3.3. Effect of PyOM addition on soil microbial community composition.
NMDS ordination of Bray-Curtis dissimilarities between (A & C) bacterial/archaeal (16S rRNA gene v4 region) communities (k=2) and (B & D) fungal (ITS2) communities (k=3) for all samples. Top panels indicate data for unamended and 350 °C PyOM-amended soil samples. Bottom panels indicate data for unamended and 550 °C PyOM-amended soil samples.

Soil C profile

The LC-MS analysis of PyOM amended and unamended soils showed that the addition of both 350 and 550 PyOM resulted in significant shifts in soil C profile (PERMANOVA, $p < 0.01$; Fig. 3.4.A and 3.4.B).

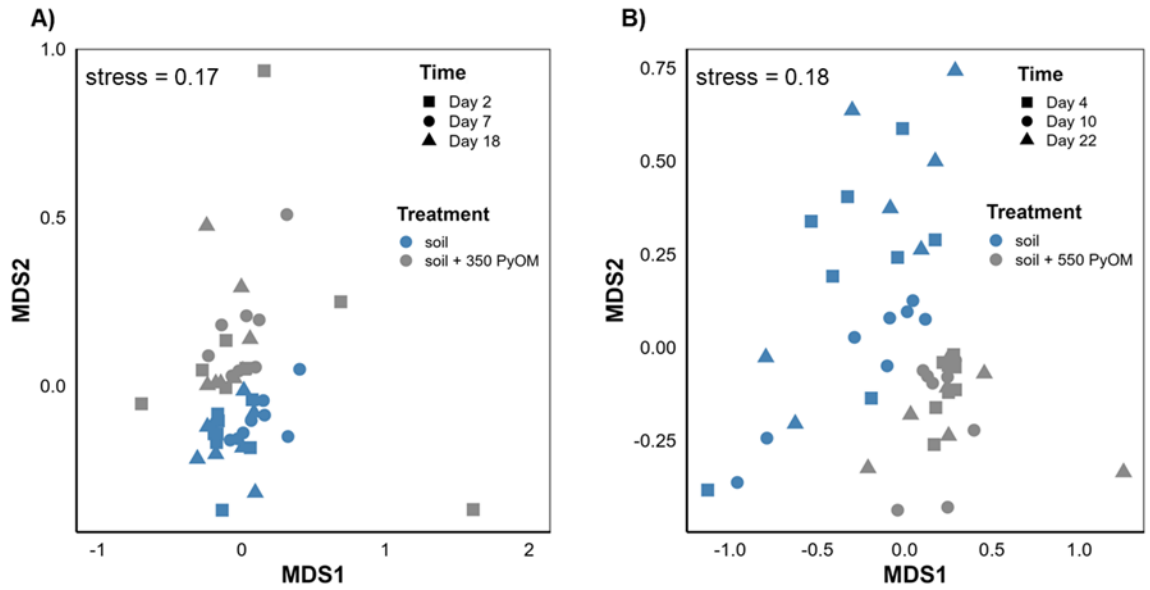

Figure 3.4. Effect of PyOM addition on soil carbon chemical profile.
NMDS ordination of Bray-Curtis distances between soil chemical peaks for A) unamended and 350 °C PyOM amended soil samples (k=2) and B) unamended and 550 °C PyOM amended soil samples (k=2).

PyOM positive responders

Using DESeq2, we identified 19 bacterial OTUs that responded positively to the addition of 350 PyOM (Fig. S3.2). After controlling for time and sample effects, these OTUs showed a significant positive response to 350 PyOM and had a mean normalized count higher than the 25th percentile. Among these, 12 OTUs belonged to the genera *Bacillus*, *Massilia*, *Ferruginibacter*, *Gemmatimonas*, *Noviherbaspirillum*, *Pseudonocardia*, *Psychroglaciecola*, *Saccharimonadales*, and *Singulisphaera*, and 7 of them were assigned to unknown genera. At the genus level, six of the identified genera showed a significant positive response to 350 PyOM at one or more time points during the incubation (Fig. 3.5). The relative abundance of all OTUs within these genera increased significantly with the addition of 350 PyOM, with the increase appearing at different points during the incubation period. In the case of fungi, we identified 5 OTUs with a mean normalized count higher than the 25th percentile that showed a significant positive response to

350 PyOM (Fig. S3.3). These OTUs belonged to the *Calyptrozyma*, *Coniochaeta*, *Holtermanniella*, *Leucosporidium* and *Solicoccozyma* genera. However, we were unable to identify a genus level response for any of the identified genera. Upon 550 PyOM addition, we identified only a single bacterial OTU from the *Gemmatimonas* genus and a single fungal OTU from the *Paraphoma* genus that responded positively to its addition.

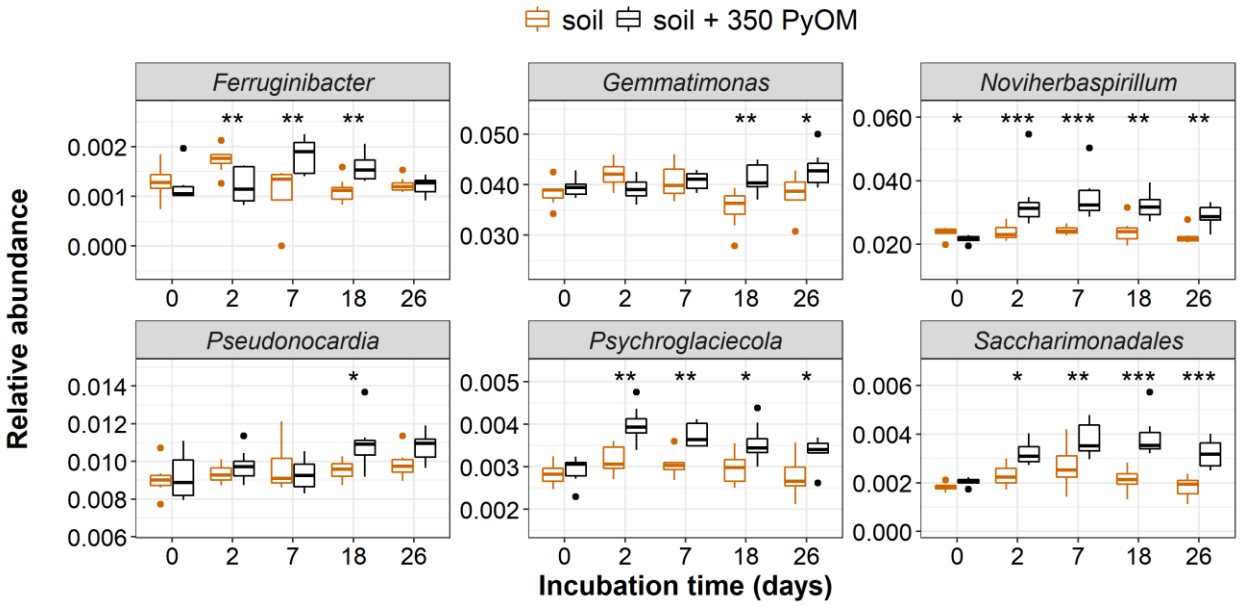

Figure 3.5. Positive bacterial responders to 350 PyOM.
*Relative abundance of positively responsive genera over time (as identified using DESeq2) observed in the unamended and 350 PyOM-amended soils (n=5-8). * indicates relative abundances that differ significantly from unamended soil at a given timepoint (t-test, *: p < 0.05; **: p < 0.01; ***: p < 0.001).*

Discussion

Carbon mineralizability differs with PyOM fraction and temperature

Consistent with our hypothesis, water-extractable PyOM-C fractions were much more readily mineralized than non-water-extractable C fractions (Fig. 3.2.A). This 10-50x difference in C mineralizability underscores the heterogeneity of the C in PyOM and the potential to

explain significant variation in PyOM decomposition rates. However, meaningful differences exist between equivalent fractions of PyOM produced at different temperatures: when we compare the C mineralization between the two different temperatures of PyOM, we see that the mineralizability of both the 350 water-extractable and non-water-extractable fractions was consistently higher. This indicates that C in low-temperature PyOM is more readily decomposed by microbes, possibly due to its lower aromaticity and lower degree of condensation compared to the C in the higher temperature 550 PyOM (Keiluweit, Nico, & Johnson, 2010; Wiedemeier et al., 2015) in addition to having a larger fraction of water-extractable C. Interestingly, compared to SOC, microbes preferred the water-extractable PyOM-C in both 350 and 550 PyOM. However, when it came to the non-water-extractable PyOM-C fractions, the non-water-extractable PyOM-C in 350 PyOM was preferred over SOC, while SOC was preferred over 550 PyOM-C. This further highlights the typically higher degrees of condensation in 550 PyOM, making the C more resistant to microbial breakdown.

Mechanisms of positive and negative priming differ over time and with PyOM temperature

The addition of 350 PyOM caused a positive priming effect on the mineralization of SOC, while the addition of 550 PyOM resulted in a negative priming effect (Fig. 3.2.B). The positive priming effect of 350 PyOM is likely due to co-metabolism / increased microbial activity, where the addition of easily mineralizable PyOM-C increases total microbial activity and accelerates the mineralization of SOC over short periods of time (DeCiucies et al., 2018; Maestrini et al., 2015; Whitman, Enders, et al., 2014). This is strongly supported by the significant positive correlation ($R^2 = 0.97$, $p < 0.001$) between the rate of PyOM-C mineralization and the rate of SOC priming observed during the incubation (Fig. 3.6.B). However, the high-frequency sampling afforded by our multiplexer CRDS system allowed us to

also detect a negative correlation between these two variables in the first 48 hours (Fig. 3.6.A). We propose that this is likely due to substrate switching. Substrate switching occurs when microbes preferentially use the easily mineralizable PyOM-C over SOC and can explain negative priming effects in the early stages of incubation (DeCiucies et al., 2018; Whitman, Zhu, et al., 2014). The higher C mineralizability observed from both fractions of 350 PyOM compared to SOC, particularly in the first 48 hours, supports the argument that the added PyOM-C is a more favorable substrate than the existing SOC, largely driven by the most available constituents of the water-extractable fraction in 350 PyOM. This preferential usage within the first two days results in a scenario where the remaining carbon in 350 PyOM and SOC are both readily used by microbes through the remaining incubation period, resulting in a net positive priming effect. Positive priming could also be a result of increased microbial activity due to alleviation of nutrient constraints or soil conditioning (creation of favorable microenvironments) upon PyOM addition (DeCiucies et al., 2018; Zimmerman & Ouyang, 2019).

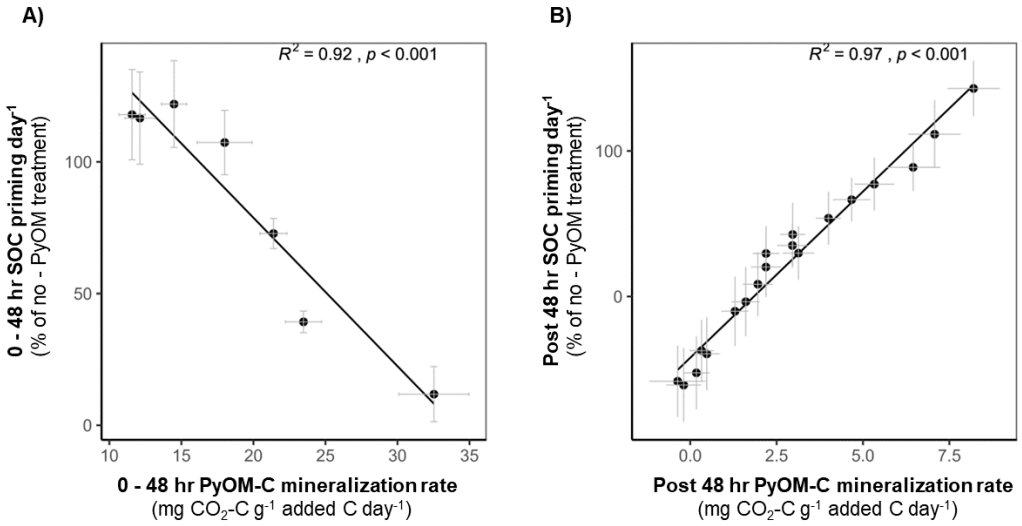

Figure 3.6. Relationships between mean PyOM-C mineralization rate and SOC priming for the 350 C PyOM.
A) *0 - 48 hours of soil-PyOM incubation and* ***B)*** *post 48 hours of soil-PyOM incubation. (n=4-5, error bars=SE). Priming calculated as: [[$SOC_{(PyOM)}$-$SOC_{(no\text{-}PyOM)}$] / $SOC_{(no\text{-}PyOM)}$]*

We can rule out substrate switching as an explanation for the negative priming effect of 550 PyOM on SOC mineralization, as no negative correlation was observed between the rate of 550 PyOM-C mineralization and the rate of SOC priming (Fig. S3.4). Instead, the short-term negative priming effect may be due to inhibition, sorption of SOC on PyOM, or dilution. Inhibitory effects of 550 PyOM on microbes (such as reduction in microbial biomass) were not investigated, but cannot be ruled out as a potential cause. Inhibition is known to occur indirectly through changes in the soil environment or directly due to toxic chemicals released upon the addition of PyOM that inhibit microbial activity (Dai et al., 2021; Smith et al., 2013). However, studies investigating the impact of PyOM produced at varying pyrolysis temperatures on microbial populations have not found a significant reduction in microbial biomass with

increasing pyrolysis temperature (DeCiucies et al., 2018; Li et al., 2020), making inhibition an unlikely explanation in this study. Sorption of SOC on high-porosity, high-surface-area 550 PyOM, may also contribute to the negative priming effect by making SOC less accessible to microbes (DeCiucies et al., 2018). Dilution of the SOC pool by the addition of PyOM-C, even with just a small mass of easily mineralizable C, may also decrease mineralization. In a previous study, DeCiucies et al. (2018) found that dilution contributed to 19% of reductions in SOC mineralization observed with PyOM produced at 450 °C over the first 7 days. The high PyOM addition rate (compared to the range of additon rates in Wang et al. (2016) and low C content in the water-extractable fraction of 550 PyOM make dilution a valid possibility in the first few days. To further understand the mechanisms behind the negative priming effect of 550 PyOM on SOC mineralization, additional research is needed. Adsorption isotherms and high-resolution imaging of ^{13}C-labeled PyOM surface could help investigate the role of sorption in negative priming. Modifying the surface properties of PyOM and understanding its relation to sorption, as well as experiments with varying addition rates, could also be valuable in determining the relative contributions of dilution vs. sorption.

350 PyOM increases the abundance of some bacterial taxa

The addition of PyOM had a significant effect on the composition of the bacterial community almost immediately. Given the absence of any pH effects, the shift in communities is most likely primarily a response to the C in PyOM. The shift in communities within the first few days of PyOM addition coincides with a sharp increase in the mineralization of the water-extractable fractions in both 350 and 550 PyOM. As PyOM-C is broken down, it creates a pool of degradation byproducts which can alter the chemical profile of soil C. A significant shift in the C profile over time was observed for 550 PyOM (PERMANOVA, $p = 0.04$) but not for 350

PyOM. We postulate that this shift over time is likely due to microbes preferentially using the easily mineralizable PyOM-C compounds first, leading to an increase in more complex, harder to break down compounds in the soil. Supporting this hypothesis, we identified four features that were specific to the 350 and 550 PyOM-amended soils and never present in any unamended soil samples. These features increased in relative abundance over time in the 350 PyOM-amended soils but declined over time in the 550 PyOM-amended soils (Fig. S3.5 and Table S3.3). The chemical formula of these features indicates that they are complex hydrocarbons, which suggests that their relative accumulation in the 350 PyOM-amended soils is due to preferential utilization of easily mineralizable PyOM-C compounds. In the case of 550 PyOM, the limited availability of easily mineralizable C would be more likely to lead to the greater use of these complex C compounds by microbes. Further characterization of these features, including confirming that they are PyOM byproducts and a byproduct of microbial breakdown, is needed to gain deeper insights into microbial utilization of PyOM-C substrates.

In line with these findings, we would expect that microbes using easily mineralizable C would increase in relative abundance first, followed by microbes that have the capacity of using complex aromatic C substrates. We observed an increase in the relative abundance of bacteria from the genera *Gemmatimonas* and *Pseudonocardia* after 18 days of incubation in the 350 PyOM-amended soils, coinciding with a period when the rate of water-extractable PyOM-C mineralization was low (Fig. S3.6). It is plausible that by this point, the most available C is already mineralized and that these bacteria are benefiting from their ability to utilize the condensed aromatic C in 350 PyOM (Dai et al., 2017; Whitman et al., 2016). This was also evident in soils amended with 550 PyOM - the only significant increase in relative abundance in

550 PyOM amended soils was observed for an OTU belonging to the genus *Gemmatimonas* on Day 10 (Fig. S3.7).

In contrast, bacteria from the genera *Noviherbaspirillum*, *Saccharimonadales*, *Ferruginibacter*, and *Psychroglaciecola*, significantly increased in relative abundance in 350 PyOM amended soils on Day 2 after PyOM addition. Previous incubation studies have observed an increase in relative abundance of *Noviherbaspirillum*, *Saccharimonadales*, and *Ferruginibacter* with PyOM, but the mechanisms by which they respond to PyOM are not well understood (De Tender et al., 2016; Song et al., 2017; Whitman et al., 2016; Woolet & Whitman, 2020). Among these, bacteria from the genus *Noviherbaspirillum* have the potential to degrade aromatic C and have been identified as fire responders, suggesting a role in aromatic PyOM-C degradation (Lin et al., 2013; Woolet & Whitman, 2020). Bacteria from *Psychroglaciecola* have not been previously identified as positive responders to PyOM, and their role in PyOM amended soils is unclear.

PyOM addition does not result in fungal community shifts

We observed no change in fungal community composition in response to the addition of PyOM and observed fewer fungal positive responders to 350 PyOM compared to bacteria. This was surprising, given that previous research has shown PyOM to impact whole community composition as well as specific fungal groups (Dai et al., 2016; Gao et al., 2021; Lehmann et al., 2011). Among the fungal responders, *Calyptrozyma* sp. has been identified as fire-responsive (Pérez-Izquierdo et al., 2021; Whitman et al., 2019). Its increased abundance was attributed to reduced competition from other fungi post fire and its capacity to grow on charred aromatic C (Pérez-Izquierdo et al., 2021). It is possible that bacteria were perhaps better able to utilize the nutrients provided by PyOM, and the effects of PyOM on fungi may become more apparent over

longer durations when the easily mineralizable carbon becomes limited. This is supported in many ways by previous studies that have investigated PyOM effects on fungi. For example, Li et al. (2019) found that bacteria may be more affected by the aqueous extractable substances of PyOM which could appear over shorter durations, while fungi may be more affected by the porous nature and aromatic carbon compounds. Yu et. al (2018) also observed that the PyOM-induced priming effect in their study was strongly associated with the increase of certain bacteria in the first 8 days, with an increase in fungal groups not observed until day 40. Liu et al. (2019) found an increase in the proportion of bacteria in fresh PyOM amended soils, and fungi in 6-year-old PyOM amended soils. Another factor that may have contributed to fewer positive fungal responders in our study is the fine grinding of PyOM particles (chosen in order to ensure effective mixing and even distribution). This may have increased the microporosity, making it more difficult for fungi to colonize the PyOM (Li et al., 2019). Additionally, sieving the soil before setting up the incubation could have affected filamentous fungi more than many bacteria (although sieving before incubations is a standard practice to homogenize soil across replicates). More research is needed to fully understand the effects of PyOM on fungal communities, including the role of time and the specific mechanisms at play. Future studies should also consider the potential impacts of particle size and porosity on fungal colonization.

Overall, the effects of PyOM on microbes are likely related to changes in nutrient provision, including both C and N. Other PyOM properties such as surface and electrochemical properties can also affect microbial response to PyOM (Sun et al., 2017; Yu et al., 2015). Ash content contributes to the alkalinity of the PyOM and is known to cause small changes in the microbial community composition (Dai et al., 2021). With our pH adjustment, the effect of ash content should be negligible compared to the effects of PyOM-C. The porous nature of PyOM

can adsorb water, organic materials and nutrients, and provide a habitat for microbes (Dai et al., 2017; Luo et al., 2013). Furthermore, PyOM sorption of acyl-homoserine lactone (AHL) intercellular signaling molecules can disrupt cell-cell communication among bacteria and affect C mineralization, especially in the short-term following addition of fresh PyOM (Masiello et al., 2013). The porosity and surface area of PyOM increase with pyrolysis temperatures (Tomczyk et al., 2020), which may influence the mineralization of 350 vs. 550 PyOM. While we did not specifically investigate the microbial colonization of 350 and 550 PyOM or other effects mentioned here, we anticipate that C availability will be the dominant factor controlling microbial response in a 30-day incubation.

Conclusion

In this study, we demonstrated that the water-extractable carbon in PyOM comprises a small fraction of PyOM-C but exhibits disproportionately high mineralizability. We calculated mineralization rates for the water-extractable PyOM-C fractions of 0.23% day^{-1} for the 350 PyOM and 0.04% day^{-1} for the 550 PyOM. These rates surpass decomposition rates estimated by Wang et al. (2016) for wood-based PyOM (mean: 0.004% day^{-1}) or PyOM produced within a similar pyrolysis temperature range (mean: < 0.04% day^{-1} for PyOM produced between 200-550 ºC), based primarily on lab incubation data. However, it is essential to recognize that mineralization rates of water-extractable PyOM-C may differ in the field under non-optimal conditions. This study was conducted for a short duration under controlled temperature and soil moisture conditions, so field rates may vary substantially, likely being lower as per Maestrini et al. (2014) or higher as shown by Ventura et al. (2015). While estimating these numbers in the field is challenging, some field evidence also exists for a rapidly cycling, easily mineralizable PyOM-C fraction (Major et al., 2010; Ventura et al., 2015). Furthermore, factors such as soil

texture and climate, including temperature and precipitation, can affect the fate of the water-extractable fraction in the short term, including whether it is lost as leachate from the soil or adsorbed to clay minerals.

We also observed that the low-temperature 350 PyOM displayed higher C mineralizability than the high-temperature 550 PyOM. Moreover, our short-term incubation study showed net positive priming of SOC upon the addition of 350 PyOM, while the addition of 550 PyOM resulted in net negative priming. Our findings align with Maestrini et al. (2014), indicating that short-term positive priming is primarily attributed to the presence of the water-extractable fraction. In contrast, high-temperature 550 PyOM exhibited a negative priming effect on SOC mineralization, potentially due to dilution, sorption of SOC on PyOM, or inhibition of microbial activity. In post-burn soils with a higher proportion of low-temperature PyOM, the less aromatic PyOM-C constituents may undergo faster turnover, especially immediately after deposition. This process could lead to a positive priming effect, where the addition of easily mineralizable PyOM-C enhances microbial activity and accelerates short-term SOC mineralization, depending on the fate of the easily mineralizable fraction and other soil and climatic factors. Conversely, in post-burn soils containing a higher proportion of high-temperature PyOM, the slower PyOM-C turnover and negative priming effects may be more likely to contribute to long-term carbon sequestration.

Furthermore, our study identified that PyOM addition influenced bacterial community composition, leading to an increased relative abundance of certain bacteria that other studies have suggested as being capable of degrading aromatic C compounds. However, it remains unclear whether these bacteria in our study, and even in the field, increase due to actual consumption of PyOM-C. Techniques like DNA Stable isotope probing (qSIP) (Hungate et al.,

2015) with ^{13}C-labeled PyOM can help identify the bacteria actively taking up the C in PyOM. In post-burn soils, microbial community responses to PyOM are likely affected by both PyOM-C availability and physico-chemical alterations in soil properties following a burn. Moreover, the presence of PyOM-C post-fire may cause shifts in microbial community composition and alterations in functional groups involved in carbon cycling. Employing qSIP with ^{13}C-labeled PyOM can help us determine whether their relative increase is due to consumption of PyOM-C, and combining SIP with metagenomics can provide further insights into the functional roles of these responders (Wang & Yao, 2021). Gaining this knowledge is crucial for predicting post-burn ecosystem recovery and potential changes in soil carbon dynamics following fire events.

Acknowledgements

This work was made possible with the financial support of the Department of Energy through awards DE-SC0016365 and DE-SC0020351. We are grateful to Harry Read for his expertise in designing and constructing the labeling chamber, and Akio Enders for designing and constructing the "charcoalator." We thank Miranda Sikora and Jamie Woolet for growing the labeled trees, and Mengmeng Luo, Dana B. Johnson, and Elias Kemna for their assistance in setting up the soil-PyOM incubations. Our gratitude also extends to Neem Patel for helping with soil collection and the Wisconsin Department of Natural Resources for providing white pine seedlings. We acknowledge Kim Sparks and the Cornell Stable Isotope Laboratory for their assistance with PyOM analyses, as well as the Center for High Throughput Computing (CHTC) for providing resources for bioinformatics and data analysis (https://chtc.cs.wisc.edu/uw-research-computing/cite-chtc.html).

Author Contributions

The author contributions to the chapter are as follows: study conception and design: NZ, TLW, TDB; data collection: NZ, TDB, MSF; analysis and interpretation of results: NZ, TDB, MSF, MFT, TLW; draft manuscript preparation: NZ; manuscript review and editing: NZ, TDB, MSF, TLW.

References

Abarenkov, K., Zirk, A., Piirmann, T., Pöhönen, R., Ivanov, F., Nilsson, R. H., & Kõljalg, U. (2021). *UNITE QIIME release for Fungi* [Application/gzip]. UNITE Community.

Bengtsson-Palme, J., Ryberg, M., Hartmann, M., Branco, S., Wang, Z., Godhe, A., De Wit, P., Sánchez-García, M., Ebersberger, I., de Sousa, F., Amend, A., Jumpponen, A., Unterseher, M., Kristiansson, E., Abarenkov, K., Bertrand, Y. J. K., Sanli, K., Eriksson, K. M., Vik, U., … Nilsson, R. H. (2013). Improved software detection and extraction of ITS1 and ITS2 from ribosomal ITS sequences of fungi and other eukaryotes for analysis of environmental sequencing data. *Methods in Ecology and Evolution*, *4*(10), 914–919.

Berry, T. D., Creelman, C., Nickerson, N., Enders, A., & Whitman, T. (2021). An open-source, automated, gas sampling peripheral for laboratory incubation experiments using cavity ring-down spectroscopy. *HardwareX*, *10*, e00208.

Bokulich, N. A., Kaehler, B. D., Rideout, J. R., Dillon, M., Bolyen, E., Knight, R., Huttley, G. A., & Gregory Caporaso, J. (2018). Optimizing taxonomic classification of marker-gene amplicon sequences with QIIME 2's q2-feature-classifier plugin. *Microbiome*, *6*(1), 90.

Bolyen, E., Rideout, J. R., Dillon, M. R., Bokulich, N. A., Abnet, C. C., Al-Ghalith, G. A., Alexander, H., Alm, E. J., Arumugam, M., Asnicar, F., Bai, Y., Bisanz, J. E., Bittinger, K., Brejnrod, A., Brislawn, C. J., Brown, C. T., Callahan, B. J., Caraballo-Rodríguez, A. M., Chase, J., … Caporaso, J. G. (2019). Reproducible, interactive, scalable and extensible microbiome data science using QIIME 2. *Nature Biotechnology*, *37*(8), Article 8.

Bray, J. R., & Curtis, J. T. (1957). An Ordination of the Upland Forest Communities of Southern Wisconsin. *Ecological Monographs*, *27*(4), 325–349.

Bruns, T. D., Chung, J. A., Carver, A. A., & Glassman, S. I. (2020). A simple pyrocosm for studying soil microbial response to fire reveals a rapid, massive response by Pyronema species. *PLOS ONE*, *15*(3), e0222691.

Bruun, E. W., Hauggaard-Nielsen, H., Ibrahim, N., Egsgaard, H., Ambus, P., Jensen, P. A., & Dam-Johansen, K. (2011). Influence of fast pyrolysis temperature on biochar labile fraction and short-term carbon loss in a loamy soil. *Biomass and Bioenergy*, *35*(3), 1182–1189.

Callahan, B. J., Mcmurdie, P. J., Rosen, M. J., Han, A. W., & A, A. J. (2016). *HHS Public Access*. *13*(7), 581–583.

Chen, Z., Wang, H., Liu, X., Zhao, X., Lu, D., Zhou, J., & Li, C. (2017). Changes in soil microbial community and organic carbon fractions under short-term straw return in a rice–wheat cropping system. *Soil and Tillage Research*, *165*, 121–127.

Dai, Z., Barberán, A., Li, Y., Brookes, P. C., & Xu, J. (2017). Bacterial Community Composition Associated with Pyrogenic Organic Matter (Biochar) Varies with Pyrolysis Temperature and Colonization Environment. *MSphere2*, *2*(2), e00085-17.

Dai, Z., Hu, J., Xu, X., Zhang, L., Brookes, P. C., He, Y., & Xu, J. (2016). Sensitive responders among bacterial and fungal microbiome to pyrogenic organic matter (biochar) addition differed greatly between rhizosphere and bulk soils. *Scientific Reports*, *6*(November), 1–11.

Dai, Z., Xiong, X., Zhu, H., Xu, H., Leng, P., Li, J., Tang, C., & Xu, J. (2021). Association of biochar properties with changes in soil bacterial, fungal and fauna communities and nutrient cycling processes. *Biochar*, *3*(3), 239–254.

De Tender, C., Haegeman, A., Vandecasteele, B., Clement, L., Cremelie, P., Dawyndt, P., Maes, M., & Debode, J. (2016). Dynamics in the Strawberry Rhizosphere Microbiome in Response to Biochar and Botrytis cinerea Leaf Infection. *Frontiers in Microbiology*, *7*, 2062.

DeCiucies, S., Whitman, T., Woolf, D., Enders, A., & Lehmann, J. (2018). Priming mechanisms with additions of pyrogenic organic matter to soil. *Geochimica et Cosmochimica Acta*, *238*, 329–342.

DeLuca, T. H., Gundale, M. J., Brimmer, R. J., & Gao, S. (2020). Pyrogenic Carbon Generation From Fire and Forest Restoration Treatments. *Frontiers in Forests and Global Change*, *3*.

Enright, D. J., Frangioso, K. M., Isobe, K., Rizzo, D. M., & Glassman, S. I. (2022). Mega-fire in redwood tanoak forest reduces bacterial and fungal richness and selects for pyrophilous taxa that are phylogenetically conserved. *Molecular Ecology*, *31*(8), 2475–2493.

Fischer, M. S., Stark, F. G., Berry, T. D., Zeba, N., Whitman, T., & Traxler, M. F. (2021). Pyrolyzed Substrates Induce Aromatic Compound Metabolism in the Post-fire Fungus, Pyronema domesticum. *Frontiers in Microbiology*, *12*.

Fox, S., Sikes, B. A., Brown, S. P., Cripps, C. L., Glassman, S. I., Hughes, K., Semenova-Nelsen, T., & Jumpponen, A. (2022). Fire as a driver of fungal diversity—A synthesis of current knowledge. *Mycologia*, *114*(2), 215–241.

Gao, W., Gao, K., Guo, Z., Liu, Y., Jiang, L., Liu, C., Liu, X., & Wang, G. (2021). Different Responses of Soil Bacterial and Fungal Communities to 3 Years of Biochar Amendment in an Alkaline Soybean Soil. *Frontiers in Microbiology*, *12*.

Güereña, D. T., Lehmann, J., Thies, J. E., Enders, A., Karanja, N., & Neufeldt, H. (2015). Partitioning the contributions of biochar properties to enhanced biological nitrogen

fixation in common bean (Phaseolus vulgaris). *Biology and Fertility of Soils*, *51*(4), 479–491.

Hamer, U., Marschner, B., Brodowski, S., & Amelung, W. (2004). Interactive priming of black carbon and glucose mineralisation. *Organic Geochemistry*, *35*(7), 823–830.

Hungate, B. A., Mau, R. L., Schwartz, E., Caporaso, J. G., Dijkstra, P., van Gestel, N., Koch, B. J., Liu, C. M., McHugh, T. A., Marks, J. C., Morrissey, E. M., & Price, L. B. (2015). Quantitative Microbial Ecology through Stable Isotope Probing. *Applied and Environmental Microbiology*, *81*(21), 7570–7581.

Kassambara, A. (2022). *rstatix: Pipe-Friendly Framework for Basic Statistical Tests*.

Keiluweit, M., Nico, P. S., & Johnson, M. G. (2010). Dynamic Molecular Structure of Plant Biomass-Derived Black Carbon (Biochar). *Environ. Sci. Technol.*, *44*(4), 1247–1253.

Keith, A., Singh, B., & Singh, B. P. (2011). Interactive priming of biochar and labile organic matter mineralization in a smectite-rich soil. *Environmental Science and Technology*, *45*(22), 9611–9618.

Kozich, J. J., Westcott, S. L., Baxter, N. T., Highlander, S. K., & Schloss, P. D. (2013). Development of a Dual-Index Sequencing Strategy and Curation Pipeline for Analyzing Amplicon Sequence Data on the MiSeq Illumina Sequencing Platform. *Applied and Environmental Microbiology*, *79*(17), 5112–5120.

Lehmann, J., & Joseph, S. (2012). Biochar for environmental management: An introduction. In *Biochar for Environmental Management: Science and Technology*.

Lehmann, J., Rillig, M. C., Thies, J., Masiello, C. A., Hockaday, W. C., & Crowley, D. (2011). Biochar effects on soil biota—A review. *Soil Biology and Biochemistry*, *43*(9), 1812–1836.

Li, X., Wang, T., Chang, S. X., Jiang, X., & Song, Y. (2020). Biochar increases soil microbial biomass but has variable effects on microbial diversity: A meta-analysis. *Science of The Total Environment*, *749*, 141593.

Li, Y., Yang, Y., Shen, F., Tian, D., Zeng, Y., Yang, G., Zhang, Y., & Deng, S. (2019). Partitioning biochar properties to elucidate their contributions to bacterial and fungal community composition of purple soil. *Science of The Total Environment*, *648*, 1333–1341.

Lin, S.-Y., Hameed, A., Arun, A. B., Liu, Y.-C., Hsu, Y.-H., Lai, W.-A., Rekha, P. D., & Young, C.-C. (2013). Description of Noviherbaspirillum malthae gen. Nov., sp. Nov., isolated from an oil-contaminated soil, and proposal to reclassify Herbaspirillum soli,Herbaspirillum aurantiacum,Herbaspirillum canariense and Herbaspirillum psychrotolerans as Noviherbaspirillum soli comb. Nov., Noviherbaspirillum aurantiacum comb. Nov., Noviherbaspirillum canariense comb. Nov. And Noviherbaspirillum psychrotolerans comb. Nov. Based on polyphasic analysis. *International Journal of Systematic and Evolutionary Microbiology*, *63*(Pt_11), 4100–4107.

Liu, Z., Zhu, M., Wang, J., Liu, X., Guo, W., Zheng, J., Bian, R., Wang, G., Zhang, X., Cheng, K., Liu, X., Li, L., & Pan, G. (2019). The responses of soil organic carbon mineralization

and microbial communities to fresh and aged biochar soil amendments. *GCB Bioenergy*, *11*(12), 1408–1420.

Love, M. I., Anders, S., Kim, V., & Huber, W. (2016). *RNA-Seq workflow: Gene-level exploratory analysis and differential expression* (4:1070). F1000Research.

Love, M. I., Huber, W., & Anders, S. (2014). Moderated estimation of fold change and dispersion for RNA-seq data with DESeq2. *Genome Biology*, *15*(12), 1–21.

Luo, Y., Durenkamp, M., De Nobili, M., Lin, Q., & Brookes, P. C. (2011). Short term soil priming effects and the mineralisation of biochar following its incorporation to soils of different pH. *Soil Biology and Biochemistry*, *43*(11), 2304–2314.

Luo, Y., Durenkamp, M., De Nobili, M., Lin, Q., Devonshire, B. J., & Brookes, P. C. (2013). Microbial biomass growth, following incorporation of biochars produced at 350 °C or 700 °C, in a silty-clay loam soil of high and low pH. *Soil Biology and Biochemistry*, *57*, 513–523.

Maestrini, B., Abiven, S., Singh, N., Bird, J., Torn, M. S., & Schmidt, M. W. I. (2014). Carbon losses from pyrolysed and original wood in a forest soil under natural and increased N deposition. *Biogeosciences*, *11*(18), 5199–5213.

Maestrini, B., Nannipieri, P., & Abiven, S. (2015). A meta-analysis on pyrogenic organic matter induced priming effect. *GCB Bioenergy*, *7*(4), 577–590.

Major, J., Lehmann, J., Rondon, M., & Goodale, C. (2010). Fate of soil-applied black carbon: Downward migration, leaching and soil respiration. *Global Change Biology*, *16*(4), 1366–1379.

Masiello, C. A., Chen, Y., Gao, X., Liu, S., Cheng, H.-Y., Bennett, M. R., Rudgers, J. A., Wagner, D. S., Zygourakis, K., & Silberg, J. J. (2013). Biochar and Microbial Signaling: Production Conditions Determine Effects on Microbial Communication. *Environmental Science & Technology*, *47*(20), 11496–11503.

McMurdie, P. J., & Holmes, S. (2013). phyloseq: An R package for reproducible interactive analysis and graphics of microbiome census data. *PLoS ONE*, *8*(4), e61217.

Oksanen, J., Simpson, G. L., Blanchet, F. G., Kindt, R., Legendre, P., Minchin, P. R., O'Hara, R. B., Solymos, P., Stevens, M. H. H., Szoecs, E., Wagner, H., Barbour, M., Bedward, M., Bolker, B., Borcard, D., Carvalho, G., Chirico, M., Caceres, M. D., Durand, S., … Weedon, J. (2022). *vegan: Community Ecology Package*.

Pedregosa, F., Varoquaux, G., Gramfort, A., Michel, V., Thirion, B., Grisel, O., Blondel, M., Prettenhofer, P., Weiss, R., Dubourg, V., Vanderplas, J., Passos, A., Cournapeau, D., Brucher, M., Perrot, M., & Duchesnay, É. (2011). Scikit-learn: Machine Learning in Python. *The Journal of Machine Learning Research*, *12*(null), 2825–2830.

Pellegrini, A. F. A., Ahlström, A., Hobbie, S. E., Reich, P. B., Nieradzik, L. P., Staver, A. C., Scharenbroch, B. C., Jumpponen, A., Anderegg, W. R. L., Randerson, J. T., & Jackson, R. B. (2018). Fire frequency drives decadal changes in soil carbon and nitrogen and ecosystem productivity. *Nature*, *553*(7687), 194–198.

Pérez-Izquierdo, L., Clemmensen, K. E., Strengbom, J., Granath, G., Wardle, D. A., Nilsson, M.-C., & Lindahl, B. D. (2021). Crown-fire severity is more important than ground-fire severity in determining soil fungal community development in the boreal forest. *Journal of Ecology*, *109*(1), 504–518.

Quast, C., Pruesse, E., Yilmaz, P., Gerken, J., Schweer, T., Yarza, P., Peplies, J., & Glöckner, F. O. (2013). The SILVA ribosomal RNA gene database project: Improved data processing and web-based tools. *Nucleic Acids Research*, *41*(D1), D590–D596.

R Core Team. (2022). *R: A Language and Environment for Statistical Computing*. R Foundation for Statistical Computing.

Robinson, D., Hayes, A., & Couch, S. (2022). *broom: Convert Statistical Objects into Tidy Tibbles*.

Santín, C., Doerr, S. H., Preston, C. M., & González-Rodríguez, G. (2015). Pyrogenic organic matter production from wildfires: A missing sink in the global carbon cycle. *Global Change Biology*, *21*(4), 1621–1633.

Santos, F., Torn, M. S., & Bird, J. A. (2012). Biological degradation of pyrogenic organic matter in temperate forest soils. *Soil Biology and Biochemistry*, *51*, 115–124.

Smith, C. R., Buzan, E. M., & Lee, J. W. (2013). Potential impact of biochar water-extractable substances on environmental sustainability. *ACS Sustainable Chemistry and Engineering*, *1*(1), 118–126.

Song, Y., Bian, Y., Wang, F., Xu, M., Ni, N., Yang, X., Gu, C., & Jiang, X. (2017). Dynamic Effects of Biochar on the Bacterial Community Structure in Soil Contaminated with Polycyclic Aromatic Hydrocarbons. *Journal of Agricultural and Food Chemistry*, *65*(32), 6789–6796.

Sun, T., Levin, B. D. A., Guzman, J. J. L., Enders, A., Muller, D. A., Angenent, L. T., & Lehmann, J. (2017). Rapid electron transfer by the carbon matrix in natural pyrogenic carbon. *Nature Communications*, *8*, 1–12.

Taylor, D. L., Walters, W. A., Lennon, N. J., Bochicchio, J., Krohn, A., Caporaso, J. G., & Pennanen, T. (2016). Accurate Estimation of Fungal Diversity and Abundance through Improved Lineage-Specific Primers Optimized for Illumina Amplicon Sequencing. *Applied and Environmental Microbiology*, *82*(24), 7217–7226.

Tomczyk, A., Sokołowska, Z., & Boguta, P. (2020). Biochar physicochemical properties: Pyrolysis temperature and feedstock kind effects. *Reviews in Environmental Science and Biotechnology*, *19*(1), 191–215.

Tsugawa, H., Cajka, T., Kind, T., Ma, Y., Higgins, B., Ikeda, K., Kanazawa, M., VanderGheynst, J., Fiehn, O., & Arita, M. (2015). MS-DIAL: Data-independent MS/MS deconvolution for comprehensive metabolome analysis. *Nature Methods*, *12*(6), Article 6.

Tu, C., Wei, J., Guan, F., Liu, Y., Sun, Y., & Luo, Y. (2020). Biochar and bacteria inoculated biochar enhanced Cd and Cu immobilization and enzymatic activity in a polluted soil. *Environment International*, *137*, 105576.

Ventura, M., Alberti, G., Viger, M., Jenkins, J. R., Girardin, C., Baronti, S., Zaldei, A., Taylor, G., Rumpel, C., Miglietta, F., & Tonon, G. (2015). Biochar mineralization and priming effect on SOM decomposition in two European short rotation coppices. *GCB Bioenergy*, *7*(5), 1150–1160.

Walters, W., Hyde, E. R., Berg-Lyons, D., Ackermann, G., Humphrey, G., Parada, A., Gilbert, J. A., Jansson, J. K., Caporaso, J. G., Fuhrman, J. A., Apprill, A., & Knight, R. (2015). Improved Bacterial 16S rRNA Gene (V4 and V4-5) and Fungal Internal Transcribed Spacer Marker Gene Primers for Microbial Community Surveys. *MSystems*, *1*(1), e00009-15.

Wang, J., Xiong, Z., & Kuzyakov, Y. (2016). Biochar stability in soil: Meta-analysis of decomposition and priming effects. *GCB Bioenergy*, *8*(3), 512–523.

Wang, J., & Yao, H. (2021). Applications of DNA/RNA-stable isotope probing (SIP) in environmental microbiology. In *Methods in Microbiology* (Vol. 48, pp. 227–267). Elsevier.

Westerling, A. L. (2016). Increasing western US forest wildfire activity: Sensitivity to changes in the timing of spring. *Philosophical Transactions of the Royal Society B: Biological Sciences*, *371*(1696), 20150178.

Whitman, T., DeCiucies, S., Hanley, K., Enders, A., Woolet, J., & Lehmann, J. (2021). Microbial community shifts reflect losses of native soil carbon with pyrogenic and fresh organic matter additions and are greatest in low-carbon soils. *Applied and Environmental Microbiology*, *January*.

Whitman, T., Enders, A., & Lehmann, J. (2014). Pyrogenic carbon additions to soil counteract positive priming of soil carbon mineralization by plants. *Soil Biology and Biochemistry*, *73*, 33–41.

Whitman, T., Pepe-Ranney, C., Enders, A., Koechli, C., Campbell, A., Buckley, D. H., & Lehmann, J. (2016). Dynamics of microbial community composition and soil organic carbon mineralization in soil following addition of pyrogenic and fresh organic matter. *ISME Journal*, *10*(12), 2918–2930.

Whitman, T., Singh, B. P., & Zimmerman, A. (2015). Priming effects in biochar-amended soils: Implications of biochar-soil organic matter interactions for carbon storage. *Biochar for Environmental Management*, 453–486.

Whitman, T., Whitman, E., Woolet, J., Flannigan, M. D., Thompson, D. K., & Parisien, M. A. (2019). Soil bacterial and fungal response to wildfires in the Canadian boreal forest across a burn severity gradient. *Soil Biology and Biochemistry*, *138*(April), 107571.

Whitman, T., Zhu, Z., & Lehmann, J. (2014). Carbon mineralizability determines interactive effects on mineralization of pyrogenic organic matter and soil organic carbon. *Environmental Science and Technology*, *48*(23), 13727–13734.

Wickham, H., Averick, M., Bryan, J., Chang, W., McGowan, L. D., François, R., Grolemund, G., Hayes, A., Henry, L., Hester, J., Kuhn, M., Pedersen, T. L., Miller, E., Bache, S. M.,

Müller, K., Ooms, J., Robinson, D., Seidel, D. P., Spinu, V., … Yutani, H. (2019). Welcome to the tidyverse. *Journal of Open Source Software*, *4*(43), 1686.

Wiedemeier, D. B., Abiven, S., Hockaday, W. C., Keiluweit, M., Kleber, M., Masiello, C. A., McBeath, A. V., Nico, P. S., Pyle, L. A., Schneider, M. P. W., Smernik, R. J., Wiesenberg, G. L. B., & Schmidt, M. W. I. (2015). Aromaticity and degree of aromatic condensation of char. *Organic Geochemistry*, *78*, 135–143.

Woolet, J., & Whitman, T. (2020). Pyrogenic organic matter effects on soil bacterial community composition. *Soil Biology and Biochemistry*, *141*, 107678.

Yao, Q., Liu, J., Yu, Z., Li, Y., Jin, J., Liu, X., & Wang, G. (2017). Three years of biochar amendment alters soil physiochemical properties and fungal community composition in a black soil of northeast China. *Soil Biology and Biochemistry*, *110*, 56–67.

Yu, L., Yuan, Y., Tang, J., Wang, Y., & Zhou, S. (2015). Biochar as an electron shuttle for reductive dechlorination of pentachlorophenol by Geobacter sulfurreducens. *Scientific Reports*, *5*(1), Article 1.

Yu, Z., Chen, L., Pan, S., Li, Y., Kuzyakov, Y., Xu, J., Brookes, P. C., & Luo, Y. (2018). Feedstock determines biochar-induced soil priming effects by stimulating the activity of specific microorganisms. *European Journal of Soil Science*, *69*(3), 521–534.

Zeba, N., Berry, T. D., Panke-Buisse, K., & Whitman, T. (2022). Effects of physical, chemical, and biological ageing on the mineralization of pine wood biochar by a Streptomyces isolate. *PLOS ONE*, *17*(4), e0265663.

Zeileis, A., & Grothendieck, G. (2005). zoo: S3 Infrastructure for Regular and Irregular Time Series. *Journal of Statistical Software*, *14*(6), 1–27.

Zimmerman, A. R., Gao, B., & Ahn, M.-Y. (2011). Soil Biology & Biochemistry Positive and negative carbon mineralization priming effects among a variety of biochar-amended soils. *Soil Biology and Biochemistry*, *43*, 1169–1179.

Zimmerman, A. R., & Ouyang, L. (2019). Priming of pyrogenic C (biochar) mineralization by dissolved organic matter and vice versa. *Soil Biology and Biochemistry*, *130*(November 2018), 105–112.

Supporting Information

Table S3.1. Properties of biomass

Property (units)	^{13}C labeled biomass		Unlabeled biomass	
	Stems	Needles	Stems	Needles
Total C (%)	41.56 ± 0.92	41.61 ± 2.05	47 ± 0.46	47.02 ± 1.05
Total N (%)	1.50 ± 0.03	2.34 ± 0.11	NA	NA
Bulk δ^{13}C vs. VPDB (‰)	914.93 ± 3.62	2071.03 ± 9.69	-28.65 ± 0.29	-29.96 ± 0.32
Bulk δ^{15}N vs. atmospheric air (‰)	10.17 ± 4.64	-2.16 ± 0.30	NA	NA

The values presented are means of five replicates ± standard deviation.

Table S3.2. Properties of non-water-extractable PyOM

Property (units)	^{13}C labeled		Unlabeled	
	350 °C	550 °C	350 °C	550 °C
pH (H_2O)	7.96	9.24	7.02	9.95
Total C (%)	64.71 ± 1.06	75.17 ± 1.9	68.64 ± 2.65	78.18 ± 0.52
Total N (%)	3.28 ± 0.04	3.05 ± 0.05	2.69 ± 0.09	2.50 ± 0.02
Bulk δ^{13}C vs. VPDB (‰)	1518.48 ± 2.34	1616.97 ± 7.39	-29.14 ± 0.14	-29.41 ± 0.02
Bulk δ^{15}N vs. atmospheric air (‰)	0.25 ± 0.29	0.39 ± 0.43	0.16 ± 0.15	0.72 ± 0.29
Total organic C (%)	56.56 ± 0.23	62.62 ± 0.2	59.25 ± 0.31	65.13 ± 0.61

The values presented represent means ± standard deviation (n = 3 for total organic C; n = 5 for total C, N, bulk δ^{13}C and bulk δ^{15}N. pH values of the original PyOM before adjustment are shown.

Table S3.3. Properties of LC-MS features identified in PyOM amended soils

Alignment ID	Average Rt (min)	Average Mz	Formula
2384	2.609	409.16467	$C_{25}H_{20}N_4O_2$
2634	2.609	425.13583	NULL
2758	2.607	432.23819	$C_{22}H_{30}O_6$
2126	2.609	387.18195	$C_{23}H_{22}N_4O_2$

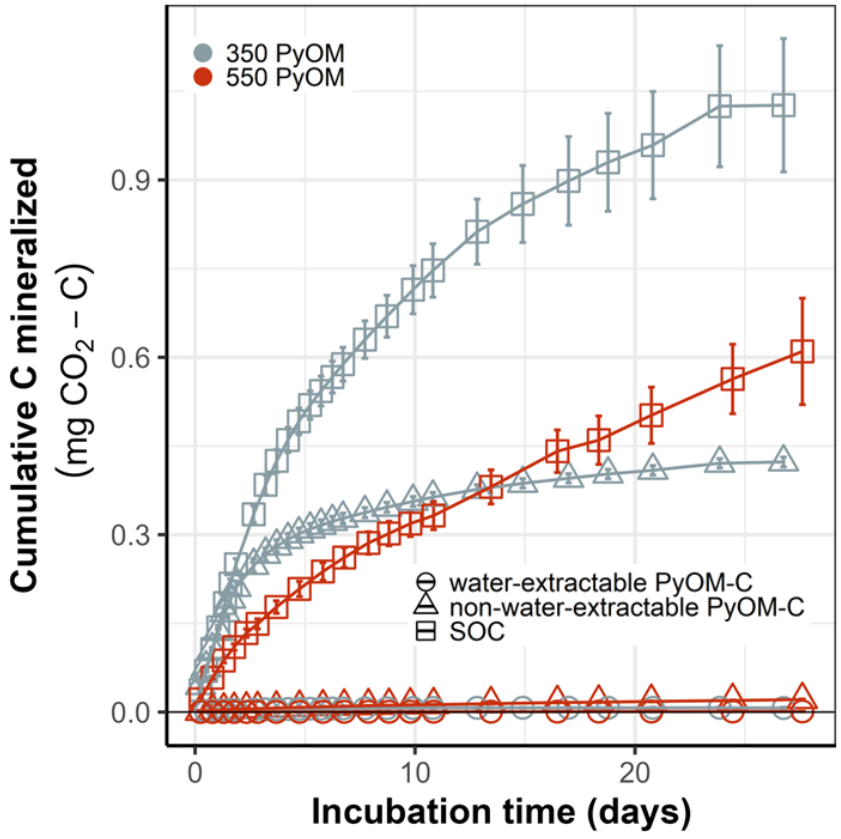

Figure S3.1. Mineralization of different fractions of PyOM over time.
Cumulative mean C mineralized for water-extractable PyOM-C, non-water-extractable PyOM-C and SOC. (n=4-5, error bars=SE).

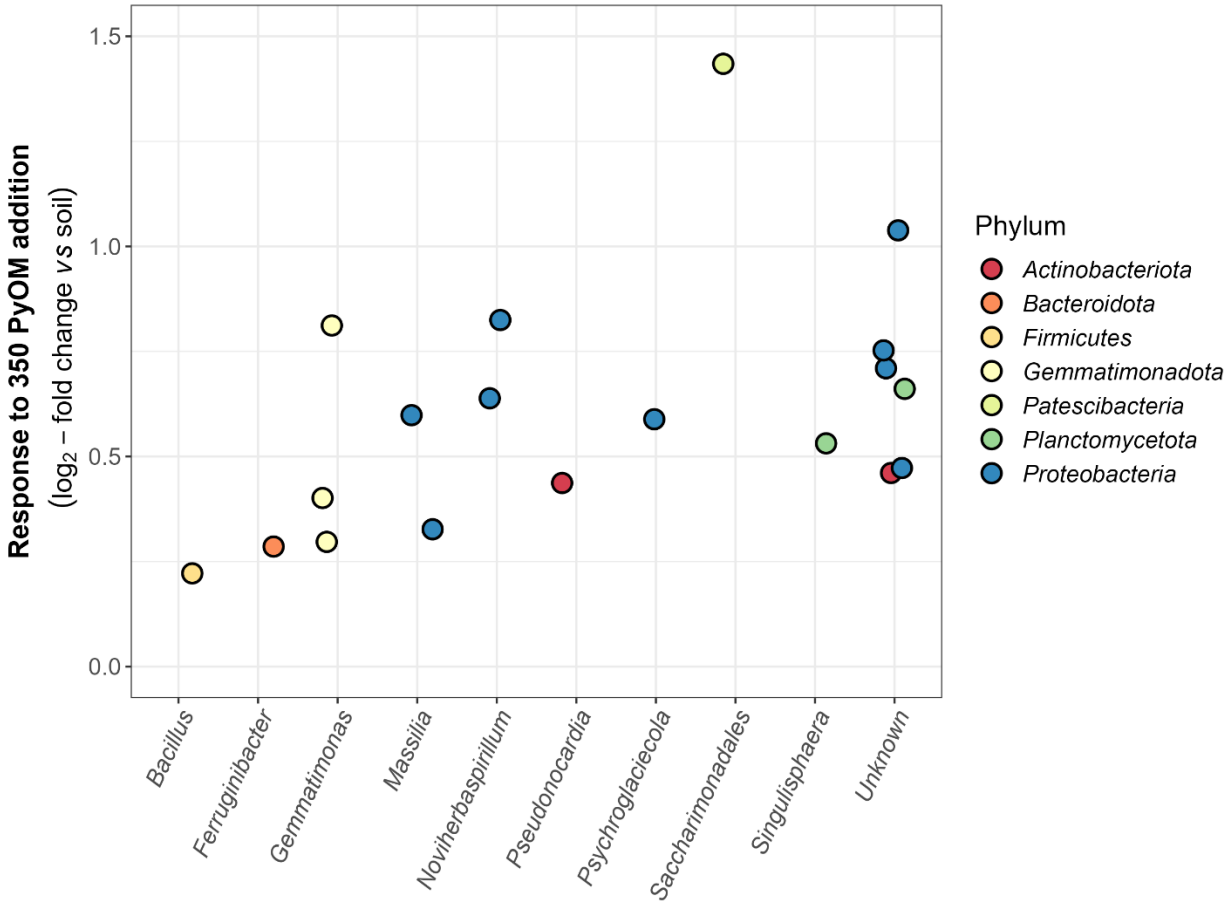

Figure S3.2. Bacterial response to 350 PyOM.
Log2-fold change in 350 PyOM amended vs. unamended soils, controlling for differences in taxon abundance across samples on Day 0 and over time. Each point represents a single 16S rRNA gene v4 region OTU with mean normalized count above the 25th percentile and that was significantly different in abundance in PyOM amended vs. unamended soils (Benjamini and Hochberg correction, adjusted p value < 0.05).

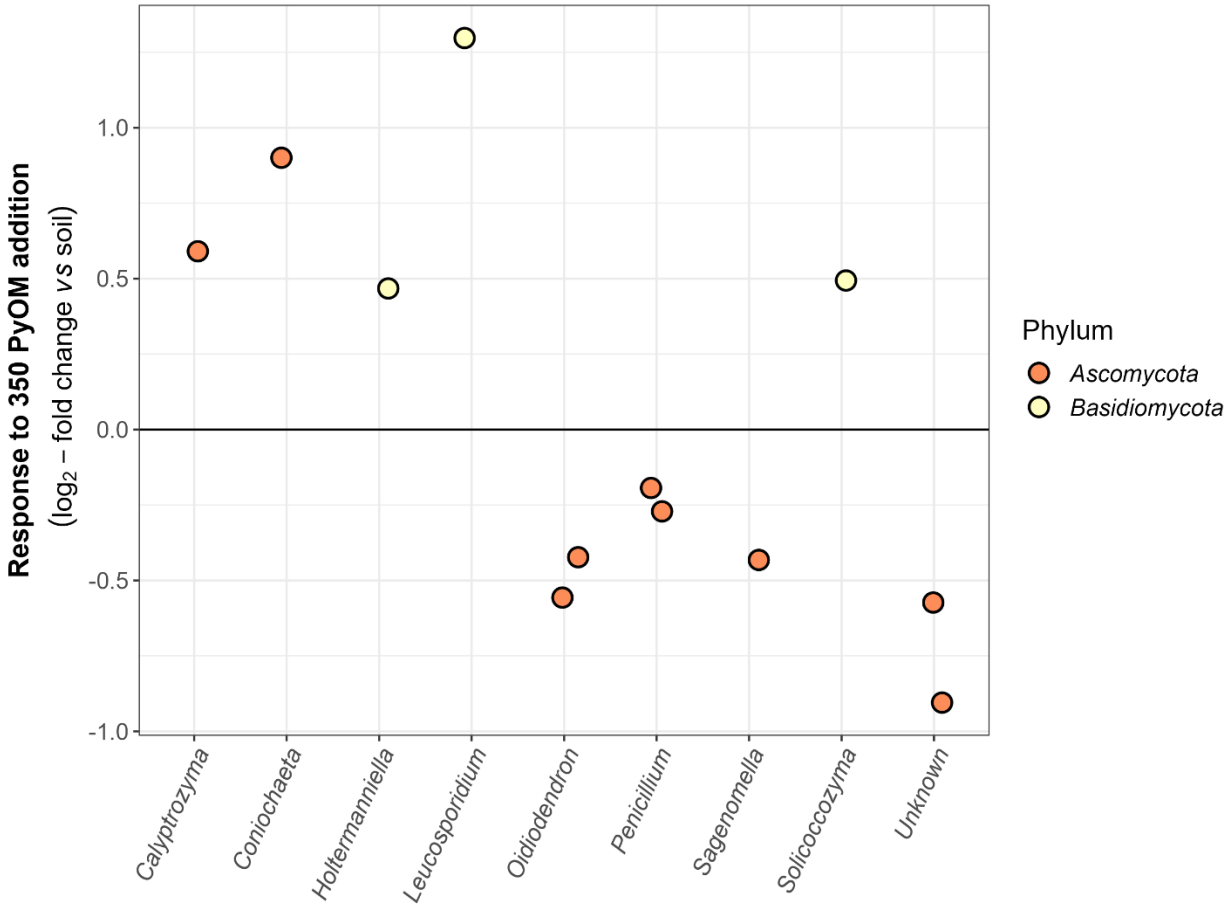

Figure S3.3. Fungal response to 350 PyOM.
Log2-fold change in 350 PyOM amended vs. unamended soils, controlling for differences in taxon abundance across samples on Day 0 and over time. Each point represents a single ITS2 gene OTU with mean normalized count above the 25th percentile and that was significantly different in abundance in PyOM amended vs. unamended soils (Benjamini and Hochberg correction, adjusted p value < 0.05).

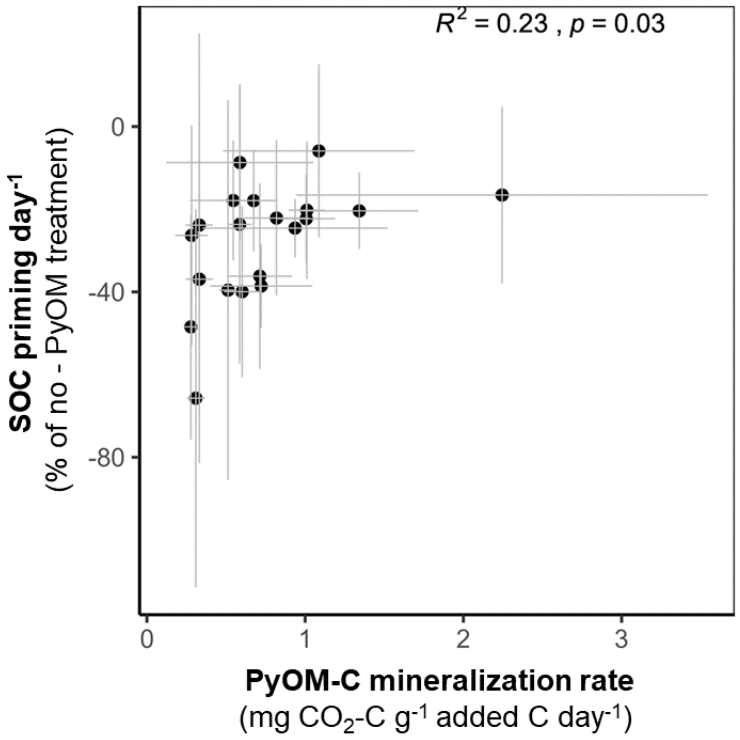

Figure S3.4. Relationship between mean PyOM-C mineralization rate and SOC priming for 550 C PyOM.
(n=4-5, error bars=SE)

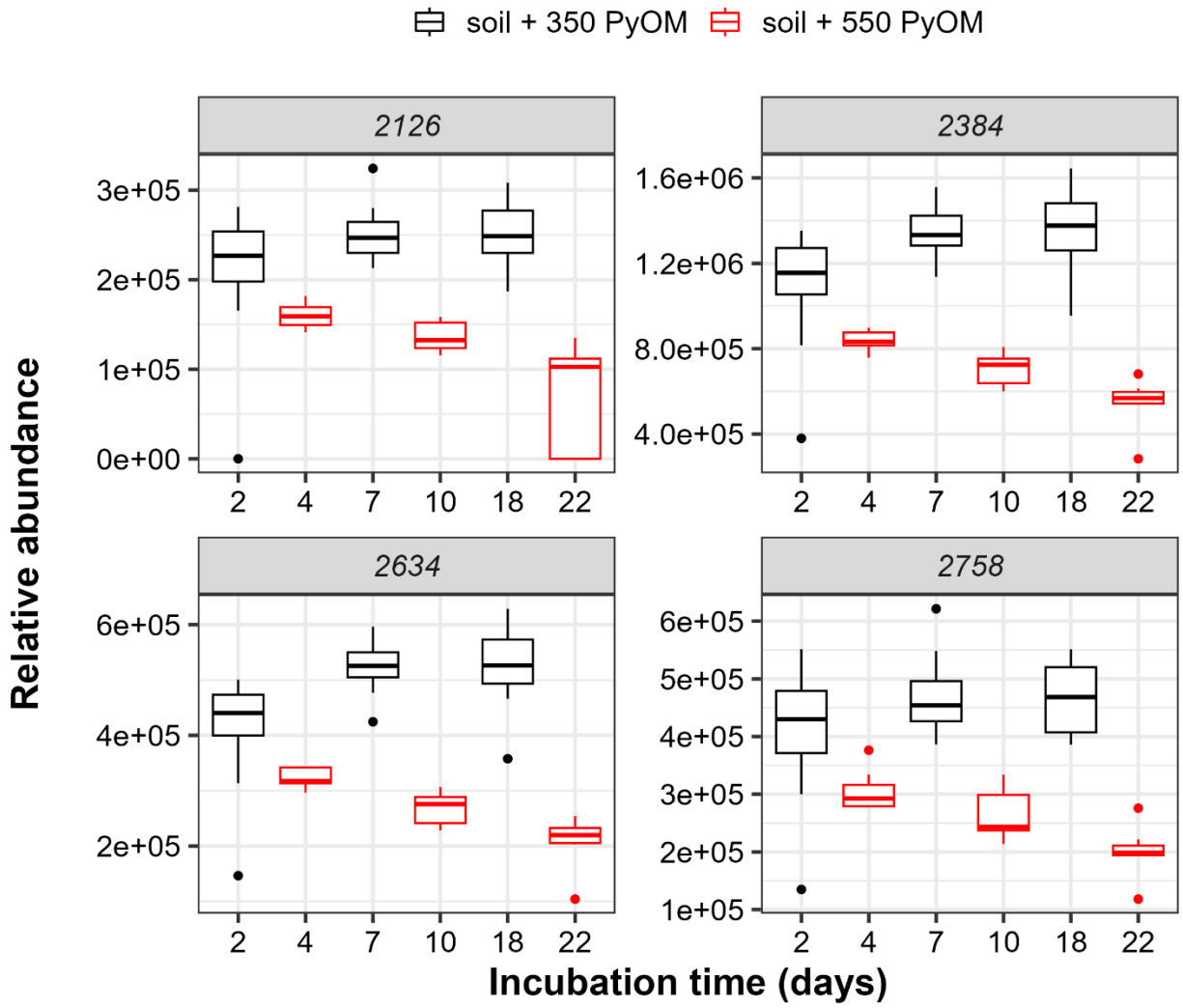

Figure S3.5. LC-MS features identified in PyOM amended soils.
Relative abundance of four LC-MS peaks over time observed only in the PyOM-amended soils (n=5-8). Colors indicate soils amended with 350 PyOM (black) and 550 PyOM (red).

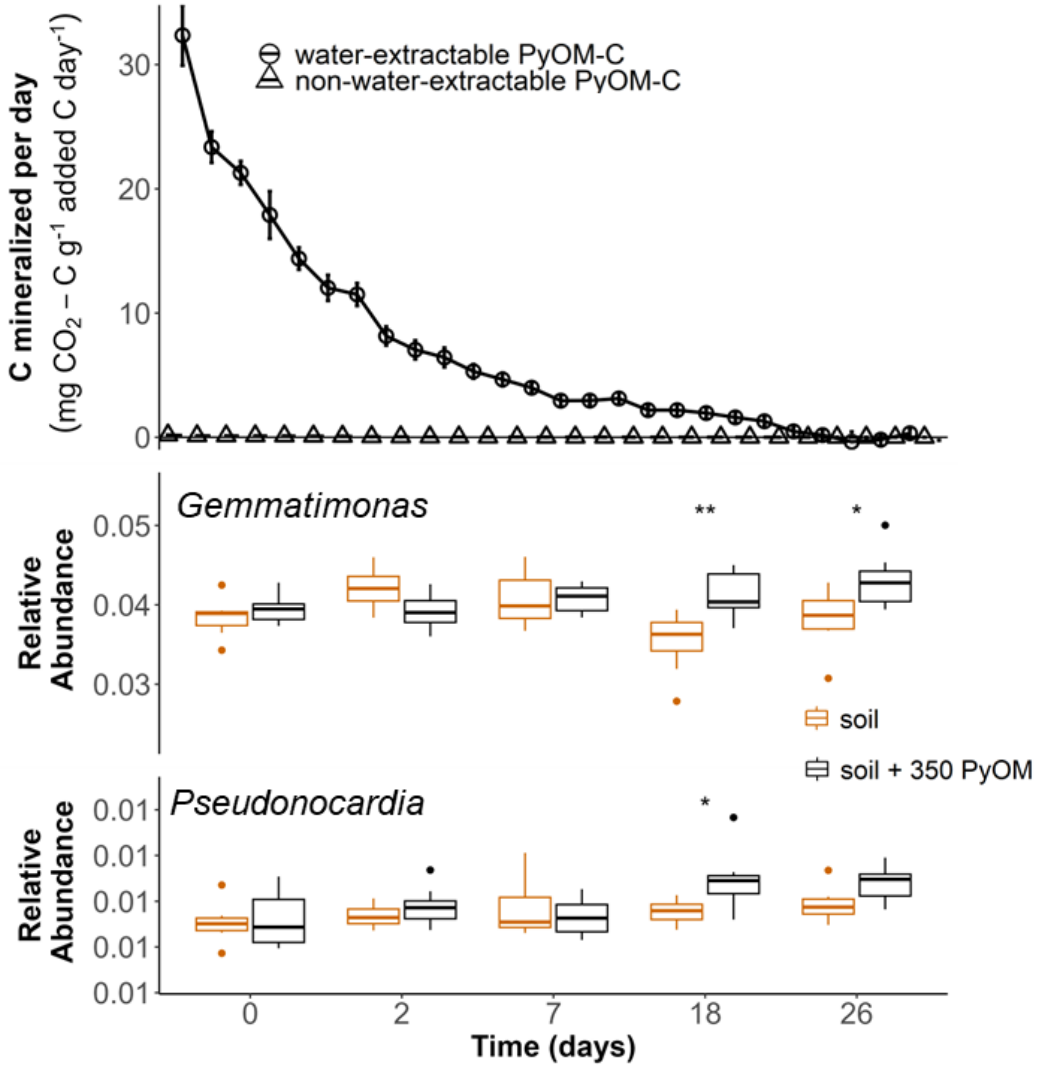

Figure S3.6. Late responders to 350 PyOM.
A) *Rate of 350 PyOM-C mineralization for water-extractable and non-water-extractable fractions (n=4-5, error bars=SE).* ***(B & C)*** *Relative abundance of positive responsive genera Gemmatimonas and Pseudonocardia over time observed in the unamended and 350 PyOM-amended soils (n=5-8). * indicates relative abundances that differ significantly from unamended soil at a given timepoint (t-test, $p < 0.05$).*

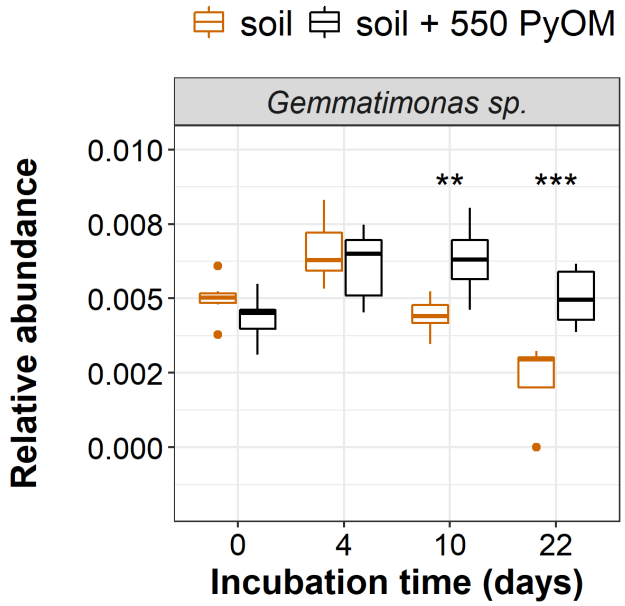

Figure S3.7. Response of Gemmatimonas sp. to 550 PyOM.
*Relative abundance of OTU belonging to genus Gemmatimonas over time in the unamended, and 550 PyOM-amended soils (n=5-8). * indicates relative abundances that differ significantly from unamended soil (t-test, *: $p < 0.05$; **: $p < 0.01$; ***: $p < 0.001$).*

Appendix S3

Additional details on $^{13}CO_2$ partitioning

We determined the fraction of CO_2 emitted from non-water-extractable PyOM ($f_{non\text{-}water\text{-}extractable\ PyOM}$) by partitioning the total CO_2 emissions from the "Soil + ^{13}C non-water-extractable PyOM" treatments into two sources: CO_2 emitted from the ^{13}C labeled non-water-extractable PyOM source and CO_2 emitted from the unlabeled soil and water-extractable PyOM source, as represented by Equation 1:

$$(1)\ f_{non\text{-}water\text{-}extractable\ PyOM} = (\delta_{Total\ CO2} - \delta_{CO2\ soil+water\text{-}extractable\ PyOM}) / (\delta_{CO2\ non\text{-}water\text{-}extractable\ PyOM} - \delta_{CO2\ soil+water\text{-}extractable\ PyOM})$$

In this equation, $\delta_{Total\ CO2}$ represents the isotopic composition of the total CO_2 emitted from the "Soil + ^{13}C non-water-extractable PyOM" treatments, $\delta_{CO2\ soil+water\text{-}extractable\ PyOM}$ represents the isotopic composition of the CO_2 emitted from soil and water-extractable PyOM fraction, determined from "Soil + unlabeled PyOM" treatments, and $\delta_{CO2\ non\text{-}water\text{-}extractable\ PyOM}$ represents the isotopic composition of the CO_2 emitted from non-water-extractable PyOM, which was assumed to be the isotopic composition of the ^{13}C labeled PyOM.

We determined the fraction of CO_2 emitted from SOC (f_{SOC}) by partitioning the total CO_2 emissions from the "Soil + ^{13}C PyOM" treatments into two sources: CO_2 emitted from the ^{13}C labeled PyOM source and CO_2 emitted from the unlabeled soil source, as represented by Equation 2:

$$(2)\quad f_{SOC} = (\delta_{total\ CO2} - \delta_{CO2\ PyOM}) / (\delta_{CO2\ SOC} - \delta_{CO2\ PyOM})$$

In this equation, δ_{total} represents the isotopic composition of the total CO_2 emitted from "Soil + ^{13}C PyOM" treatments, $\delta_{CO2\ PyOM}$ represents the isotopic composition of the CO_2 emitted from PyOM, which was assumed to be the isotopic composition of the ^{13}C labeled PyOM, and $\delta_{CO2\ SOC}$ represents the isotopic composition of the CO_2 emitted from SOC, determined from the "Unamended soil control" treatments.

CHAPTER FOUR: USING QUANTITATIVE STABLE ISOTOPE PROBING OF DNA TO IDENTIFY SOIL MICROBES THAT INCORPORATE PYROGENIC ORGANIC MATTER-CARBON

Nayela Zeba[1], Kelsey Kruger[1], Jamie Woolet[2], Timothy D. Berry[1] and Thea Whitman[1]

[1]Department of Soil Science, University of Wisconsin-Madison

[2] Department of Forest and Rangeland Stewardship, Colorado State University

Abstract

In the previous chapter, we demonstrated that the addition of pyrogenic organic matter (PyOM) affects microbial community composition and C mineralization and leads to a positive response in several groups of bacteria detectable at the genus level. However, the mechanisms underlying their response, particularly whether they are actually incorporating PyOM-C, remain unknown. In this study, we employed quantitative stable isotope probing (qSIP) of DNA with non-water-extractable ^{13}C-labeled PyOM to identify and quantify PyOM-C assimilation by specific bacterial taxa. We produced PyOM at 350 °C and amended soils that burned in 2014 in California with labeled ^{13}C non-water extractable PyOM. In parallel, we also measured CO_2 flux from PyOM-amended soils to investigate trends in non-water-extractable PyOM-C mineralizability.

We identified 30 true incorporators of non-water-extractable PyOM-C, many of which have been previously recognized as responders to both fire and PyOM amendments, such as species from the genera *Arthrobacter* and *Noviherbaspirillum*. Some of the incorporators, like those from the genus *Noviherbaspirillum*, exhibited high sequence similarity to significant positive responders identified in Chapter 3. All of the incorporators displayed low relative abundance in unamended soils (less than 1%) and most did not significantly increase upon PyOM addition. Only three incorporators, including one from the family *Blastocetallaceae*, showed significant increases in relative abundance (pairwise t-test, $p < 0.05$). Furthermore, we were able to detect evidence for predation, underscoring the role PyOM may play in the post-fire food web. Overall, this study provides valuable insights into the capacity of specific taxa to degrade PyOM-C and highlights the importance of PyOM-C availability as a substrate in post-fire soils.

Introduction

The addition of pyrogenic organic matter (PyOM) to soil has been observed to cause a shift in microbial community structure and an increase in the relative abundance of certain microbes (Whitman et al., 2021; Woolet & Whitman, 2020). In the previous chapter, we conducted a short-term study to examine the effects of PyOM on both the overall microbial community structure and individual taxa. We identified specific bacterial genera that increased in relative abundance in response to PyOM addition, many of which were noted for increased abundance in other PyOM-amended soil studies. However, a crucial question remains: *is this response due to the availability of carbon (C) or other changes in soil properties associated with PyOM addition?* Interestingly, some of the observed PyOM responders have previously been identified as pyrophilous, suggesting that the presence of PyOM might be as or more important for these microbes as other factors that enable them to thrive in post-fire environments, such as heat tolerance (Lee et al., 2017), fast growth, and tolerance or preference for fire-altered soil properties (Pérez-Valera et al., 2018). However, it remains unclear whether the relative increase of these taxa results from PyOM-C incorporation or other factors related to PyOM presence. To investigate these questions and determine whether previously documented PyOM responders increased in relative abundance due to PyOM-C consumption, we employed DNA Stable Isotope Probing (DNA-SIP) using ^{13}C-labeled PyOM, paired with bulk soil community sequencing.

Several studies suggest that microbial response to PyOM, over the short term, is mediated by PyOM-C availability (Lehmann et al., 2011; Whitman et al., 2014), but there is limited concrete evidence of actual PyOM-C consumption by microbes. Apart from lab incubations measuring the mineralization of ^{13}C-labeled PyOM-C substrates, as described in the previous chapter, other methods that have been used to infer PyOM-C consumption include pure culture

studies using PyOM-C as the sole carbon source (Fischer et al., 2021; Zeba et al., 2022), transcriptomics during growth on PyOM-C (Fischer et al., 2021), genome-resolved metagenomics identifying genes and pathways that are likely related to PyOM-C degradation (Dove et al., 2022; Nelson et al., 2022), and visualization of microbial colonization of PyC particles using microscopy techniques (Dai et al., 2017). However, in studies that rely on changes in relative abundance, accounting for and/or ruling out changes in soil properties such as pH and moisture upon PyOM addition may not be sufficient to infer PyOM-C consumption, as factors like PyOM's electrochemical and structural properties could still play a crucial role in microbial responses, as discussed in the previous chapter. Additionally, while isolate-based studies are powerful for confirming PyOM-C mineralization, they are fundamentally limited by cultivation techniques, in that we cannot study uncultivated organisms, and isolate-based studies also cannot capture complex ecological dynamics that would occur in a natural soil and may affect PyOM-C uptake.

Using a DNA-SIP approach enables us to identify microbes that definitively incorporate the ^{13}C labeled C in PyOM into their DNA, providing a direct link between the microbial identity and its metabolic activity *in situ* in PyOM-amended soils (Neufeld et al., 2007; Radajewski et al., 2000). We opted for quantitative stable isotope probing (qSIP) of DNA, as it not only identifies microbes that assimilate the labeled substrate but also allows quantification of the amount of ^{13}C incorporated into their DNA (Hungate et al., 2015). This offers valuable insights into the substrate utilization levels and metabolic preferences of different microbial taxa.

In Chapter 3, we demonstrated that the mineralizability of water-extractable PyOM-C was higher than both soil organic carbon (SOC) and non-water extractable PyOM-C. We also observed a temporal trend among the positively responsive bacteria, with certain genera like

Noviherbaspirillum increasing in relative abundance early on, corresponding with high rates of water-extractable PyOM-C mineralization in the incubation. In contrast, members of the *Pseudonocardia* genus increased at later time points, corresponding with lower rates of water-extractable as well as non-water-extractable PyOM-C mineralization. To capture microbes that respond to both fractions of PyOM-C, we performed qSIP at two separate time points, which were chosen based on the mineralization trends observed in the previous study (earlier for water-extractable and later for non-water-extractable PyOM-C). We focused on bacteria and 350 PyOM, which had the most responders. Using the same approach as in Chapter 3, we worked with PyOM produced from highly enriched ^{13}C-labeled pine trees and a set of control trees grown under natural abundance $^{13}CO_2$ conditions to detect taxa that can take up PyOM-C. While the experiment has been performed for both PyOM-C fractions, only the non-water-extractable data are presented in this chapter.

We hypothesized that PyOM-C would be incorporated by taxa previously identified as 350 PyOM responders, such as *Pseudonocardia* and *Gemmatimonas* sp. that were identified as late responders in Chapter 3. In addition, we hypothesized that taxa from other PyOM responsive genera like *Nocardioides* and *Mesorhizobium*, identified in Woolet and Whitman's (2020) meta-analysis would incorporate PyOM-C. We also expected to identify *Arthrobacter* and *Massilia* sp., known to be fire-responsive (Enright et al., 2022; Pulido-Chavez et al., 2023; Whitman et al., 2019), as true incorporators of PyOM-C. Finally, we also anticipated discovering previously undocumented taxa with potential aromatic degradation capacity.

Material and Methods

Soil description

The soil used in this study was the same as the one used in Chapter 3, collected in the winter of 2020 from sites that burned during the 2014 King Fire in California. The soil properties are provided in Table 3.1.

Biomass production

Two sets of eastern white pine seedlings (12 pots each) were grown from seed, one in a $^{13}CO_2$ rich atmosphere inside a custom ^{13}C-labelling growth chamber and another in ambient $^{13}CO_2$. The seedlings were pulse labelled with 99% $^{13}CO_2$ at regular intervals over a 6-month long growth period The seedlings were watered every other day and fertilized with a modified Hoagland solution once every two watering periods, while humidity and temperature were maintained at 60% RH and 21 °C, respectively, with an 18-hour photoperiod. The labeled biomass properties are shown in Table S4.1.

PyOM production and analyses

The aboveground biomass of eastern white pine trees was used to produce PyOM as described in the previous chapters. The stems and needles were ground separately, mixed at a 1:4 ratio, and pyrolyzed at 350 °C (referred to as "350 PyOM"). The resulting PyOM was ground and sieved to collect particles < 53 μm. Its pH was measured as described in Chapter 2, and other PyOM properties like total organic C, N, H and O and bulk $\delta^{13}C$ and $\delta^{15}N$ were measured at the Cornell Stable Isotope Laboratory (COIL). The properties of all PyOM materials are provided in Table 4.1.

Table 4.1. Properties of 350 PyOM

Property (units)	^{13}C labeled	Unlabeled
pH (H_2O)	8.37	8.25
Total organic C (%)	70.41 ± 3.9	65.23 ± 0.53
Total N (%)	3.55 ± 0.1	2.39 ± 0.02
Total H (%)	3.87 ± 1.71	3.03 ± 0.11
Total O (%)	22.93 ± 9.05	15.48 ± 0.59
Bulk $\delta^{13}C$ vs. VPDB (‰)	76,200.62 ± 744.10	-24.91 ± 0.67
Bulk $\delta^{15}N$ vs. atmospheric air (‰)	0.4 ± 8.11	0.78 ± 0.1
Total water extractable C (DOC) (mg g^{-1} PyOM)	2.18 ± 0.01	2.67 ± 0.03

The values presented for total organic C, total N, total H, total O, bulk $\delta^{13}C$ and bulk $\delta^{15}N$ are means of five replicates ± standard deviation. The values for water-extractable C represent DOC in original PyOM before exchange. pH values of the PyOM before adjustment are shown.

Water-extractable PyOM-C extraction and exchange

To study the microbial assimilation of PyOM-C fractions, we removed and exchanged the water-extractable fraction from the ^{13}C labeled and unlabeled 350 PyOM following the protocol described in Chapter 3. This resulted in two PyOM treatments: PyOM where the water-extractable fraction is ^{13}C-labeled and PyOM where the non-water-extractable fraction is ^{13}C-labeled. We also extracted the water-extractable fraction for the unlabeled PyOM sample and returned it at the same rate, using it as a control in the SIP experiment to compare the extent of ^{13}C incorporation in the labeled incubations.

The samples were pH-adjusted to match the soil pH and dried at 70 °C before use in the incubation study. The total dissolved organic carbon (DOC) content of the water-extractable PyOM-C fraction was measured at the Water Science and Engineering Laboratory, UW-Madison using a Sievers M5310C Total Organic Carbon Analyzer (GE Analytical Instruments Inc., CO,

USA). Before returning the DOC to the non-water-extractable PyOM, we measured properties of the non-water-extractable PyOM (Table 4.2). The concentration of water-extractable PyOM-C in all PyOM treatments was selected to match the DOC concentration of the water-extracted PyOM for the ^{13}C labeled 350 PyOM treatment (Table 4.1). Thus, all 350 PyOM treatments had 2.18 mg water-extractable PyOM-C g^{-1} PyOM, ensuring equivalent levels of water-extractable PyOM-C in both the labeled and unlabeled PyOM treatments.

Table 4.2. Properties of non-water-extractable 350 PyOM

Property (units)	^{13}C labeled	Unlabeled
pH (H_2O)	7.81	7.95
Total organic C (%)	68.67 ± 1.96	65.49 ± 0.47
Total N (%)	3.56 ± 0.16	2.35 ± 0.02
Total H (%)	3.21 ± 0.73	3.10 ± 0.03
Total O (%)	17.70 ± 2.99	15.21 ± 0.19
Bulk $\delta^{13}C$ vs. VPDB (‰)	70068.54 ± 5924.88	-26.06 ± 0.15
Bulk $\delta^{15}N$ vs. atmospheric air (‰)	-7.28 ± 2.88	0.98 ± 0.13

The values presented for total organic C, total N, total H, total O, bulk $\delta^{13}C$ and bulk $\delta^{15}N$ are means of five replicates ± standard deviation. pH values of the PyOM before adjustment are shown.

Incubation setup

To prepare for incubation, the soil was thawed, sieved to < 2 mm, and kept moist and at room temperature for two weeks with exposure to the air. To ensure equivalent moisture levels, we determined the field capacity for unamended soil and 350 PyOM-amended soil separately by using a sub-sample of the soil (following Whitman et al. 2021). The moisture content of the thawed soils was measured one day before the start of incubation to determine the water required to achieve the target moisture level of 65% field capacity for each treatment.

All incubations were conducted in sterile 30 mL polypropylene jars (Dynalab Corp., NY, USA) placed inside half-pint-sized Mason jars (118 mL). Each 30 mL jar received 2 g soil on a dry mass basis, and the soil-PyOM amended jars received PyOM at a consistent rate of 50 mg PyOM g^{-1} dry soil (*i.e.*, 2.5% dry mass addition rate). This addition rate was comparable to the addition rate for 350 PyOM in the previous chapter (3.1% dry mass addition), designed to represent locally high inputs of PyOM after a wildfire and enable sufficient ^{13}C isotope incorporation to be detectable using qSIP. We temporarily capped the jars and rolled them to mix the soil with PyOM. Unamended soil jars were also capped and rolled to maintain consistency. We added water drop-wise to gradually bring up the moisture of each jar to the target moisture level of 65% field capacity.

For the qSIP pipeline, six replicates each of the Soil + ^{13}C water-extractable PyOM and the control Soil + unlabeled PyOM treatments were destructively sampled after 7 days of incubation to identify microbes that incorporated the water-extractable PyOM-C fraction, and six replicates each of the Soil + ^{13}C non-water-extractable PyOM and the control Soil + unlabeled PyOM treatments were destructively sampled after 21 days of incubation to identify incorporators of the non-water-extractable PyOM-C fraction. These sampling time points were selected based on the C mineralization pattern of the PyOM fractions observed in Chapter 3 to maximize our chances of identifying incorporators specific to each fraction. While all treatments were collected and processed as described below, in this chapter, we only consider qSIP data for the Soil + ^{13}C non-water-extractable PyOM treatment (and its unlabeled control). At each sampling time point, six jars were destructively sampled and stored at -80 °C until DNA extraction was performed. In addition, six replicate unamended soil jars were also destructively sampled at both these time points to assess changes in microbial community composition with

PyOM additions. Six unamended soil samples were also randomly selected and frozen during setup to represent the community profile on Day 0.

We extracted DNA from each soil sample using the DNEasy PowerLyzer PowerSoil DNA extraction kit (QIAGEN, Germantown, MD), following the manufacturer's instructions. One blank extraction without soil was included for every 24 samples. Extracted DNA was quantified, and 3-4 µg DNA of each sample chosen for qSIP analysis was shipped on dry ice to the DOE Joint Genome Institute, Lawrence Berkeley National Laboratory, California, USA for density gradient centrifugation and fraction collection. Briefly, DNA samples were separated into 24 SIP density gradient fractions of approximately 220 µL in a buffer containing cesium chloride ($CsCl_4$) by centrifuging at 190,600 x g for 120 h at 20 ºC in a Beckman Coulter ultracentrifuge using a VTi65.2 rotor (cat# 362754; Beckman Coulter Inc., IN, USA). The density of each fraction was measured, and the DNA was purified, resuspended, and quantified for downstream analysis. The detailed procedure for fractionation and subsequent purification is described in Nuccio et al. (2022) and Vyshenska et al. (2022).

Quantitative PCR (qPCR) of the 16S rRNA gene

We determined the total numbers of bacterial 16S rRNA gene copies in each density fraction by quantitative PCR (qPCR) using the methods described in Whitman et al. (2019). All fractions were analyzed in triplicate targeting the 16S rRNA gene v4 region with 515f and 806r primers (Carini et al., 2016). The reactions were carried out in a UV-sterilized PCR Workstation to minimize the risk of contamination. We used Hard-Shell® low profile, skirted 96-Well PCR Plates (cat# HSP9665, Bio-Rad Laboratories, Inc., CA, USA) to perform the reactions, with each well containing a total volume of 20 µL. The reaction mix consisted of 10 µL SsoAdvanced™ Universal SYBR® Green Supermix (Bio-Rad Laboratories, Inc., CA, USA), 1 µL each of the

forward and reverse primers (10 µM), 1 µL of DNA extract (diluted 1:5), 1 µL of bovine serum albumin (BSA) (20 mg ml^{-1}) (VWR, PA, USA), and 6 µL of PCR-grade water. We sealed the PCR plates with Microseal® 'B' Adhesive Seals (cat# MSB1001, Bio-Rad Laboratories, Inc., CA, USA). The reactions were carried out on a CFX96 Touch™ Real-Time PCR Detection System (Bio-Rad Laboratories, CA, USA), using the following cycling conditions: 98 °C for 3 min, followed by 45 cycles of 95 °C for 15 s, 60 °C for 30 s, and a plate read. After amplification, we performed a melt curve analysis to ensure specificity, by heating the samples to 65 °C for 5 s, followed by a 0.5 °C $cycle^{-1}$ temperature ramp, and a plate read, repeated for a total of 60 cycles.

We included calibration standards and no-template controls (NTCs) on each plate in triplicate. To generate calibration standards, we used genomic DNA from a *Streptomyces* sp. isolate with a known 16S rRNA gene sequence, which we sourced from our lab's collection. We prepared two calibration standards, Std-1 (2.89×10^9 copies μL^{-1}) and Std-2 (3.94×10^9 copies μL^{-1}), which were aliquoted and stored in a -20 °C freezer. To create standard curves, we serially-diluted the calibration standards to create a 7-point calibration curve spanning 2.89×10^3 - 2.89×10^8 copies μL^{-1} for Std-1 and 3.94×10^2 - 3.94×10^7 copies μL^{-1} for Std-2, which encompassed the range of sample values.

After amplification, we analyzed the data using Bio-Rad CFX Manager 3.1 (Bio-Rad Laboratories, Inc., Hercules, CA), exporting the results as .csv files. To calculate the number of bacterial 16S rRNA gene copies in each sample, we generated standard curve equations by plotting the average Cq values of each standard against the known copy number in Microsoft Excel (Version 2302) and fitting a logarithmic regression curve. We re-amplified samples if the

R^2-value of the calibration curve was less than 0.99 using at least 5 points in the standard curve. Raw Cq values and calibration curve results are provided in Appendix S4.

Sequencing the 16S rRNA gene, data processing and taxonomic assignments

To characterize community composition of each fraction, we performed PCR in triplicate on all density fractions to amplify the 16S rRNA gene v4 region with the barcoded 515f and 806r primers (Walters et al., 2015), and Illumina sequencing adapters added as per Kozich et al. (2013). During PCR, we included one negative control (PCR-grade water) and one positive control (known microbial community mix) for every 30 samples. The PCR amplicon triplicates for all DNA fractions including the extraction blanks and PCR controls were pooled, purified and normalized and library cleanup was performed. A detailed procedure for the PCR amplification and purification is described in Chapter 3 and Whitman et al. (2019). We submitted the pooled library to the UW Madison Biotechnology Center (UW-Madison, WI) for 2x250 paired end Illumina MiSeq sequencing.

We used the QIIME2 pipeline (QIIME2, version 2020.6; Bolyen et al., 2019) to process the sequences following the steps described in Chapter 3 and Woolet and Whitman (2020). The sequence processing steps were performed on the UW-Madison Centre for High Throughput Computing cluster (Madison, WI).

qSIP analysis

We used R Studio (version 4.2.2; R Core Team, 2022) for data analysis and visualization. The raw OTU table consisted of 20,259 taxa which were further quality-filtered using the 'tidyverse' (Wickham et al., 2019) and 'phyloseq' (McMurdie & Holmes, 2013) packages based on the steps described in Coskun et al. (2022). We removed 1576 OTUs that belonged to "Chloroplast" and "Mitochondria". We subsetted taxa originating from soil as those for which

the total number of reads summed across all soil samples (PyOM amended and unamended) was at least 10 times greater than the total reads summed across all negative control samples (extraction blanks and PCR controls). A total of 1680 OTUs were removed based on comparing sequence reads in negative controls to the samples, comprising 1.68% of the entire 16S rRNA gene dataset (81,142 sequence reads out of 4,837,961). This OTU table was used for qSIP assessment as well as comparing relative abundances between the bulk unfractionated DNA samples from different soil treatments and measurement time points.

For qSIP, only OTUs that had sequences present for every sample (summed across all density fractions) were selected for assessment. The ^{13}C atom fraction excess (AFE) value for each OTU was calculated, following the qSIP workflow embedded in the 'HTS-SIP' R package (Hungate et al., 2015; Youngblut et al., 2018). We ran bootstrap replicates (n = 1000) within each treatment to estimate taxon - specific 90% confidence intervals (CI) for change in density and to identify significant isotope incorporation. An OTU was considered a true incorporator if the lower boundary of the CI was above the 0% AFE cutoff (Hungate et al., 2015).

We used the "pairwise.t.test" function from the 'stats' R package to test for significant differences in relative abundances between the bulk unfractionated DNA of the unlabeled PyOM-amended and unamended soils for the incorporators identified using qSIP. We used the same test to compare relative abundance of incorporators in the bulk unfractionated DNA of the unamended soils at different sampling time points. The Github repository github.com/nayelazeba/Chapter4 contains files related to quality filtering and qSIP analysis.

CO_2 flux monitoring, partitioning and statistical analyses

We monitored CO_2 emissions in all jars until they were destructively sampled to trace both PyOM-C and SOC mineralization. To inform flux partitioning, six replicates of the Soil +

^{13}C PyOM treatment, as well as an additional six replicates of the Soil + ^{13}C water-extractable PyOM treatment, were included, and gas fluxes from these jars were sampled until the end of the incubation period. We included two empty jars as gas flux blanks.

To maintain humidity and prevent water loss, we placed the 30 mL jars inside half-pint-sized Mason jars (118 mL) containing 10 mL of acidified deionized water (pH ~4) and capped them with sterile, gas-tight lids fitted with CO_2 gas measurement fittings. The jars were connected to randomly selected positions on distribution manifolds (Berry et al., 2021), and flushed with a 400 ppm CO_2 -air gas mixture to reset the headspace CO_2 concentration at the initial time point. We measured the emitted CO_2 in the headspace of each jar at frequent intervals by withdrawing 20 mL of gas using a 25 mL SGE gastight syringe (cat # 009462, Trajan Scientific and Medical, Victoria, Australia). The collected gas was injected into evacuated Labco® 12 mL Exetainer vials (Labco Limited, Ceredigion, United Kingdom), and the headspace CO_2 concentration and $\delta^{13}C$ were measured at COIL using the Thermo Delta V isotope ratio mass spectrometer interfaced to a Gas Bench II. We collected headspace gas samples at intervals of 48 h during the first week and intervals of 72 h during the last two weeks of incubation. After each gas sampling, we flushed the jars with the 400 ppm CO_2 - air gas mixture to prevent oxygen depletion and excessive CO_2 accumulation inside the jars. The precise concentration after flushing each jar was measured and subtracted from the next time point reading to calculate the emitted CO_2 in the jar during that interval. We checked the mass of the jars once a week to determine moisture loss and added water to return jars to target moisture levels.

We processed raw CO_2 readings from the multiplexer-Picarro system and partitioned CO_2 emissions from the flux monitoring treatments using stable isotope partitioning (as described in

Chapter 3) to determine the fraction of CO_2 emitted from water-extractable PyOM, non-water-extractable PyOM, and soil in the soil-PyOM amended incubations. We normalized the amount of C mineralized with the quantity of each carbon source added to the jars to determine the mineralizability of each PyOM-C fraction.

We assessed normality and homogeneity of variance across treatment groups using the Shapiro and Bartlett test functions in the R 'stats' package. Welch's ANOVA was employed to test for significant differences in mineralizability between the PyOM-C fractions and SOC, due to unequal variances. The Games-Howell post-hoc test function in the 'rstatix' package (Kassambara, 2022) was used to compare mineralizability between different treatment pairs. All code used for flux partitioning, analyses and figures in this chapter is available at github.com/nayelazeba/Chapter4.

Results

PyOM – C incorporators

In all ^{13}C-non-water-extractable PyOM soil incubations, a shift in peak DNA buoyant density was observed in the range of 0.0023 and 0.01124 g mL^{-1} compared to the average peak DNA buoyant density of control unlabeled PyOM soil incubations, indicating ^{13}C incorporation in the 16S rRNA genes (Fig. 4.1). Despite this small shift in density of total DNA, we were able to detect significant shifts in ^{13}C atom fraction excess (AFE) for 30 taxa (Fig. 4.2). Among these, the phylum *Proteobacteria* had the most taxa that showed ^{13}C PyOM incorporation (Fig. 4.3). The highest PyOM-C incorporation was observed for taxa belonging to the families *Sphingomonadaceae* (0.4 AFE), *Xanthobacteraceae* (0.34 AFE), and *Oxalobacteraceae* (0.24 AFE).

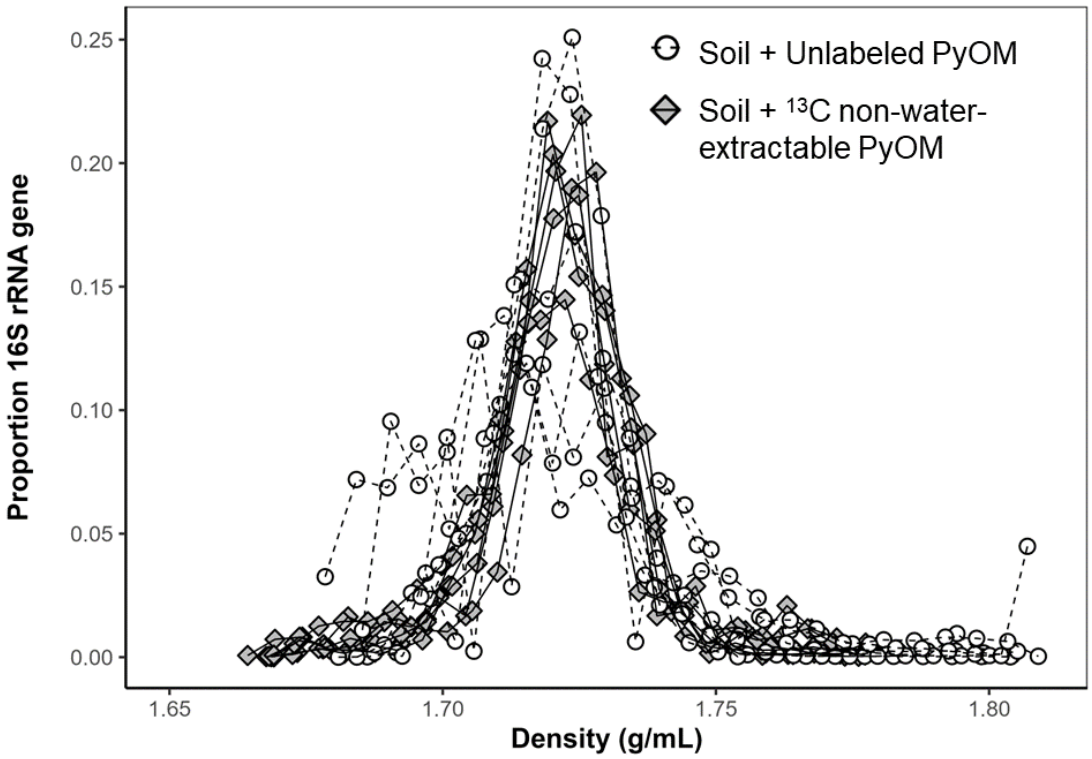

Figure 4.1. The relative abundance of bacterial 16S rRNA gene copies as a function of density of CsCl in the corresponding fraction.

Soils amended with ^{13}C non-water-extractable PyOM (n = 6) are represented by solid lines and filled diamonds, and soils amended with unlabeled PyOM (control; n = 6) are represented by dashed lines and open circles. The y-axis represents the relative abundance of 16S rRNA genes in each density gradient fraction quantified with qPCR, normalized to maximal abundance across all density fractions in that replicate.

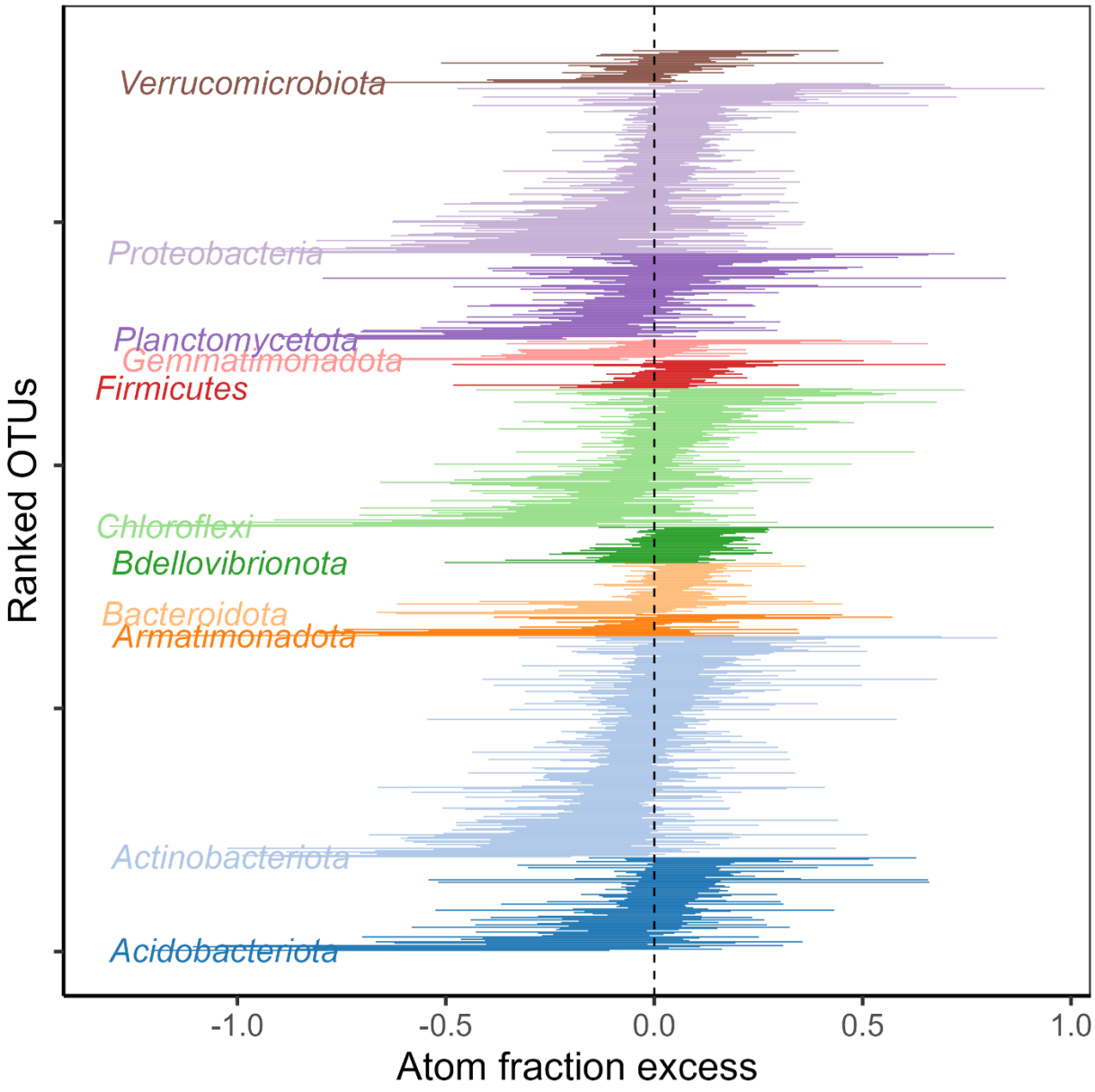

Figure 4.2. OTU-specific shifts in the ^{13}C atom fraction excess (AFE) for ^{13}C non-water-extractable PyOM.

Each line represents the AFE values of all OTUs in the 11 most abundant phyla in the qSIP samples, color-coded and labeled by phylum. Error bars indicate 90% confidence intervals across six replicates. OTUs with non-overlapping 90% CIs with 0 are considered to be significantly ^{13}C-enriched.

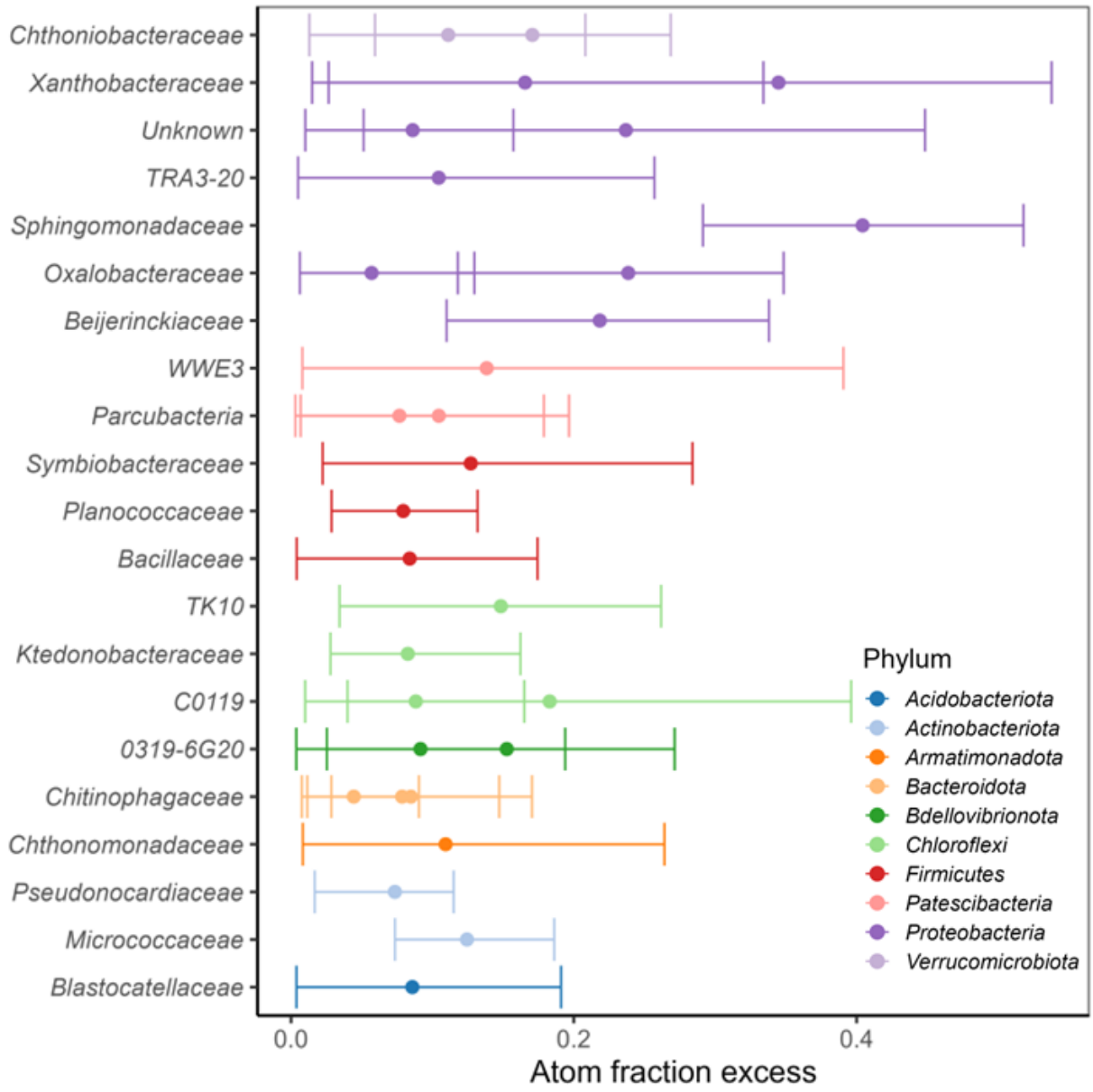

Figure 4.3. ^{13}C AFE values of significant non-water-extractable PyOM-C incorporators.
Each data point represents the AFE value of incorporator OTUs identified using qSIP, labeled by their family assignments and color-coded by phylum. Error bars represent 90% CI across six replicates.

Effect of PyOM addition on bacterial communities

We observed significant shifts in the overall bacterial community composition in response to the addition of 350 PyOM on Day 21 (PERMANOVA, $p_{PyOM} < 0.01$, $R^2_{PyOM} = 0.11$,

Fig. 4.4). We also observed a shift in the bacterial communities of unamended soils from Day 0 to Day 21 (PERMANOVA, $p_{time} < 0.01$, $R^2_{time} = 0.10$).

Of the twelve incorporators most abundant in initial unamended soils, only the OTU from the family *Blastocatellaceae* showed a significant increase in median relative abundance in PyOM-amended soils on Day 21, which was 4 times higher than unamended soils (Fig. 4.5). However, for the other incorporators, there was no significant change in relative abundance between PyOM-amended and unamended soils. Furthermore, the median relative abundance of nine of the most abundant incorporators remained very low, close to 0, in both unamended soils and PyOM-amended soils.

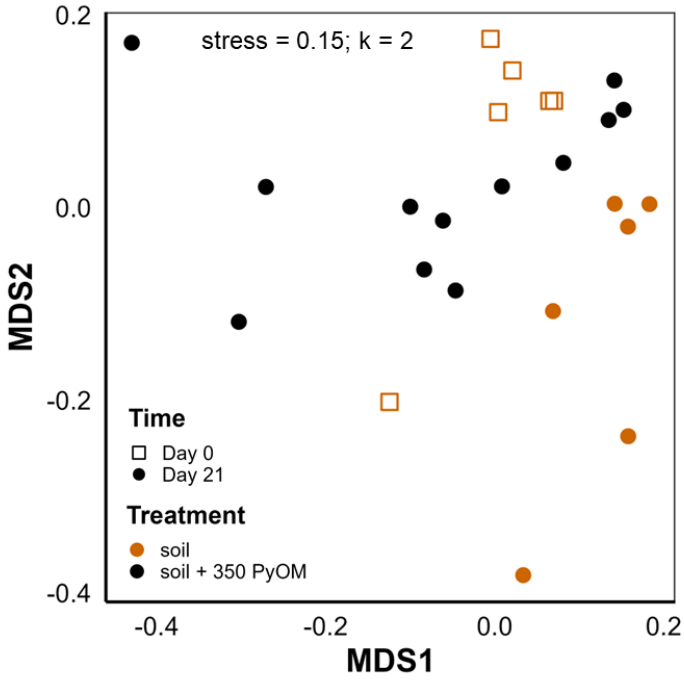

Figure 4.4. Effect of 350 PyOM addition on soil bacterial community composition.
Non-metric multidimensional scaling (NMDS) ordination plot of Bray-Curtis dissimilarities between bacterial/archaeal communities (16S rRNA gene v4 region). Orange points represent data from unfractionated DNA of unamended soil controls on Day 0 (squares) and Day 21 (circles). Black points represent data from unfractionated DNA of 350 PyOM-amended soils (both ^{13}C labeled and unlabeled PyOM) on Day 21.

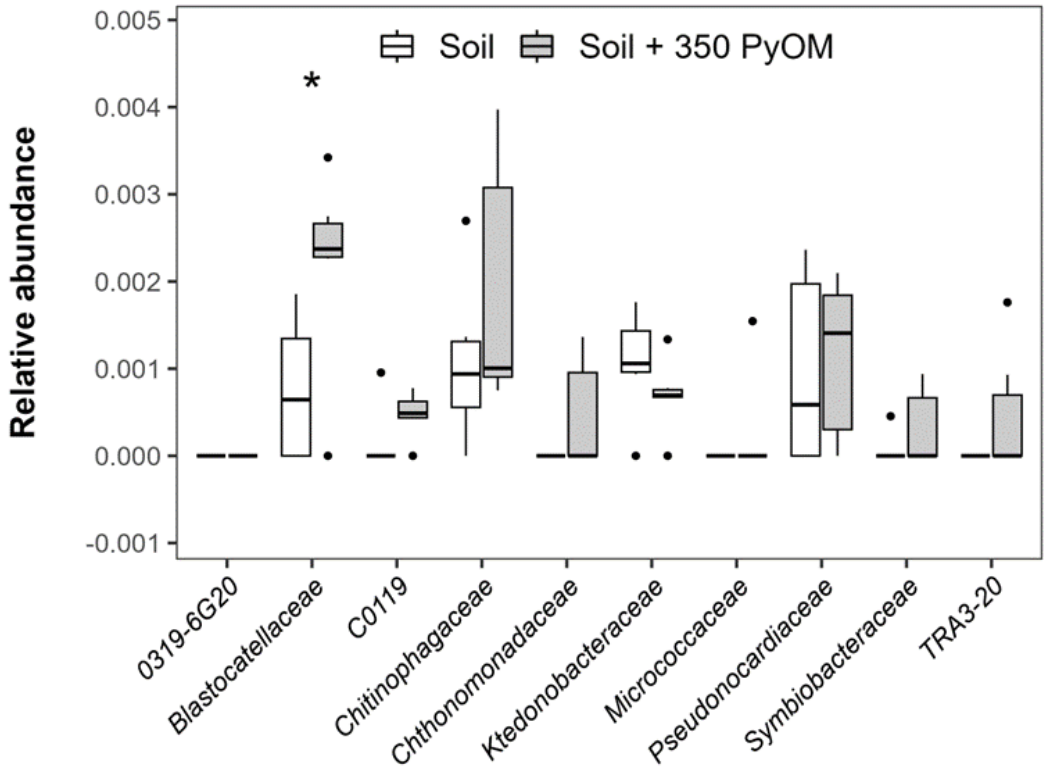

Figure 4.5. Relative abundance changes among the 350 PyOM-C incorporators.
Relative abundance of the twelve most abundant PyOM-C incorporator OTUs (identified using qSIP) in unfractionated DNA of unamended soils (n = 6) and unlabeled 350 PyOM-amended soils (n=6) on Day 21. The x-axis labels indicate the family level assignment of the OTUs. Where multiple incorporator OTUs were present in a family (Chitinophagaceae, n=3), all OTUs are summed. Asterisks indicate statistically significant differences in relative abundance (= $p < 0.05$).*

PyOM-C and SOC flux dynamics

At the end of the incubation period, mineralizability of the water-extractable fraction of 350 PyOM-C was significantly higher than that of the non-water-extractable PyOM-C fraction and SOC ($p < 0.05$, Games-Howell post-hoc test; Fig. 4.6.A). The amount of C mineralized per gram of added C from the water-extractable fraction was 64 and 55 times higher than the non-water-extractable PyOM-C and SOC, respectively. However, total C mineralization from the water-extractable PyOM-C fractions was lower due to the small fraction of total carbon it

represented in each jar (Fig. 4.6.B). Until day 15, the C mineralizability of the non-water-extractable PyOM-C fraction was higher than that of SOC but this trend reversed after that (Fig. 4.6.C). The addition of 350 PyOM did not significantly affect the mineralizability of the SOC (Fig. 4.6.D).

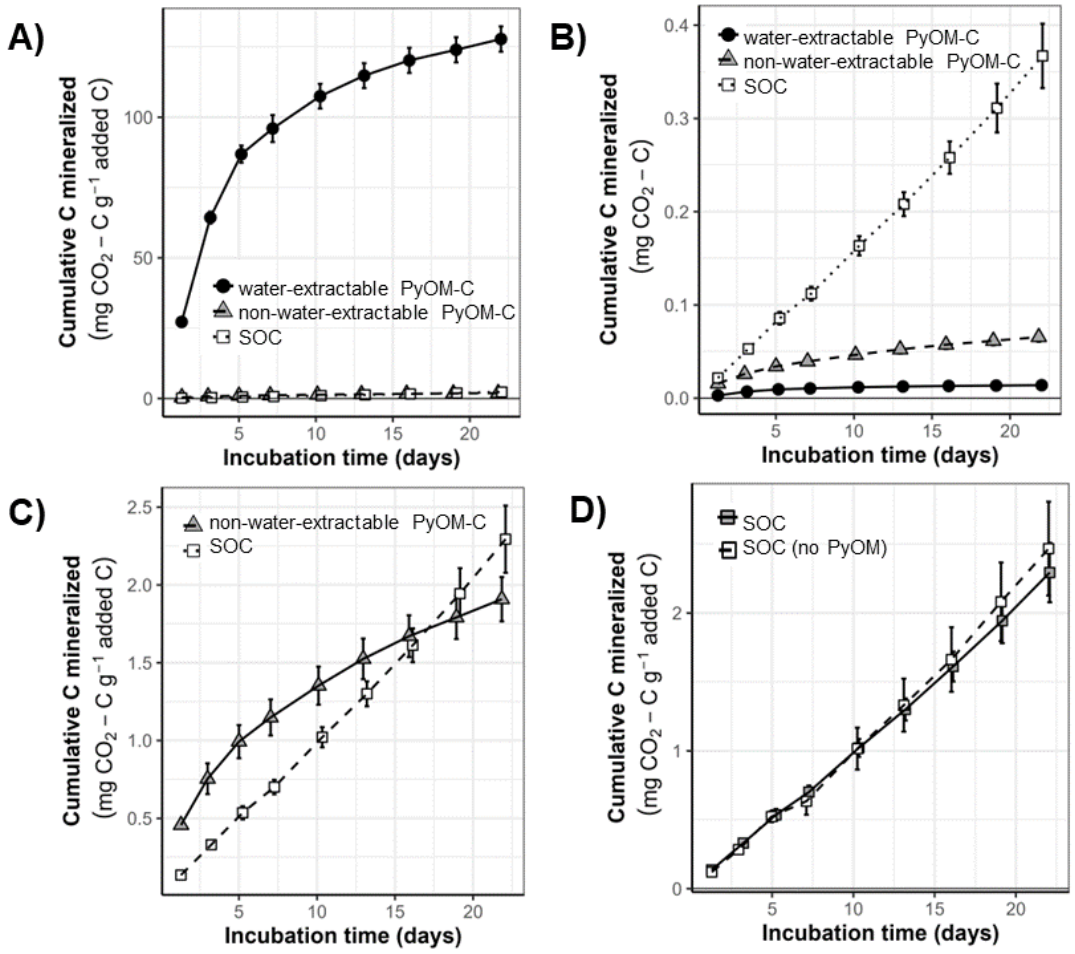

Figure 4.6. Carbon mineralization of 350 PyOM fractions over time.
A) *Cumulative mean C mineralization per gram of added C (mineralizability) for water-extractable PyOM-C, non-water-extractable PyOM-C, and SOC.* ***B)*** *Cumulative mean C mineralization for water-extractable PyOM-C, non-water-extractable PyOM-C and SOC in each jar.* ***C)*** *Mineralizability of non-water-extractable PyOM-C and SOC.* ***D)*** *Mineralizability of SOC in unamended soil control and 350 PyOM amended soils. (n = 6-12, error bars=SE).*

Discussion

The analysis of peak DNA density in ^{13}C non-water-extractable PyOM-amended soils compared to unlabeled PyOM-amended soils (controls) revealed a small and variable shift in peak DNA density (Fig. 4.1). This indicates that only a small fraction of the microbial community took up the ^{13}C label in PyOM, as expected, since PyOM-C incorporation is likely carried out by a select group of microbes capable of breaking down the high proportion of condensed aromatic C structures in PyOM. The variability between replicates also suggests inconsistent ^{13}C incorporation and may also help explain why only 30 true incorporators of non-water-extractable PyOM-C were identified. However, to our knowledge there have been no previous studies of DNA-SIP with ^{13}C-labelled PyOM, making the conclusive identification of even a handful of PyOM-consuming species of interest.

Taxa incorporating PyOM-C include known fire and PyOM responders

Interestingly, many of the incorporators have been identified as responders to both fire and PyOM amendments (Fig. 4.3). For instance, members of the genus *Arthrobacter* (*Micrococcaceae* family) were significant positive fire responders one-year post-fire and continued to be enriched in the same soils five years later. This enrichment was partially attributed to their potential ability to degrade PyOM but could not be confirmed under that experimental design (Whitman et al., 2019, 2022). Our study adds further support to these findings by confirming the capacity of an *Arthrobacter* species to consume PyOM-C. Notably, the *Arthrobacter* incorporator also exhibited high sequence similarity (> 98% identity) to a significant responder from the *Micrococcaceae* family in our previous 350 PyOM incubation in Chapter 3.

Similarly, two incorporator taxa from the *Oxalobacteraceae* family had high sequence similarity (> 98% identity) to *Noviherbaspirillum* species identified as positive responders to 350 PyOM. In Chapter 3, we also demonstrated a significant positive response to 350 PyOM for *Noviherbaspirillum* at the genus level, which was one of the three genera that consistently responded to PyOM across various studies (Woolet & Whitman, 2020). This congruence of results validates our previous findings and highlights the ability of *Noviherbaspirillum* species to degrade PyOM-C. Additionally, Pulido-Chavez et al. (2023) reported an increase in the abundance of *Noviherbaspirillum* in post-fire soils over time. These bacteria became more prevalent 95 days after the fire and maintained their increased presence throughout the study. The authors attributed this increase to *Noviherbaspirillum's* ability to exploit post fire resources like PyOM. The evidence supporting *Noviherbaspirillum's* ability to degrade PyOM includes isolating a strain from oil-polluted sediments in crude oil enrichment cultures (Lin et al., 2013) and examining the genome of a different strain within the *Oxalobacteraceae* family that contained genes coding for the degradation of certain aromatic compounds (Baldani et al., 2014). In this study, we provide confirmation that *Noviherbaspirillum* species are indeed capable of incorporating PyOM-C.

The incorporators from the *Bacillus* genus (*Bacillaceae* family) and the *Beijerinckiaceae* family displayed high sequence similarity to previously identified significant 350 PyOM responders within the *Bacillus* genus and *Beijerinckiaceae* family, respectively (> 98% identity for both). Interestingly, *Bacillus* species, belonging to *Firmicutes*, have also been found to be dominant in early post-fire soils (Pulido-Chavez et al., 2023). Although they have not been directly linked to PyOM-C degradation, their increased presence in post-fire soils is believed to be due to stress and heat tolerance traits common among *Firmicutes*. Our study suggests that part

of the reason these species dominate post-fire soils may be by exploiting PyOM-C that becomes available immediately after fire.

We identified an incorporator from the *Pseudonocardiaceae* family; however, it did not belong to the *Pseudonocardia* genus, which we hypothesized as the likely incorporator group, based on the genus-level response observed in the previous study. Additionally, the sequence similarity between the incorporator and responder identified in Chapter 3 was low, with less than 97% similarity. These findings suggest the possibility of other members within the *Pseudonocardiaceae* family being capable of incorporating PyOM-C. Finally, the incorporators from the genus *Segetibacter* (*Chitinophagaceae* family) have been documented as positive fire responders (Adkins et al., 2022), and they are also known to increase in abundance upon PyOM addition (Whitman et al., 2016; Zhang et al., 2019).

PyOM-C incorporation is not always accompanied by increased relative abundance

For many incorporator OTUs, significant increases in relative abundance upon PyOM addition were not observed (Fig. 4.5), suggesting that active PyOM-C incorporation doesn't necessarily result in rapid growth for many microbes. It is plausible that PyOM-C, as a complex substrate, is utilized by a select group of slow-growing and persistent microbes that have the pathways to metabolize complex C substrates. For instance, a *Sphingomonadaceae* species showed the highest ^{13}C incorporation (0.4 AFE; Fig. 4.3). Bacteria from this family are commonly found in high abundance in soils contaminated with (poly)aromatic compounds, such as oil spills, and are known for their ability to degrade xenobiotic and (poly)aromatic compounds (Ghosal et al., 2016; Glaeser & Kämpfer, 2014). They have been identified as PyOM responders in several studies (Han et al., 2017; Whitman et al., 2016; Zhang et al., 2019), and *Sphingomonadaceae* was one of the families for which a consistent response could be detected at

the family level (Woolet & Whitman, 2020). Similarly, the *Xanthobacteraceae* family, for which we also identified a high PyOM-C incorporator (0.3 AFE), is known to possess pathways for aromatic carbon degradation (Oren, 2014). Perhaps, the chemical nature of PyOM-C does not provide a competitive advantage that many bacteria can exploit, and hence, it would not necessarily result in higher fitness or growth response that would appear as significant increase in relative abundance in soils.

On the other hand, significant increases in relative abundance after PyOM addition were detected for PyOM-C incorporating taxa from the *Blastocatellaceae* and *Oxalobacteraceae* families (Fig. S4.1). This is intriguing and may indicate a different life history strategy compared to incorporators that did not show an increase in relative numbers. These bacteria may be fast growers and could exploit post-fire environments containing PyOM-C, potentially giving them a competitive advantage. As discussed earlier, there is substantial evidence supporting *Oxalobacteraceae* as a PyOM and fire-responsive family, capable of exploiting post-fire carbon resources. In the case of *Blastocatellaceae,* however, there is limited evidence to support that members of this family respond to PyOM presence in incubation studies or post-fire soils. Some representatives are documented to degrade complex carbon compounds (Huber et al., 2017), and one study found increased abundance upon PyOM addition (Zhang et al., 2019). However, another study noted lower abundance of this family in burned soils (Adkins et al., 2020) highlighting that PyOM degradation alone may not be sufficient to give this OTU a competitive advantage post-fire. The low level of ^{13}C incorporation (0.08 AFE) accompanied by an increase in relative abundance for this OTU could also suggest secondary incorporation of the ^{13}C label via cross-feeding (discussed in detail in the next section).

In interpreting the lack of increased abundances in many of the PyOM incorporators, it is essential to remember that these soils were collected from sites that burned in 2014 and likely already contained some PyOM, supporting the establishment of bacteria capable of degrading PyOM. Comparing post-burn soils with unburned soils may reveal an increase in the relative abundance of many incorporating taxa, which was not observed in the current or previous studies. The same could be true for soils without a history of burning, which may show a detectable increase in relative abundance upon receiving PyOM. In such cases, the relative increase may be attributed to the ability of these bacteria to colonize environments containing the newly added complex C in PyOM. It is also important to note that the change in relative abundance was measured at only one timepoint, and other trends may have been detected through multiple timepoint sampling, as observed in the previous incubation. Moreover, the reported findings focus specifically on the incorporation of the non-water-extractable PyOM-C, which contains a high proportion of aromatic carbon compared to the water-extractable fraction. It is possible that additional responders might increase in abundance due to the incorporation of the water-extractable fraction.

Some taxa may incorporate ^{13}C in their DNA by cross-feeding and predation

Cross-feeding is common in ^{13}C-SIP studies, where an incorporator may not directly consume the substrate but instead takes up the byproduct of other taxa's metabolism of the substrate (Neufeld et al., 2007; Wang & Yao, 2021). This means that some bacteria identified as incorporators might not be primary consumers of PyOM-C, but rather could incorporate the ^{13}C label from byproducts of PyOM-C metabolism by primary consumers. In this study, our aim was to identify taxa incorporating ^{13}C-non-water-extractable PyOM by sampling on Day 21, when we expected to detect taxa specifically targeting this fraction after much of the water-extractable

fraction had been consumed. Our choice of this time point was based on PyOM-C mineralization trends observed in Chapter 3. Despite this, we anticipated cross-feeding to occur, and cannot guarantee that all identified incorporators were primary consumers of the ^{13}C non-water-extractable PyOM-C. There is strong evidence for primary consumption in incorporators with documented responses to fire or PyOM additions. For others, the incorporation may be due to uptake of by-products of PyOM-C metabolism. In addition, the availability of simpler byproducts might trigger a faster growth response due to increased competition for these substrates, leading to an increase in abundance, as suggested in the case of the *Blastocatellaceae*.

While some bacteria may use metabolic byproducts, others might acquire the ^{13}C label by feeding directly on bacteria that consume the ^{13}C-non-water-extractable PyOM-C. We found some evidence supporting this, with two incorporator taxa from the family *0319-6G20,* an uncultivated clade of the phylum *Bdellovibrionota,* which includes many predatory bacteria (Rendulic et al., 2004; Zhang et al., 2023). This has interesting implications, as predatory bacteria have been shown to grow faster and consume more carbon upon substrate addition than non-predatory bacteria, exerting top-down control on resource acquisition by prey populations and playing a vital role in carbon cycling (Hungate et al., 2021).

Hence, although cross-feeding in SIP studies may be unavoidable, it can be useful for tracking the flow of carbon within the microbial food web (Pepe-Ranney et al., 2016; Wilhelm et al., 2021). Studying cross-feeding and predator prey interactions in soils can be crucial for insights into both microbial community structure and carbon cycling processes (D'Souza et al., 2018; Hungate et al., 2021).

It is important to note that examining ^{13}C incorporation at only one timepoint limits our ability to differentiate between primary consumers and secondary consumers of non-water

extractable PyOM-C. To achieve this distinction, we would need to monitor incorporation and changes in relative abundance at multiple timepoints. Additionally, SIP combined with metagenomics can help identify metabolic pathways present in the incorporators (Dumont et al., 2006; Eyice et al., 2015), providing insights into their role in PyOM-C degradation and distinguishing between primary and secondary incorporation.

PyOM properties besides C substrate availability affect microbial communities

In this study, although a PyOM-specific effect on the bacterial community was observed (Fig. 4.4), only a small number of microbes were actively consuming PyOM-C, with even fewer showing an increase in relative abundance. Furthermore, all incorporator taxa exhibited very low relative abundances in unamended soils on Day 0 and Day 21 (Fig. S4.2). Incorporators from the *Blastocatellaceae* family were identified as having the highest relative abundance on Day 0, with a mean relative abundance of 0.37% ± 0.14. This indicates that while community-wide shifts may occur, the microbes actively incorporating labeled ^{13}C-non-water-extractable PyOM are very few and low in abundance.

This discrepancy between substrate consumption and community and abundance trends inferred from sequencing data has been previously noted (Bryson et al., 2017) and could be expected for this study. As discussed earlier, the consumption of a complex substrate like non-water-extractable PyOM might not offer a fitness advantage to most bacteria and could be limited to a select few. Furthermore, PyOM-induced shifts in community compositions may be mediated more by the water-extractable PyOM-C, which is more readily mineralizable and potentially favorable to a broader range of microbes.

In addition to carbon-related effects, other PyOM properties, such as its structural characteristics as well as its influence on soil properties like moisture, pH and nutrient

availability, may also contribute to the observed community shifts (Dai et al., 2021, p. 202; Lehmann et al., 2011). Although we controlled both pH and moisture, the presence of PyOM may have created favorable microsites in soils (Zimmerman & Ouyang, 2019b), influencing the abundance of different microbial groups (Delgado-Baquerizo et al., 2016). The porous structure of PyOM provides a potential habitat for microbes (Pietikäinen et al., 2000), enabling certain bacteria to colonize its surface and access the carbon within it. For example, *Pseudonocardiaceae* have been observed to colonize high temperature PyOM surfaces, which have a porous structure and high surface area (Dai et al., 2017a). Additionally, members of the *Sphingomonadaceae* family have traits that help them effectively colonize membrane surfaces (de Vries et al., 2019). Conversely, negative effects of PyOM on microbes such as toxicity have been reported, which could adversely affect certain microbes (Lehmann et al., 2011; Smith et al., 2013).

Overall, while the incorporation of non-water-extractable PyOM-C by some bacteria was observed, multiple factors, including the properties of PyOM and its impact on soil properties, may have contributed to the observed community-wide shifts. The specific application rates and experimental conditions of this study were designed to identify true incorporators of ^{13}C non-water-extractable PyOM but may not fully represent the behavior of microbes in the field. Additionally, it is important to note that the detection of PyOM-C incorporation and changes in community dynamics and relative abundance were limited to a single timepoint in this study. Longer incubation periods or multiple sampling points could reveal different patterns of PyOM-C consumption and microbial community dynamics.

Water-extractable PyOM-C is highly mineralizable

The mineralization data showed similar trends as in Chapter 3's incubation with 350 PyOM, where the water-extractable fraction had the highest mineralizability. This is further proof that microbes preferentially utilize the water-extractable PyOM-C over the SOC or the non-water-extractable PyOM-C, most likely due to a higher proportion of easy to break down aliphatic C carbon. The non-water-extractable PyOM-C in 350 PyOM was also preferred over SOC, also consistent with the previous finding. However, a statistically significant positive priming effect was not observed in this experiment, potentially due to larger measurement uncertainty resulting from the lack of high-resolution CO_2 sampling. Despite the lack of a significant priming effect, we do note that the trends we observed in this incubation with PyOM produced from a completely different set of pine trees were similar to those observed in the previous experiment. This demonstrates consistent trends for PyOM-C mineralization and supports the validity of our findings.

Overall, our findings highlight the importance of considering the heterogeneity of PyOM-C fractions in short-term C cycling in post-fire soils. The water-extractable fraction may be particularly important for understanding the effect of PyOM on soil microbial communities and ecosystem processes in soils containing a high proportion of low-temperature PyOM.

Conclusion

In conclusion, this study provides valuable insights into the bacterial taxa actively incorporating PyOM-C in soil microbial communities. We use PyOM-C SIP for the first time to reveal that several bacteria known to respond to fire and PyOM amendments are indeed capable of degrading PyOM-C that has relatively higher proportion of condensed aromatic C.

Acknowledgements

This research was made possible with the financial support of the Department of Energy awards DE-SC0016365 and DE-SC0020351. We would like to thank Harry Read for labelling chamber design and construction, as well as Akio Enders for the design and construction of the "charcoalator". We also extend our gratitude to Monika Fischer and Neem Patel for collection of the burned soil, and to the Wisconsin Department of Natural Resources for providing us with the white pine seedlings used to grow both sets of trees in this study. Additionally, we would like to acknowledge Kim Sparks and the Cornell Stable Isotope Laboratory for their assistance with PyOM and flux gas sample analysis, and Rex Malstrom and the DOE Joint Genome Institute for conducting DNA-SIP fractionation. We would also like to thank Shan Shan for assistance with qPCR. Finally, we are grateful for the support provided by CHTC for bioinformatics and data analysis (https://chtc.cs.wisc.edu/uw-research-computing/cite-chtc.html).

Author Contributions

The author contributions to the chapter are as follows: study conception and design: NZ, TLW, TDB; data collection: NZ, KK, JW, TDB; analysis and interpretation of results: NZ, TDB, TLW; draft manuscript preparation: NZ; manuscript review and editing: NZ, TLW.

References

Adkins, J., Docherty, K. M., Gutknecht, J. L. M., & Miesel, J. R. (2020). How do soil microbial communities respond to fire in the intermediate term? Investigating direct and indirect effects associated with fire occurrence and burn severity. *Science of The Total Environment*, *745*, 140957.

Adkins, J., Docherty, K. M., & Miesel, J. R. (2022). Copiotrophic Bacterial Traits Increase With Burn Severity One Year After a Wildfire. *Frontiers in Forests and Global Change*, *5*.

Baldani, J. I., Rouws, L., Cruz, L. M., Olivares, F. L., Schmid, M., & Hartmann, A. (2014). The Family Oxalobacteraceae. In E. Rosenberg, E. F. DeLong, S. Lory, E. Stackebrandt, & F. Thompson (Eds.), *The Prokaryotes* (pp. 919–974). Springer Berlin Heidelberg.

Berry, T. D., Creelman, C., Nickerson, N., Enders, A., & Whitman, T. (2021). An open-source, automated, gas sampling peripheral for laboratory incubation experiments using cavity ring-down spectroscopy. *HardwareX*, *10*, e00208.

Bolyen, E., Rideout, J. R., Dillon, M. R., Bokulich, N. A., Abnet, C. C., Al-Ghalith, G. A., Alexander, H., Alm, E. J., Arumugam, M., Asnicar, F., Bai, Y., Bisanz, J. E., Bittinger, K., Brejnrod, A., Brislawn, C. J., Brown, C. T., Callahan, B. J., Caraballo-Rodríguez, A. M., Chase, J., … Caporaso, J. G. (2019). Reproducible, interactive, scalable and extensible microbiome data science using QIIME 2. *Nature Biotechnology*, *37*(8), Article 8.

Bryson, S., Li, Z., Chavez, F., Weber, P. K., Pett-Ridge, J., Hettich, R. L., Pan, C., Mayali, X., & Mueller, R. S. (2017). Phylogenetically conserved resource partitioning in the coastal microbial loop. *The ISME Journal*, *11*(12), Article 12.

Carini, P., Marsden, P., Leff, J., Morgan, E., Strickland, M., & Fierer, N. (2016). Relic DNA is abundant in soil and obscures estimates of soil microbial diversity. *Relic DNA Is Abundant in Soil and Obscures Estimates of Soil Microbial Diversity*, *March*, 043372.

Coskun, Ö. K., Vuillemin, A., Schubotz, F., Klein, F., Sichel, S. E., Eisenreich, W., & Orsi, W. D. (2022). Quantifying the effects of hydrogen on carbon assimilation in a seafloor microbial community associated with ultramafic rocks. *The ISME Journal*, *16*(1), Article 1.

Dai, Z., Barberán, A., Li, Y., Brookes, P. C., & Xu, J. (2017). Bacterial Community Composition Associated with Pyrogenic Organic Matter (Biochar) Varies with Pyrolysis Temperature and Colonization Environment. *MSphere2*, *2*(2), e00085-17.

Dai, Z., Xiong, X., Zhu, H., Xu, H., Leng, P., Li, J., Tang, C., & Xu, J. (2021). Association of biochar properties with changes in soil bacterial, fungal and fauna communities and nutrient cycling processes. *Biochar*, *3*(3), 239–254.

de Vries, H. J., Beyer, F., Jarzembowska, M., Lipińska, J., van den Brink, P., Zwijnenburg, A., Timmers, P. H. A., Stams, A. J. M., & Plugge, C. M. (2019). Isolation and characterization of Sphingomonadaceae from fouled membranes. *Npj Biofilms and Microbiomes*, *5*(1), Article 1.

Delgado-Baquerizo, M., Maestre, F. T., Eldridge, D. J., & Singh, B. K. (2016). Microsite Differentiation Drives the Abundance of Soil Ammonia Oxidizing Bacteria along Aridity Gradients. *Frontiers in Microbiology*, *7*.

Dove, N. C., Taş, N., & Hart, S. C. (2022). Ecological and genomic responses of soil microbiomes to high-severity wildfire: Linking community assembly to functional potential. *The ISME Journal*, *16*(7), Article 7.

D'Souza, G., Shitut, S., Preussger, D., Yousif, G., Waschina, S., & Kost, C. (2018). Ecology and evolution of metabolic cross-feeding interactions in bacteria. *Natural Product Reports*, *35*(5), 455–488.

Dumont, M. G., Radajewski, S. M., Miguez, C. B., McDonald, I. R., & Murrell, J. C. (2006). Identification of a complete methane monooxygenase operon from soil by combining stable isotope probing and metagenomic analysis. *Environmental Microbiology*, *8*(7), 1240–1250.

Enright, D. J., Frangioso, K. M., Isobe, K., Rizzo, D. M., & Glassman, S. I. (2022). Mega-fire in redwood tanoak forest reduces bacterial and fungal richness and selects for pyrophilous taxa that are phylogenetically conserved. *Molecular Ecology*, *31*(8), 2475–2493.

Eyice, Ö., Namura, M., Chen, Y., Mead, A., Samavedam, S., & Schäfer, H. (2015). SIP metagenomics identifies uncultivated Methylophilaceae as dimethylsulphide degrading bacteria in soil and lake sediment. *The ISME Journal*, *9*(11), Article 11.

Fischer, M. S., Stark, F. G., Berry, T. D., Zeba, N., Whitman, T., & Traxler, M. F. (2021). Pyrolyzed Substrates Induce Aromatic Compound Metabolism in the Post-fire Fungus, Pyronema domesticum. *Frontiers in Microbiology*, *12*.

Ghosal, D., Ghosh, S., Dutta, T. K., & Ahn, Y. (2016). Current state of knowledge in microbial degradation of polycyclic aromatic hydrocarbons (PAHs): A review. *Frontiers in Microbiology*, *7*(AUG).

Glaeser, S. P., & Kämpfer, P. (2014). The Family Sphingomonadaceae. In E. Rosenberg, E. F. DeLong, S. Lory, E. Stackebrandt, & F. Thompson (Eds.), *The Prokaryotes* (pp. 641–707). Springer Berlin Heidelberg.

Han, G., Lan, J., Chen, Q., Yu, C., & Bie, S. (2017). Response of soil microbial community to application of biochar in cotton soils with different continuous cropping years. *Scientific Reports*, *7*(1), 1–11.

Huber, K. J., Pascual, J., Foesel, B. U., & Overmann, J. (2017). *B lastocatellaceae* . In W. B. Whitman, F. Rainey, P. Kämpfer, M. Trujillo, J. Chun, P. DeVos, B. Hedlund, & S. Dedysh (Eds.), *Bergey's Manual of Systematics of Archaea and Bacteria* (1st ed., pp. 1–4). Wiley.

Hungate, B. A., Marks, J. C., Power, M. E., Schwartz, E., van Groenigen, K. J., Blazewicz, S. J., Chuckran, P., Dijkstra, P., Finley, B. K., Firestone, M. K., Foley, M., Greenlon, A., Hayer, M., Hofmockel, K. S., Koch, B. J., Mack, M. C., Mau, R. L., Miller, S. N., Morrissey, E. M., … Pett-Ridge, J. (2021). The Functional Significance of Bacterial Predators. *MBio*, *12*(2), e00466-21.

Hungate, B. A., Mau, R. L., Schwartz, E., Caporaso, J. G., Dijkstra, P., van Gestel, N., Koch, B. J., Liu, C. M., McHugh, T. A., Marks, J. C., Morrissey, E. M., & Price, L. B. (2015). Quantitative Microbial Ecology through Stable Isotope Probing. *Applied and Environmental Microbiology*, *81*(21), 7570–7581.

Kassambara, A. (2022). *rstatix: Pipe-Friendly Framework for Basic Statistical Tests*.

Kozich, J. J., Westcott, S. L., Baxter, N. T., Highlander, S. K., & Schloss, P. D. (2013). Development of a Dual-Index Sequencing Strategy and Curation Pipeline for Analyzing Amplicon Sequence Data on the MiSeq Illumina Sequencing Platform. *Applied and Environmental Microbiology*, *79*(17), 5112–5120.

Lee, S.-H., Sorensen, J. W., Grady, K. L., Tobin, T. C., & Shade, A. (2017). Divergent extremes but convergent recovery of bacterial and archaeal soil communities to an ongoing subterranean coal mine fire. *The ISME Journal*, *11*(6), Article 6.

Lehmann, J., Rillig, M. C., Thies, J., Masiello, C. A., Hockaday, W. C., & Crowley, D. (2011). Biochar effects on soil biota—A review. *Soil Biology and Biochemistry*, *43*(9), 1812–1836.

Lin, S.-Y., Hameed, A., Arun, A. B., Liu, Y.-C., Hsu, Y.-H., Lai, W.-A., Rekha, P. D., & Young, C.-C. (2013). Description of Noviherbaspirillum malthae gen. Nov., sp. Nov., isolated from an oil-contaminated soil, and proposal to reclassify Herbaspirillum soli,Herbaspirillum aurantiacum,Herbaspirillum canariense and Herbaspirillum psychrotolerans as Noviherbaspirillum soli comb. Nov., Noviherbaspirillum aurantiacum comb. Nov., Noviherbaspirillum canariense comb. Nov. And Noviherbaspirillum psychrotolerans comb. Nov. Based on polyphasic analysis. *International Journal of Systematic and Evolutionary Microbiology*, *63*(Pt_11), 4100–4107.

McMurdie, P. J., & Holmes, S. (2013). phyloseq: An R package for reproducible interactive analysis and graphics of microbiome census data. *PLoS ONE*, *8*(4), e61217.

Nelson, A. R., Narrowe, A. B., Rhoades, C. C., Fegel, T. S., Daly, R. A., Roth, H. K., Chu, R. K., Amundson, K. K., Young, R. B., Steindorff, A. S., Mondo, S. J., Grigoriev, I. V., Salamov, A., Borch, T., & Wilkins, M. J. (2022). Wildfire-dependent changes in soil microbiome diversity and function. *Nature Microbiology*, *7*(9), 1419–1430.

Neufeld, J. D., Vohra, J., Dumont, M. G., Lueders, T., Manefield, M., Friedrich, M. W., & Murrell, C. J. (2007). DNA stable-isotope probing. *Nature Protocols*, *2*(4), 860–866.

Nuccio, E. E., Blazewicz, S. J., Lafler, M., Campbell, A. N., Kakouridis, A., Kimbrel, J. A., Wollard, J., Vyshenska, D., Riley, R., Tomatsu, A., Hestrin, R., Malmstrom, R. R., Firestone, M., & Pett-Ridge, J. (2022). HT-SIP: A semi-automated stable isotope probing pipeline identifies cross-kingdom interactions in the hyphosphere of arbuscular mycorrhizal fungi. *Microbiome*, *10*(1), 199.

Oren, A. (2014). The Family Xanthobacteraceae. In E. Rosenberg, E. F. DeLong, S. Lory, E. Stackebrandt, & F. Thompson (Eds.), *The Prokaryotes* (pp. 709–726). Springer Berlin Heidelberg.

Pepe-Ranney, C., Campbell, A. N., Koechli, C. N., Berthrong, S., & Buckley, D. H. (2016). Unearthing the Ecology of Soil Microorganisms Using a High Resolution DNA-SIP Approach to Explore Cellulose and Xylose Metabolism in Soil. *Frontiers in Microbiology*, *7*.

Pérez-Valera, E., Verdú, M., Navarro-Cano, J. A., & Goberna, M. (2018). Resilience to fire of phylogenetic diversity across biological domains. *Molecular Ecology*, *27*(13), 2896–2908.

Pietikäinen, J., Kiikkilä, O., & Fritze, H. (2000). Charcoal as a habitat for microbes and its effect on the microbial community of the underlying humus. *Oikos*, *89*(2), 231–242.

Pulido-Chavez, M. F., Randolph, J. W. J., Zalman, C., Larios, L., Homyak, P. M., & Glassman, S. I. (2023). Rapid bacterial and fungal successional dynamics in first year after chaparral wildfire. *Molecular Ecology*, *32*(7), 1685–1707.

R Core Team. (2022). *R: A Language and Environment for Statistical Computing*. R Foundation for Statistical Computing.

Radajewski, S., Ineson, P., Parekh, N. R., & Murrell, J. C. (2000). Stable-isotope probing as a tool in microbial ecology. *Nature*, *403*(6770), 646–649.

Rendulic, S., Jagtap, P., Rosinus, A., Eppinger, M., Baar, C., Lanz, C., Keller, H., Lambert, C., Evans, K. J., Goesmann, A., Meyer, F., Sockett, R. E., & Schuster, S. C. (2004). A Predator Unmasked: Life Cycle of *Bdellovibrio bacteriovorus* from a Genomic Perspective. *Science*, *303*(5658), 689–692.

Smith, C. R., Buzan, E. M., & Lee, J. W. (2013). Potential impact of biochar water-extractable substances on environmental sustainability. *ACS Sustainable Chemistry and Engineering*, *1*(1), 118–126.

Vyshenska, D., Sampara, P., Singh, K., Tomatsu, A., Kauffman, W. B., Nuccio, E. E., Blazewicz, S. J., Pett-Ridge, J., Varghese, N., Kellom, M., Clum, A., Riley, R., Roux, S., Eloe-Fadrosh, E. A., Ziels, R. M., & Malmstrom, R. R. (2022). *A standardized quantitative analysis strategy for stable isotope probing metagenomics* (p. 2022.12.20.521340). bioRxiv.

Walters, W., Hyde, E. R., Berg-Lyons, D., Ackermann, G., Humphrey, G., Parada, A., Gilbert, J. A., Jansson, J. K., Caporaso, J. G., Fuhrman, J. A., Apprill, A., & Knight, R. (2015). Improved Bacterial 16S rRNA Gene (V4 and V4-5) and Fungal Internal Transcribed Spacer Marker Gene Primers for Microbial Community Surveys. *MSystems*, *1*(1), e00009-15.

Wang, J., & Yao, H. (2021). Applications of DNA/RNA-stable isotope probing (SIP) in environmental microbiology. In *Methods in Microbiology* (Vol. 48, pp. 227–267). Elsevier.

Whitman, T., DeCiucies, S., Hanley, K., Enders, A., Woolet, J., & Lehmann, J. (2021). Microbial community shifts reflect losses of native soil carbon with pyrogenic and fresh organic matter additions and are greatest in low-carbon soils. *Applied and Environmental Microbiology*, *January*.

Whitman, T., Enders, A., & Lehmann, J. (2014). Pyrogenic carbon additions to soil counteract positive priming of soil carbon mineralization by plants. *Soil Biology and Biochemistry*, *73*, 33–41.

Whitman, T., Pepe-Ranney, C., Enders, A., Koechli, C., Campbell, A., Buckley, D. H., & Lehmann, J. (2016). Dynamics of microbial community composition and soil organic carbon mineralization in soil following addition of pyrogenic and fresh organic matter. *ISME Journal*, *10*(12), 2918–2930.

Whitman, T., Whitman, E., Woolet, J., Flannigan, M. D., Thompson, D. K., & Parisien, M. A. (2019). Soil bacterial and fungal response to wildfires in the Canadian boreal forest across a burn severity gradient. *Soil Biology and Biochemistry*, *138*(April), 107571.

Whitman, T., Woolet, J., Sikora, M., Johnson, D. B., & Whitman, E. (2022). Resilience in soil bacterial communities of the boreal forest from one to five years after wildfire across a severity gradient. *Soil Biology and Biochemistry*, *172*, 108755.

Wickham, H., Averick, M., Bryan, J., Chang, W., McGowan, L. D., François, R., Grolemund, G., Hayes, A., Henry, L., Hester, J., Kuhn, M., Pedersen, T. L., Miller, E., Bache, S. M., Müller, K., Ooms, J., Robinson, D., Seidel, D. P., Spinu, V., … Yutani, H. (2019). Welcome to the tidyverse. *Journal of Open Source Software*, *4*(43), 1686.

Wilhelm, R. C., Pepe-Ranney, C., Weisenhorn, P., Lipton, M., & Buckley, D. H. (2021). Competitive Exclusion and Metabolic Dependency among Microorganisms Structure the Cellulose Economy of an Agricultural Soil. *MBio*, *12*(1), e03099-20.

Woolet, J., & Whitman, T. (2020). Pyrogenic organic matter effects on soil bacterial community composition. *Soil Biology and Biochemistry*, *141*, 107678.

Youngblut, N. D., Barnett, S. E., & Buckley, D. H. (2018). HTSSIP: An R package for analysis of high throughput sequencing data from nucleic acid stable isotope probing (SIP) experiments. *PLOS ONE*, *13*(1), e0189616.

Zeba, N., Berry, T. D., Panke-Buisse, K., & Whitman, T. (2022). Effects of physical, chemical, and biological ageing on the mineralization of pine wood biochar by a Streptomyces isolate. *PLOS ONE*, *17*(4), e0265663.

Zhang, L., Huang, X., Zhou, J., & Ju, F. (2023). Active predation, phylogenetic diversity, and global prevalence of myxobacteria in wastewater treatment plants. *The ISME Journal*, 1–11.

Zhang, M., Riaz, M., Zhang, L., El-desouki, Z., & Jiang, C. (2019). Biochar Induces Changes to Basic Soil Properties and Bacterial Communities of Different Soils to Varying Degrees at 25 mm Rainfall: More Effective on Acidic Soils. *Frontiers in Microbiology*, *10*, 1321.

Zimmerman, A. R., & Ouyang, L. (2019). Priming of pyrogenic C (biochar) mineralization by dissolved organic matter and vice versa. *Soil Biology and Biochemistry*, *130*(November 2018), 105–112.

Supporting Information

Table S4.1. Properties of ^{13}C labeled biomass

Property (units)	Stems	Needles
Total C (%)	49.72 ± 8.03	47.08 ± 8.29
Bulk $^{13}C/^{12}C$ (AT %)	75.29 ± 2.91	81.76 ± 2.09

The values presented are means of five replicates ± standard deviation.

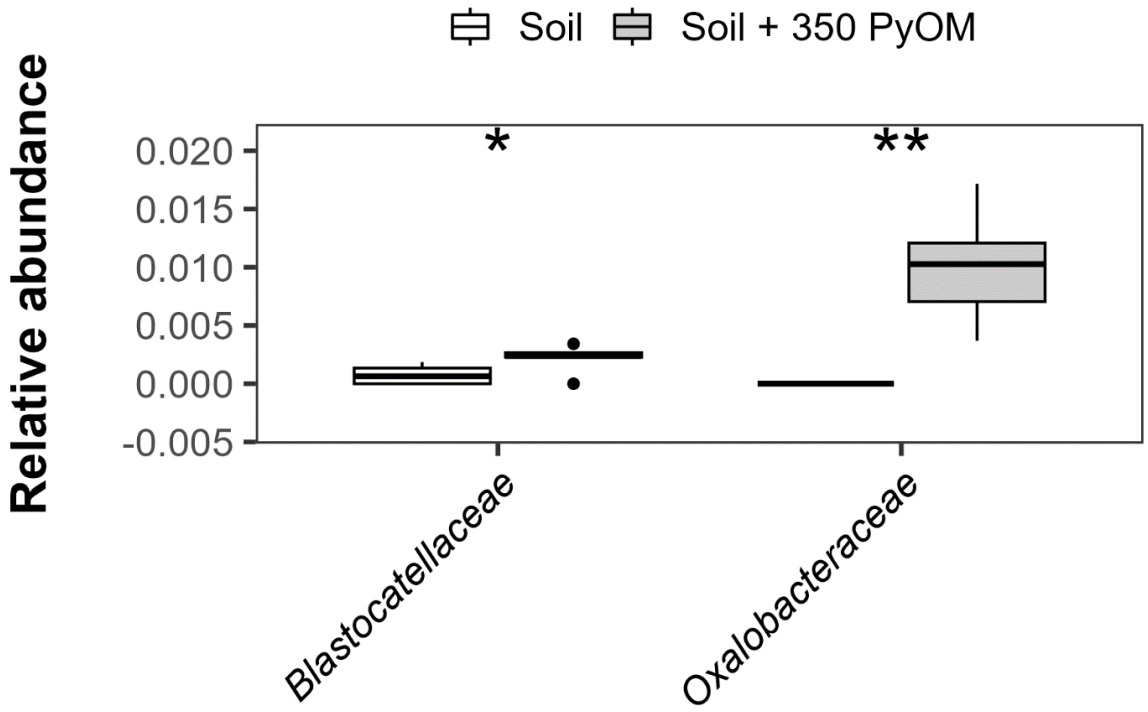

Figure S4.1. Significant relative abundance changes among 350 PyOM-C incorporators. *Relative abundance of three PyOM-C incorporator OTUs (identified using qSIP) in unfractionated DNA of unamended soils (n = 6) and unlabeled 350 PyOM-amended soils (n=6) on Day 21. The incorporator OTUs are grouped by family shown on the x-axis. Asterisks indicate statistically significant differences in relative abundance ('*': <= 0.05;'**' : p < = 0.01).*

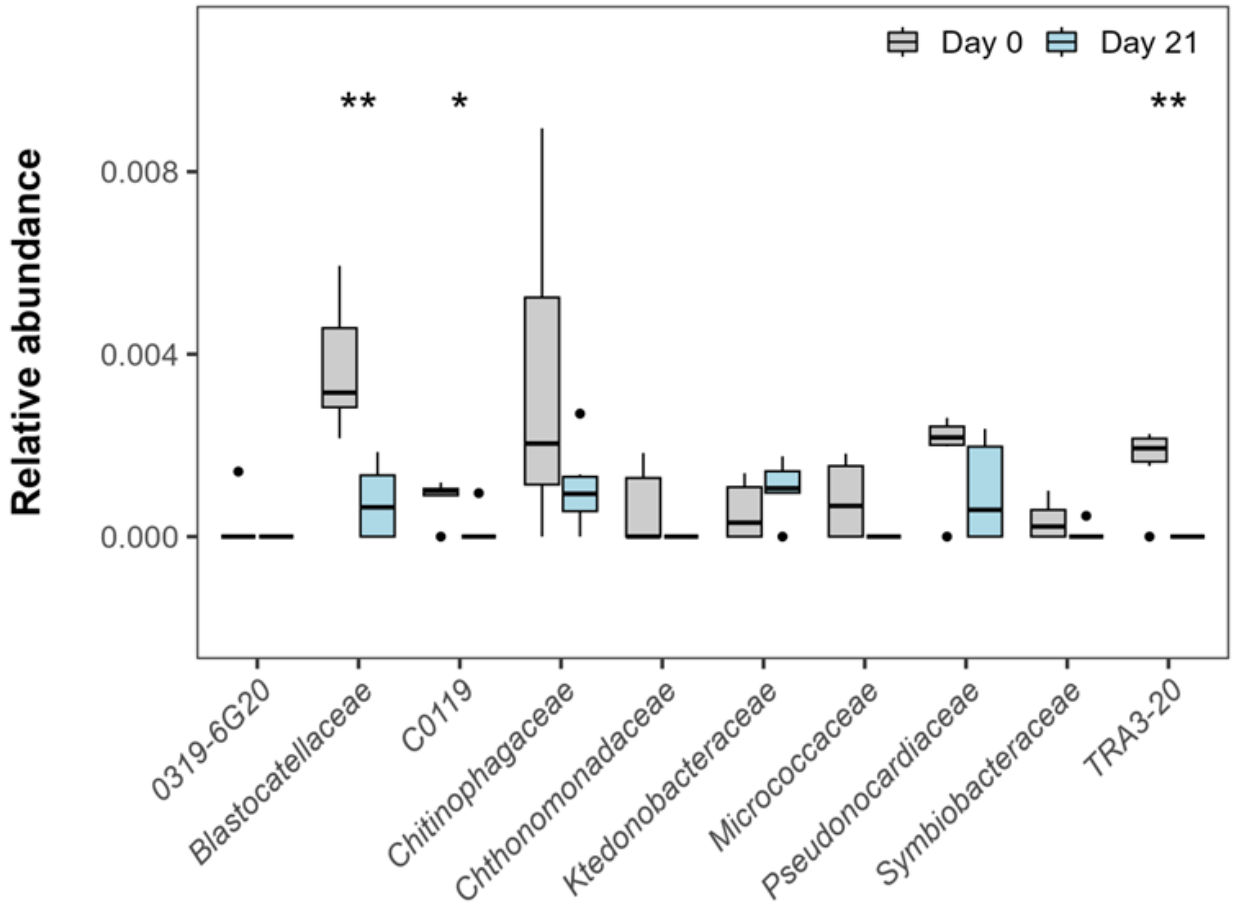

Figure S4.2. Relative abundance changes with time among the 350 PyOM-C incorporators in unamended soil.

Relative abundance of twelve most abundant PyOM-C incorporator OTUs (identified using qSIP) in unfractionated DNA of unamended soils on Day 0 (n = 6) and Day 21 (n = 6). The incorporator OTUs are grouped by family shown on the x-axis. Asterisks indicate statistically significant differences in relative abundance ('': <= 0.05;'**' : p < = 0.01).*

Appendix S4

qPCR calibration table

Date	Content	Starting Qua	Cq_Ave	Cq_sd	Equation	R2	Not included
3/14/2023	Std-01	289000000	15.88	1.09	y = -1.755ln(x) + 50.7	0.99	
3/14/2023	Std-02	28900000	20.53	1.52			
3/14/2023	Std-03	2890000	24.80	1.19			
3/14/2023	Std-04	289000	29.47	0.77			
3/14/2023	Std-05	57800	32.06	0.66			
3/14/2023	Std-06	28900	32.94	1.12			
3/14/2023	Std-07	2890	35.49	1.00			
3/14/2023	Neg Ctrl	0	36.36	0.55			
3/3/2023	Std-01	39400000	13.78	0.13	y = -1.848ln(x) + 45.832	0.99	
3/3/2023	Std-02	3940000	17.11	2.33			
3/3/2023	Std-03	394000	22.11	0.19			
3/3/2023	Std-04	78800	25.02	0.04			
3/3/2023	Std-05	39400	26.71	0.20			
3/3/2023	Std-06	3940	30.74	0.05			
3/3/2023	Std-07	394	34.46	0.48			
3/3/2023	Neg Ctrl	0	37.86	0.06			
3/7/2023	Std-01	39400000	17.54	0.41	y = -2.17ln(x) + 56.066	0.99	
3/7/2023	Std-02	3940000	23.68	0.46			
3/7/2023	Std-03	394000	28.27	0.48			
3/7/2023	Std-04	78800	31.44	0.33			
3/7/2023	Std-05	39400	33.64	0.49			
3/7/2023	Std-06	3940	37.60	0.23			
3/7/2023	Std-07	394		0.96			39.64
3/7/2023	Neg Ctrl	0	40.33	0.45			
3/8/2023	Std-01	289000000	9.19	2.06	y = -2.876ln(x) + 65.529	0.99	
3/8/2023	Std-02	28900000	16.07	2.38			
3/8/2023	Std-03	2890000		7.04			26.82
3/8/2023	Std-04	289000	30.64	6.97			
3/8/2023	Std-05	57800	34.58	2.67			
3/8/2023	Std-06	28900	34.52	2.25			
3/8/2023	Std-07	2890		0.99			36.32
3/8/2023	Neg Ctrl	0	39.08				
3/9/2023	Std-01	289000000	15.16	0.72	y = -1.987ln(x) + 53.767	0.99	
3/9/2023	Std-02	28900000	18.87	0.40			
3/9/2023	Std-03	2890000	24.13	0.48			
3/9/2023	Std-04	289000	29.50	0.62			
3/9/2023	Std-05	57800	32.73	0.72			
3/9/2023	Std-06	28900	33.81	0.91			
3/9/2023	Std-07	2890	36.79	0.62			
3/9/2023	Neg Ctrl	0	37.65	1.95			

3/9/2023	Std-01	289000000	15.12	0.40	y = -1.851ln(x) + 51.445	0.99	
3/9/2023	Std-02	28900000	19.39	0.31			
3/9/2023	Std-03	2890000	23.80	0.09			
3/9/2023	Std-04	289000	28.97	0.23			
3/9/2023	Std-05	57800	31.74	0.58			
3/9/2023	Std-06	28900	32.81	0.41			
3/9/2023	Std-07	2890	35.58	0.30			
3/9/2023	Neg Ctrl	0	37.62	0.59			
3/9/2023	Std-01	289000000	15.43	0.37	y = -2.016ln(x) + 54.903	0.99	
3/9/2023	Std-02	28900000	20.16	0.60			
3/9/2023	Std-03	2890000	25.12	1.53			
3/9/2023	Std-04	289000	30.17	1.51			
3/9/2023	Std-05	57800	33.02	1.42			
3/9/2023	Std-06	28900	33.45	1.03			
3/9/2023	Std-07	2890		0.67			35.72
3/9/2023	Neg Ctrl	0	37.55	0.39			
3/10/2023	Std-01	289000000	14.55	0.97	y = -2.032ln(x) + 53.571	0.99	
3/10/2023	Std-02	28900000	17.62	2.73			
3/10/2023	Std-03	2890000	22.82	0.55			
3/10/2023	Std-04	289000	28.68	0.67			
3/10/2023	Std-05	57800	32.03	0.66			
3/10/2023	Std-06	28900	33.33	0.70			
3/10/2023	Std-07	2890	36.35	0.78			
3/10/2023	Neg Ctrl	0	39.11	1.18			
3/10/2023	Std-01	289000000	14.48	0.97	y = -2.067ln(x) + 54.659	0.99	
3/10/2023	Std-02	28900000	19.28	0.77			
3/10/2023	Std-03	2890000	23.33	0.38			
3/10/2023	Std-04	289000	29.00	1.52			
3/10/2023	Std-05	57800		3.29			34.44
3/10/2023	Std-06	28900		5.15			37.08
3/10/2023	Std-07	2890		19.69			34.10
3/10/2023	Neg Ctrl	0	36.04	20.81			
3/13/2023	Std-01	289000000	15.33	0.29	y = -1.771ln(x) + 49.603	0.99	
3/13/2023	Std-02	28900000	19.00	0.21			
3/13/2023	Std-03	2890000	22.94	0.58			
3/13/2023	Std-04	289000	27.54	0.57			
3/13/2023	Std-05	57800	30.23	0.81			
3/13/2023	Std-06	28900	31.84	0.48			
3/13/2023	Std-07	2890	34.17	0.13			
3/13/2023	Neg Ctrl	0	35.69	1.46			

3/13/2023	Std-01	2.89E+08	13.79	1.99	y = -2.383ln(x) + 60.772	0.99	
3/13/2023	Std-02	28900000	20.12	1.48			
3/13/2023	Std-03	2890000	25.68	2.19			
3/13/2023	Std-04	289000	31.26	2.82			
3/13/2023	Std-05	57800	35.10	2.89			
3/13/2023	Std-06	28900	35.26	2.78			
3/13/2023	Std-07	2890		1.71			37.84
3/13/2023	Neg Ctrl	0	40.38	1.28			
3/14/2023	Std-01	2.89E+08	14.55	0.68	y = -1.979ln(x) + 53.314	0.99	
3/14/2023	Std-02	28900000	19.52	0.65			
3/14/2023	Std-03	2890000	23.89	0.60			
3/14/2023	Std-04	289000	28.69	0.30			
3/14/2023	Std-05	57800	31.40	0.52			
3/14/2023	Std-06	28900	32.93	0.12			
3/14/2023	Std-07	2890		0.18			35.13
3/14/2023	Neg Ctrl	0	37.05	0.58			

qPCR analysis of SIP fractions

Date	Sample	Cq_Ave	Cq_SD	Equation	SQ	DF	Vol_frac_µL	Copies_frac
3/14/2023	SB-UN-1-T3_1	36.55	0.26	y = -1.755ln(x) + 50.7	3177.37	5	149	2.37E+06
3/14/2023	SB-UN-1-T3_2	36.19	1.48	y = -1.755ln(x) + 50.7	3899.51	5	221	4.31E+06
3/14/2023	SB-UN-1-T3_3	36.09	0.86	y = -1.755ln(x) + 50.7	4133.15	5	213	4.40E+06
3/14/2023	SB-UN-1-T3_4	36.15	0.42	y = -1.755ln(x) + 50.7	3989.32	5	228	4.55E+06
3/14/2023	SB-UN-1-T3_5	35.76	0.34	y = -1.755ln(x) + 50.7	4973.00	5	219	5.45E+06
3/14/2023	SB-UN-1-T3_6	35.82	0.16	y = -1.755ln(x) + 50.7	4810.88	5	227	5.46E+06
3/14/2023	SB-UN-1-T3_7	35.53	0.26	y = -1.755ln(x) + 50.7	5690.58	5	216	6.15E+06
3/14/2023	SB-UN-1-T3_8	35.32	0.41	y = -1.755ln(x) + 50.7	6393.66	5	205	6.55E+06
3/14/2023	SB-UN-1-T3_9	34.00	0.19	y = -1.755ln(x) + 50.7	13588.47	5	216	1.47E+07
3/14/2023	SB-UN-1-T3_10	33.95	0.25	y = -1.755ln(x) + 50.7	13991.22	5	224	1.57E+07
3/14/2023	SB-UN-1-T3_11	32.52	0.11	y = -1.755ln(x) + 50.7	31466.72	5	214	3.37E+07
3/14/2023	SB-UN-1-T3_12	30.85	0.10	y = -1.755ln(x) + 50.7	81753.29	5	226	9.24E+07
3/14/2023	SB-UN-1-T3_13	28.54	0.05	y = -1.755ln(x) + 50.7	305342.36	5	218	3.33E+08
3/14/2023	SB-UN-1-T3_14	26.45	0.01	y = -1.755ln(x) + 50.7	1004941.87	5	218	1.10E+09
3/14/2023	SB-UN-1-T3_15	24.69	0.24	y = -1.755ln(x) + 50.7	2733759.79	5	206	2.82E+09
3/14/2023	SB-UN-1-T3_16	24.13	0.11	y = -1.755ln(x) + 50.7	3763717.51	5	210	3.95E+09
3/14/2023	SB-UN-1-T3_17	24.36	0.25	y = -1.755ln(x) + 50.7	3299553.60	5	204	3.37E+09
3/14/2023	SB-UN-1-T3_18	25.45	0.27	y = -1.755ln(x) + 50.7	1769557.16	5	218	1.93E+09
3/14/2023	SB-UN-1-T3_19	26.04	0.20	y = -1.755ln(x) + 50.7	1263366.05	5	221	1.40E+09
3/14/2023	SB-UN-1-T3_20	30.49	4.34	y = -1.755ln(x) + 50.7	100354.21	5	205	1.03E+08
3/14/2023	SB-UN-1-T3_21	27.66	0.07	y = -1.755ln(x) + 50.7	503453.27	5	213	5.36E+08
3/14/2023	SB-UN-1-T3_22	32.23	3.70	y = -1.755ln(x) + 50.7	37114.02	5	155	2.88E+07
3/14/2023	SB-UN-1-T3_23	35.03	1.07	y = -1.755ln(x) + 50.7	7526.22	5	66	2.48E+06
3/14/2023	SB-UN-1-T3_24	36.44	0.89	y = -1.755ln(x) + 50.7	3377.59	5	17	2.87E+05

Date	Sample	Cq_Ave	Cq_SD	Equation	SQ	DF	Vol_frac_µL	Copies_frac
3/3/2023	SB-UN-3-T3_1	34.66	0.23	y = -1.848ln(x) + 45.832	422.49	5	174	3.68E+05
3/3/2023	SB-UN-3-T3_2	29.87	0.27	y = -1.848ln(x) + 45.832	5641.50	5	268	7.56E+06
3/3/2023	SB-UN-3-T3_3	33.41	0.16	y = -1.848ln(x) + 45.832	830.69	5	237	9.84E+05
3/3/2023	SB-UN-3-T3_4	33.60	0.89	y = -1.848ln(x) + 45.832	749.82	5	214	8.02E+05
3/3/2023	SB-UN-3-T3_5	32.81	0.26	y = -1.848ln(x) + 45.832	1150.40	5	233	1.34E+06
3/3/2023	SB-UN-3-T3_6	33.36	0.17	y = -1.848ln(x) + 45.832	850.36	5	215	9.14E+05
3/3/2023	SB-UN-3-T3_7	32.37	0.10	y = -1.848ln(x) + 45.832	1453.33	5	206	1.50E+06
3/3/2023	SB-UN-3-T3_8	31.56	0.12	y = -1.848ln(x) + 45.832	2259.94	5	212	2.40E+06
3/3/2023	SB-UN-3-T3_9	32.47	1.12	y = -1.848ln(x) + 45.832	1381.67	5	222	1.53E+06
3/3/2023	SB-UN-3-T3_10	29.55	0.30	y = -1.848ln(x) + 45.832	6685.12	5	206	6.89E+06
3/3/2023	SB-UN-3-T3_11	28.58	0.04	y = -1.848ln(x) + 45.832	11291.63	5	213	1.20E+07
3/3/2023	SB-UN-3-T3_12	27.62	0.21	y = -1.848ln(x) + 45.832	18994.61	5	209	1.98E+07
3/3/2023	SB-UN-3-T3_13	26.92	0.32	y = -1.848ln(x) + 45.832	27728.43	5	229	3.17E+07
3/3/2023	SB-UN-3-T3_14	25.28	0.09	y = -1.848ln(x) + 45.832	67647.76	5	208	7.04E+07
3/3/2023	SB-UN-3-T3_15	24.71	0.14	y = -1.848ln(x) + 45.832	91769.97	5	209	9.59E+07
3/3/2023	SB-UN-3-T3_16	23.98	0.05	y = -1.848ln(x) + 45.832	136246.19	5	201	1.37E+08
3/3/2023	SB-UN-3-T3_17	24.43	0.32	y = -1.848ln(x) + 45.832	107216.35	5	215	1.15E+08
3/3/2023	SB-UN-3-T3_18	24.42	0.27	y = -1.848ln(x) + 45.832	107308.46	5	227	1.22E+08
3/3/2023	SB-UN-3-T3_19	25.27	0.26	y = -1.848ln(x) + 45.832	67823.67	5	212	7.19E+07
3/3/2023	SB-UN-3-T3_20	26.42	0.38	y = -1.848ln(x) + 45.832	36418.99	5	218	3.97E+07
3/3/2023	SB-UN-3-T3_21	27.01	0.32	y = -1.848ln(x) + 45.832	26491.76	5	224	2.97E+07
3/3/2023	SB-UN-3-T3_22	27.67	0.32	y = -1.848ln(x) + 45.832	18478.09	5	223	2.06E+07
3/3/2023	SB-UN-3-T3_23	29.31	0.19	y = -1.848ln(x) + 45.832	7633.72	5	104	3.97E+06
3/3/2023	SB-UN-3-T3_24	34.60	0.18	y = -1.848ln(x) + 45.832	435.35	5	21	4.57E+04

Date	Sample	Cq_Ave	Cq_SD	Equation	SQ	DF	Vol_frac_µL	Copies_frac
3/7/2023	SB-UN-4-T3_1	31.74	0.48	y = -2.17ln(x) + 56.066	73949.89	5	114	4.22E+07
3/7/2023	SB-UN-4-T3_2	35.32	0.38	y = -2.17ln(x) + 56.066	14184.02	5	167	1.18E+07
3/7/2023	SB-UN-4-T3_3	36.23	0.15	y = -2.17ln(x) + 56.066	9310.18	5	230	1.07E+07
3/7/2023	SB-UN-4-T3_4	36.36	0.20	y = -2.17ln(x) + 56.066	8799.46	5	242	1.06E+07
3/7/2023	SB-UN-4-T3_5	36.32	0.05	y = -2.17ln(x) + 56.066	8933.57	5	232	1.04E+07
3/7/2023	SB-UN-4-T3_6	37.11	0.24	y = -2.17ln(x) + 56.066	6213.14	5	233	7.24E+06
3/7/2023	SB-UN-4-T3_7	37.22	0.23	y = -2.17ln(x) + 56.066	5915.75	5	231	6.83E+06
3/7/2023	SB-UN-4-T3_8	36.69	0.17	y = -2.17ln(x) + 56.066	7535.62	5	225	8.48E+06
3/7/2023	SB-UN-4-T3_9	35.85	0.23	y = -2.17ln(x) + 56.066	11137.82	5	224	1.25E+07
3/7/2023	SB-UN-4-T3_10	33.56	0.23	y = -2.17ln(x) + 56.066	31930.21	5	228	3.64E+07
3/7/2023	SB-UN-4-T3_11	38.33	0.90	y = -2.17ln(x) + 56.066	3542.82	5	213	3.77E+06
3/7/2023	SB-UN-4-T3_12	30.37	0.76	y = -2.17ln(x) + 56.066	138972.51	5	221	1.54E+08
3/7/2023	SB-UN-4-T3_13	28.73	0.79	y = -2.17ln(x) + 56.066	295449.87	5	207	3.06E+08
3/7/2023	SB-UN-4-T3_14	27.94	0.64	y = -2.17ln(x) + 56.066	426071.35	5	230	4.90E+08
3/7/2023	SB-UN-4-T3_15	26.27	0.57	y = -2.17ln(x) + 56.066	916955.75	5	215	9.86E+08
3/7/2023	SB-UN-4-T3_16	24.70	0.66	y = -2.17ln(x) + 56.066	1890502.23	5	209	1.98E+09
3/7/2023	SB-UN-4-T3_17	23.30	0.22	y = -2.17ln(x) + 56.066	3604752.31	5	220	3.97E+09
3/7/2023	SB-UN-4-T3_18	23.02	0.14	y = -2.17ln(x) + 56.066	4106289.28	5	205	4.21E+09
3/7/2023	SB-UN-4-T3_19	24.25	0.31	y = -2.17ln(x) + 56.066	2325573.82	5	225	2.62E+09
3/7/2023	SB-UN-4-T3_20	25.79	0.41	y = -2.17ln(x) + 56.066	1148205.61	5	215	1.23E+09
3/7/2023	SB-UN-4-T3_21	26.66	0.66	y = -2.17ln(x) + 56.066	765985.15	5	218	8.35E+08
3/7/2023	SB-UN-4-T3_22	28.19	0.70	y = -2.17ln(x) + 56.066	378718.02	5	216	4.09E+08
3/7/2023	SB-UN-4-T3_23	36.86	1.01	y = -2.17ln(x) + 56.066	6979.88	5	213	7.43E+06

Sample	Cq_Ave	Cq_SD	Equation	SQ	DF	Vol_frac_µL	Copies_frac
SB-UN-5-T3_1	36.05	2.86	y = -2.876ln(x) + 65.529	28315.84	5	3877	5.49E+08
SB-UN-5-T3_2	35.30	0.32	y = -2.876ln(x) + 65.529	36701.98	5	41	7.52E+06
SB-UN-5-T3_3	37.58		y = -2.876ln(x) + 65.529	16641.15	5	181	1.51E+07
SB-UN-5-T3_4	35.47	0.49	y = -2.876ln(x) + 65.529	34568.29	5	176	3.04E+07
SB-UN-5-T3_5	34.69		y = -2.876ln(x) + 65.529	45352.00	5	191	4.33E+07
SB-UN-5-T3_6	33.62	0.12	y = -2.876ln(x) + 65.529	65752.66	5	138	4.54E+07
SB-UN-5-T3_7	33.38	0.33	y = -2.876ln(x) + 65.529	71681.19	5	179	6.42E+07
SB-UN-5-T3_8	32.85	0.17	y = -2.876ln(x) + 65.529	85926.80	5	166	7.13E+07
SB-UN-5-T3_9	31.07		y = -2.876ln(x) + 65.529	159590.07	5	175	1.40E+08
SB-UN-5-T3_10	30.30		y = -2.876ln(x) + 65.529	208489.28	5	177	1.85E+08
SB-UN-5-T3_11	30.14		y = -2.876ln(x) + 65.529	220806.90	5	167	1.84E+08
SB-UN-5-T3_12	32.47		y = -2.876ln(x) + 65.529	98064.69	5	181	8.87E+07
SB-UN-5-T3_13	27.36		y = -2.876ln(x) + 65.529	580156.08	5	184	5.34E+08
SB-UN-5-T3_14	26.26		y = -2.876ln(x) + 65.529	851044.61	5	177	7.53E+08
SB-UN-5-T3_15	25.83		y = -2.876ln(x) + 65.529	987412.07	5	177	8.74E+08
SB-UN-5-T3_16	26.05	0.44	y = -2.876ln(x) + 65.529	915497.19	5	172	7.87E+08
SB-UN-5-T3_17	25.01		y = -2.876ln(x) + 65.529	1315635.44	5	176	1.16E+09
SB-UN-5-T3_18	24.19		y = -2.876ln(x) + 65.529	1745563.98	5	184	1.61E+09
SB-UN-5-T3_19	25.58		y = -2.876ln(x) + 65.529	1079069.92	5	178	9.60E+08
SB-UN-5-T3_20	24.46		y = -2.876ln(x) + 65.529	1592656.09	5	183	1.46E+09
SB-UN-5-T3_21	24.77		y = -2.876ln(x) + 65.529	1426336.17	5	175	1.25E+09
SB-UN-5-T3_22	35.78	1.57	y = -2.876ln(x) + 65.529	31066.55	5	190	2.95E+07
SB-UN-5-T3_23	26.36		y = -2.876ln(x) + 65.529	820648.02	5	265	1.09E+09
SB-UN-5-T3_24	29.47		y = -2.876ln(x) + 65.529	278965.78	5	215	3.00E+08

Date	Sample	Cq_Ave	Cq_SD	Equation	SQ	DF	Vol_frac_µL	Copies_frac
3/9/2023	SB-UN-10-T3_1	33.60	0.21	y = -1.987ln(x) + 53.767	25579.52	5	147	1.88E+07
3/9/2023	SB-UN-10-T3_2	37.03	0.73	y = -1.987ln(x) + 53.767	4546.55	5	204	4.64E+06
3/9/2023	SB-UN-10-T3_3	37.02	0.41	y = -1.987ln(x) + 53.767	4581.56	5	243	5.57E+06
3/9/2023	SB-UN-10-T3_4	36.85	0.69	y = -1.987ln(x) + 53.767	4994.24	5	245	6.12E+06
3/9/2023	SB-UN-10-T3_5	37.40	0.43	y = -1.987ln(x) + 53.767	3771.50	5	243	4.58E+06
3/9/2023	SB-UN-10-T3_6	37.19	0.39	y = -1.987ln(x) + 53.767	4208.46	5	237	4.99E+06
3/9/2023	SB-UN-10-T3_7	38.04	0.35	y = -1.987ln(x) + 53.767	2739.91	5	243	3.33E+06
3/9/2023	SB-UN-10-T3_8	36.38	0.36	y = -1.987ln(x) + 53.767	6307.12	5	236	7.44E+06
3/9/2023	SB-UN-10-T3_9	35.88	0.12	y = -1.987ln(x) + 53.767	8123.80	5	236	9.59E+06
3/9/2023	SB-UN-10-T3_10	34.79	0.19	y = -1.987ln(x) + 53.767	14028.37	5	246	1.73E+07
3/9/2023	SB-UN-10-T3_11	33.52	0.10	y = -1.987ln(x) + 53.767	26688.60	5	237	3.16E+07
3/9/2023	SB-UN-10-T3_12	31.56	0.87	y = -1.987ln(x) + 53.767	71405.24	5	232	8.28E+07
3/9/2023	SB-UN-10-T3_13	30.34	0.07	y = -1.987ln(x) + 53.767	132251.09	5	233	1.54E+08
3/9/2023	SB-UN-10-T3_14	37.35	0.37	y = -1.987ln(x) + 53.767	3870.22	5	225	4.35E+06
3/9/2023	SB-UN-10-T3_15	28.91	0.13	y = -1.987ln(x) + 53.767	271192.69	5	227	3.08E+08
3/9/2023	SB-UN-10-T3_16	29.71	0.05	y = -1.987ln(x) + 53.767	181305.72	5	221	2.00E+08
3/9/2023	SB-UN-10-T3_17	28.62	0.18	y = -1.987ln(x) + 53.767	313986.52	5	224	3.52E+08
3/9/2023	SB-UN-10-T3_18	32.84	0.23	y = -1.987ln(x) + 53.767	37410.96	5	223	4.17E+07
3/9/2023	SB-UN-10-T3_19	28.41	0.19	y = -1.987ln(x) + 53.767	348261.15	5	227	3.95E+08
3/9/2023	SB-UN-10-T3_20	31.25	0.98	y = -1.987ln(x) + 53.767	83493.19	5	238	9.94E+07
3/9/2023	SB-UN-10-T3_21	29.61	0.41	y = -1.987ln(x) + 53.767	190265.63	5	228	2.17E+08
3/9/2023	SB-UN-10-T3_22	30.29	0.64	y = -1.987ln(x) + 53.767	135096.08	5	228	1.54E+08
3/9/2023	SB-UN-10-T3_23	30.16	0.44	y = -1.987ln(x) + 53.767	144708.72	5	228	1.65E+08
3/9/2023	SB-UN-10-T3_24	30.12	0.36	y = -1.987ln(x) + 53.767	147361.74	5	102	7.52E+07

Date	Sample	Cq_Av	Cq_SD	Equation	SQ	DF	Vol_frac_µL	Copies_frac
3/9/2023	SB-UN-12-T3_1	36.35	1.20	y = -1.851ln(x) + 51.445	3479.19	5	103	1.79E+06
3/9/2023	SB-UN-12-T3_2	35.99	0.31	y = -1.851ln(x) + 51.445	4232.17	5	213	4.51E+06
3/9/2023	SB-UN-12-T3_3	35.41	0.45	y = -1.851ln(x) + 51.445	5778.00	5	230	6.64E+06
3/9/2023	SB-UN-12-T3_4	35.41	0.11	y = -1.851ln(x) + 51.445	5784.23	5	232	6.71E+06
3/9/2023	SB-UN-12-T3_5	35.66	0.24	y = -1.851ln(x) + 51.445	5046.85	5	237	5.98E+06
3/9/2023	SB-UN-12-T3_6	35.12	0.08	y = -1.851ln(x) + 51.445	6758.61	5	225	7.60E+06
3/9/2023	SB-UN-12-T3_7	35.20	0.07	y = -1.851ln(x) + 51.445	6494.28	5	252	8.18E+06
3/9/2023	SB-UN-12-T3_8	35.00	0.12	y = -1.851ln(x) + 51.445	7214.34	5	230	8.30E+06
3/9/2023	SB-UN-12-T3_9	33.88	0.01	y = -1.851ln(x) + 51.445	13247.69	5	230	1.52E+07
3/9/2023	SB-UN-12-T3_10	31.20	0.11	y = -1.851ln(x) + 51.445	56280.29	5	227	6.39E+07
3/9/2023	SB-UN-12-T3_11	30.64	0.16	y = -1.851ln(x) + 51.445	76003.80	5	230	8.74E+07
3/9/2023	SB-UN-12-T3_12	30.35	0.15	y = -1.851ln(x) + 51.445	88901.60	5	209	9.29E+07
3/9/2023	SB-UN-12-T3_13	30.81	0.47	y = -1.851ln(x) + 51.445	69512.36	5	231	8.03E+07
3/9/2023	SB-UN-12-T3_14	30.58	0.14	y = -1.851ln(x) + 51.445	78635.76	5	225	8.85E+07
3/9/2023	SB-UN-12-T3_15	29.71	0.13	y = -1.851ln(x) + 51.445	125490.95	5	228	1.43E+08
3/9/2023	SB-UN-12-T3_16	29.08	0.19	y = -1.851ln(x) + 51.445	176514.02	5	218	1.92E+08
3/9/2023	SB-UN-12-T3_17	29.48	0.68	y = -1.851ln(x) + 51.445	142611.77	5	222	1.58E+08
3/9/2023	SB-UN-12-T3_18	28.31	0.16	y = -1.851ln(x) + 51.445	267984.69	5	217	2.91E+08
3/9/2023	SB-UN-12-T3_19	27.93	0.38	y = -1.851ln(x) + 51.445	329605.61	5	223	3.68E+08
3/9/2023	SB-UN-12-T3_20	28.12	0.50	y = -1.851ln(x) + 51.445	297519.73	5	229	3.41E+08
3/9/2023	SB-UN-12-T3_21	28.85	0.15	y = -1.851ln(x) + 51.445	199880.65	5	221	2.21E+08
3/9/2023	SB-UN-12-T3_22	29.16	0.31	y = -1.851ln(x) + 51.445	168860.70	5	219	1.85E+08
3/9/2023	SB-UN-12-T3_23	28.67	0.42	y = -1.851ln(x) + 51.445	220310.07	5	231	2.54E+08
3/9/2023	SB-UN-12-T3_24	30.83	0.17	y = -1.851ln(x) + 51.445	68678.42	5	85	2.92E+07

Date	Sample	Cq_Ave	Cq_SD	Equation	SQ	DF	Vol_frac_µL	Copies_frac
3/9/2023	SB-13CNWX-1-T3_1	33.76	0.29	y = -2.016ln(x) + 54.903	35784.71	5	158	2.83E+07
3/9/2023	SB-13CNWX-1-T3_2	32.90	0.45	y = -2.016ln(x) + 54.903	55068.67	5	216	5.95E+07
3/9/2023	SB-13CNWX-1-T3_3	35.14	0.16	y = -2.016ln(x) + 54.903	18088.54	5	241	2.18E+07
3/9/2023	SB-13CNWX-1-T3_4	35.56	0.79	y = -2.016ln(x) + 54.903	14722.95	5	220	1.62E+07
3/9/2023	SB-13CNWX-1-T3_5	34.73	0.38	y = -2.016ln(x) + 54.903	22158.61	5	226	2.50E+07
3/9/2023	SB-13CNWX-1-T3_6	34.92	0.33	y = -2.016ln(x) + 54.903	20190.24	5	231	2.33E+07
3/9/2023	SB-13CNWX-1-T3_7	31.88	0.08	y = -2.016ln(x) + 54.903	91347.63	5	224	1.02E+08
3/9/2023	SB-13CNWX-1-T3_8	29.79	0.30	y = -2.016ln(x) + 54.903	256494.88	5	198	2.54E+08
3/9/2023	SB-13CNWX-1-T3_9	27.72	0.31	y = -2.016ln(x) + 54.903	715947.10	5	233	8.34E+08
3/9/2023	SB-13CNWX-1-T3_10	26.23	0.15	y = -2.016ln(x) + 54.903	1503970.13	5	212	1.59E+09
3/9/2023	SB-13CNWX-1-T3_11	25.67	0.31	y = -2.016ln(x) + 54.903	1988652.91	5	221	2.20E+09
3/9/2023	SB-13CNWX-1-T3_12	25.36	0.26	y = -2.016ln(x) + 54.903	2313599.47	5	222	2.57E+09
3/9/2023	SB-13CNWX-1-T3_13	24.92	0.31	y = -2.016ln(x) + 54.903	2871428.23	5	227	3.26E+09
3/9/2023	SB-13CNWX-1-T3_14	26.11	0.26	y = -2.016ln(x) + 54.903	1592713.94	5	220	1.75E+09
3/9/2023	SB-13CNWX-1-T3_15	27.44	0.17	y = -2.016ln(x) + 54.903	824783.12	5	222	9.16E+08
3/9/2023	SB-13CNWX-1-T3_16	29.96	0.22	y = -2.016ln(x) + 54.903	236662.97	5	212	2.51E+08
3/9/2023	SB-13CNWX-1-T3_17	29.33	0.44	y = -2.016ln(x) + 54.903	322161.16	5	225	3.62E+08
3/9/2023	SB-13CNWX-1-T3_18	30.72	0.18	y = -2.016ln(x) + 54.903	161779.85	5	228	1.84E+08
3/9/2023	SB-13CNWX-1-T3_19	30.40	0.48	y = -2.016ln(x) + 54.903	190345.25	5	227	2.16E+08
3/9/2023	SB-13CNWX-1-T3_20	32.58	0.29	y = -2.016ln(x) + 54.903	64543.10	5	216	6.97E+07
3/9/2023	SB-13CNWX-1-T3_21	33.47	0.32	y = -2.016ln(x) + 54.903	41475.47	5	233	4.83E+07
3/9/2023	SB-13CNWX-1-T3_22	31.53	0.22	y = -2.016ln(x) + 54.903	108460.06	5	226	1.23E+08
3/9/2023	SB-13CNWX-1-T3_23	31.75	0.37	y = -2.016ln(x) + 54.903	97344.50	5	223	1.09E+08
3/9/2023	SB-13CNWX-1-T3_24	34.00	0.25	y = -2.016ln(x) + 54.903	31888.58	5	64	1.02E+07

Date	Sample	Cq_Ave	Cq_SD	Equation	SQ	DF	Vol_frac_µL	Copies_frac
3/10/2023	SB-13CNWX-2-T3_1	30.68	0.41	y = -2.032ln(x) + 53.571	78208.01	5	210	8.21E+07
3/10/2023	SB-13CNWX-2-T3_2	33.99	0.24	y = -2.032ln(x) + 53.571	15345.15	5	239	1.83E+07
3/10/2023	SB-13CNWX-2-T3_3	33.47	0.04	y = -2.032ln(x) + 53.571	19729.14	5	241	2.38E+07
3/10/2023	SB-13CNWX-2-T3_4	34.24	0.12	y = -2.032ln(x) + 53.571	13539.38	5	241	1.63E+07
3/10/2023	SB-13CNWX-2-T3_5	35.08	0.07	y = -2.032ln(x) + 53.571	8966.17	5	244	1.09E+07
3/10/2023	SB-13CNWX-2-T3_6	32.24	0.54	y = -2.032ln(x) + 53.571	36205.63	5	237	4.29E+07
3/10/2023	SB-13CNWX-2-T3_7	31.75	0.37	y = -2.032ln(x) + 53.571	46026.58	5	254	5.85E+07
3/10/2023	SB-13CNWX-2-T3_8	29.98	0.70	y = -2.032ln(x) + 53.571	110116.52	5	221	1.22E+08
3/10/2023	SB-13CNWX-2-T3_9	27.63	0.26	y = -2.032ln(x) + 53.571	350474.42	5	227	3.98E+08
3/10/2023	SB-13CNWX-2-T3_10	25.33	0.37	y = -2.032ln(x) + 53.571	1085891.36	5	227	1.23E+09
3/10/2023	SB-13CNWX-2-T3_11	25.49	0.42	y = -2.032ln(x) + 53.571	1005530.29	5	231	1.16E+09
3/10/2023	SB-13CNWX-2-T3_12	23.42	0.25	y = -2.032ln(x) + 53.571	2777854.73	5	227	3.15E+09
3/10/2023	SB-13CNWX-2-T3_13	23.68	0.29	y = -2.032ln(x) + 53.571	2451935.74	5	231	2.83E+09
3/10/2023	SB-13CNWX-2-T3_14	24.24	0.38	y = -2.032ln(x) + 53.571	1861252.58	5	223	2.08E+09
3/10/2023	SB-13CNWX-2-T3_15	25.20	0.26	y = -2.032ln(x) + 53.571	1159933.11	5	227	1.32E+09
3/10/2023	SB-13CNWX-2-T3_16	26.11	0.25	y = -2.032ln(x) + 53.571	741027.06	5	216	8.00E+08
3/10/2023	SB-13CNWX-2-T3_17	26.89	0.14	y = -2.032ln(x) + 53.571	503898.31	5	233	5.87E+08
3/10/2023	SB-13CNWX-2-T3_18	28.70	0.20	y = -2.032ln(x) + 53.571	206355.80	5	215	2.22E+08
3/10/2023	SB-13CNWX-2-T3_19	30.97	0.28	y = -2.032ln(x) + 53.571	67588.68	5	224	7.57E+07
3/10/2023	SB-13CNWX-2-T3_20	32.98	0.58	y = -2.032ln(x) + 53.571	25182.34	5	226	2.85E+07
3/10/2023	SB-13CNWX-2-T3_21	32.26	0.24	y = -2.032ln(x) + 53.571	35944.35	5	229	4.12E+07
3/10/2023	SB-13CNWX-2-T3_22	31.94	0.15	y = -2.032ln(x) + 53.571	41910.30	5	229	4.80E+07
3/10/2023	SB-13CNWX-2-T3_23	33.05	0.31	y = -2.032ln(x) + 53.571	24283.86	5	225	2.73E+07
3/10/2023	SB-13CNWX-2-T3_24	34.98	0.28	y = -2.032ln(x) + 53.571	9423.30	5	53	2.50E+06

Date	Sample	Cq_Ave	Cq_SD	Equation	SQ	DF	Vol_frac_µL	Copies_frac
3/10/2023	SB-13CNWX-3-T3_1	37.95	0.52	y = -2.067ln(x) + 54.659	3235.22	5	249	4.03E+06
3/10/2023	SB-13CNWX-3-T3_2	35.56	0.46	y = -2.067ln(x) + 54.659	10302.73	5	222	1.14E+07
3/10/2023	SB-13CNWX-3-T3_3	33.88	0.59	y = -2.067ln(x) + 54.659	23203.78	5	240	2.78E+07
3/10/2023	SB-13CNWX-3-T3_4	32.88	0.40	y = -2.067ln(x) + 54.659	37690.65	5	224	4.22E+07
3/10/2023	SB-13CNWX-3-T3_5	31.12	0.33	y = -2.067ln(x) + 54.659	88098.06	5	236	1.04E+08
3/10/2023	SB-13CNWX-3-T3_6	33.16	0.42	y = -2.067ln(x) + 54.659	32864.68	5	211	3.47E+07
3/10/2023	SB-13CNWX-3-T3_7	29.00	0.32	y = -2.067ln(x) + 54.659	246029.13	5	227	2.79E+08
3/10/2023	SB-13CNWX-3-T3_8	29.81	0.16	y = -2.067ln(x) + 54.659	166632.25	5	216	1.80E+08
3/10/2023	SB-13CNWX-3-T3_9	26.56	0.28	y = -2.067ln(x) + 54.659	801624.52	5	219	8.78E+08
3/10/2023	SB-13CNWX-3-T3_10	26.08	0.24	y = -2.067ln(x) + 54.659	1009936.83	5	217	1.10E+09
3/10/2023	SB-13CNWX-3-T3_11	24.99	0.14	y = -2.067ln(x) + 54.659	1713003.52	5	223	1.91E+09
3/10/2023	SB-13CNWX-3-T3_12	25.05	0.39	y = -2.067ln(x) + 54.659	1663489.08	5	222	1.85E+09
3/10/2023	SB-13CNWX-3-T3_13	25.90	0.38	y = -2.067ln(x) + 54.659	1102613.58	5	227	1.25E+09
3/10/2023	SB-13CNWX-3-T3_14	26.79	0.19	y = -2.067ln(x) + 54.659	715700.52	5	222	7.94E+08
3/10/2023	SB-13CNWX-3-T3_15	28.59	0.33	y = -2.067ln(x) + 54.659	300455.15	5	223	3.35E+08
3/10/2023	SB-13CNWX-3-T3_16	29.75	0.13	y = -2.067ln(x) + 54.659	170950.75	5	213	1.82E+08
3/10/2023	SB-13CNWX-3-T3_17	30.99	0.50	y = -2.067ln(x) + 54.659	93759.18	5	213	9.99E+07
3/10/2023	SB-13CNWX-3-T3_18	30.95	0.34	y = -2.067ln(x) + 54.659	95695.95	5	224	1.07E+08
3/10/2023	SB-13CNWX-3-T3_19	30.30	0.33	y = -2.067ln(x) + 54.659	130941.53	5	230	1.51E+08
3/10/2023	SB-13CNWX-3-T3_20	30.76	0.17	y = -2.067ln(x) + 54.659	105209.35	5	216	1.14E+08
3/10/2023	SB-13CNWX-3-T3_21	30.23	0.15	y = -2.067ln(x) + 54.659	135927.15	5	233	1.58E+08
3/10/2023	SB-13CNWX-3-T3_22	32.59	0.92	y = -2.067ln(x) + 54.659	43383.53	5	228	4.95E+07
3/10/2023	SB-13CNWX-3-T3_23	32.01	0.37	y = -2.067ln(x) + 54.659	57479.44	5	226	6.50E+07
3/10/2023	SB-13CNWX-3-T3_24	35.34	0.52	y = -2.067ln(x) + 54.659	11451.28	5	16	9.16E+05

Date	Sample	Cq_Ave	Cq_SD	Equation	SQ	DF	Vol_frac_µL	Copies_frac
3/13/2023	SB-13CNWX-4-T3_2	32.79	0.20	y = -1.771ln(x) + 49.603	13296.87	5	250	1.66E+07
3/13/2023	SB-13CNWX-4-T3_3	31.75	0.42	y = -1.771ln(x) + 49.603	23940.71	5	231	2.77E+07
3/13/2023	SB-13CNWX-4-T3_4	32.34	0.66	y = -1.771ln(x) + 49.603	17067.72	5	243	2.07E+07
3/13/2023	SB-13CNWX-4-T3_5	32.43	0.22	y = -1.771ln(x) + 49.603	16220.31	5	234	1.90E+07
3/13/2023	SB-13CNWX-4-T3_6	31.23	0.17	y = -1.771ln(x) + 49.603	32058.29	5	241	3.86E+07
3/13/2023	SB-13CNWX-4-T3_7	33.44	0.50	y = -1.771ln(x) + 49.603	9169.91	5	231	1.06E+07
3/13/2023	SB-13CNWX-4-T3_8	29.02	0.08	y = -1.771ln(x) + 49.603	111601.33	5	222	1.24E+08
3/13/2023	SB-13CNWX-4-T3_9	29.30	0.22	y = -1.771ln(x) + 49.603	95138.41	5	237	1.13E+08
3/13/2023	SB-13CNWX-4-T3_10	26.16	0.11	y = -1.771ln(x) + 49.603	560369.23	5	223	6.25E+08
3/13/2023	SB-13CNWX-4-T3_11	25.48	0.43	y = -1.771ln(x) + 49.603	824423.46	5	229	9.44E+08
3/13/2023	SB-13CNWX-4-T3_12	25.30	0.11	y = -1.771ln(x) + 49.603	912903.42	5	227	1.04E+09
3/13/2023	SB-13CNWX-4-T3_13	24.83	0.07	y = -1.771ln(x) + 49.603	1187451.25	5	230	1.37E+09
3/13/2023	SB-13CNWX-4-T3_14	25.27	0.10	y = -1.771ln(x) + 49.603	927318.48	5	228	1.06E+09
3/13/2023	SB-13CNWX-4-T3_15	26.14	0.14	y = -1.771ln(x) + 49.603	566903.26	5	228	6.46E+08
3/13/2023	SB-13CNWX-4-T3_16	27.22	0.07	y = -1.771ln(x) + 49.603	307802.17	5	218	3.36E+08
3/13/2023	SB-13CNWX-4-T3_17	28.28	0.45	y = -1.771ln(x) + 49.603	169256.76	5	231	1.95E+08
3/13/2023	SB-13CNWX-4-T3_18	30.70	0.53	y = -1.771ln(x) + 49.603	43186.02	5	217	4.69E+07
3/13/2023	SB-13CNWX-4-T3_19	32.36	0.68	y = -1.771ln(x) + 49.603	16887.22	5	227	1.92E+07
3/13/2023	SB-13CNWX-4-T3_20	31.48	0.76	y = -1.771ln(x) + 49.603	27840.49	5	239	3.33E+07
3/13/2023	SB-13CNWX-4-T3_21	33.39	0.30	y = -1.771ln(x) + 49.603	9476.66	5	223	1.06E+07
3/13/2023	SB-13CNWX-4-T3_22	32.06	0.06	y = -1.771ln(x) + 49.603	20011.19	5	237	2.37E+07
3/13/2023	SB-13CNWX-4-T3_23	34.00	1.51	y = -1.771ln(x) + 49.603	6692.89	5	222	7.43E+06
3/13/2023	SB-13CNWX-4-T3_24	34.42	0.39	y = -1.771ln(x) + 49.603	5293.75	5	55	1.46E+06

Date	Sample	Cq_Ave	Cq_SD	Equation	SQ	DF	Vol_frac_µL	Copies_frac
3/13/2023	SB-13CNWX-5-T3_2	30.35	0.48	y = -2.383ln(x) + 60.772	350631.44	5	228	4.00E+08
3/13/2023	SB-13CNWX-5-T3_3	29.08	0.57	y = -2.383ln(x) + 60.772	595674.91	5	246	7.33E+08
3/13/2023	SB-13CNWX-5-T3_4	30.96	0.53	y = -2.383ln(x) + 60.772	271005.14	5	224	3.04E+08
3/13/2023	SB-13CNWX-5-T3_5	30.32	0.28	y = -2.383ln(x) + 60.772	354466.61	5	243	4.31E+08
3/13/2023	SB-13CNWX-5-T3_6	30.34	0.43	y = -2.383ln(x) + 60.772	351291.67	5	220	3.86E+08
3/13/2023	SB-13CNWX-5-T3_7	28.64	0.45	y = -2.383ln(x) + 60.772	718646.40	5	217	7.80E+08
3/13/2023	SB-13CNWX-5-T3_8	28.66	0.49	y = -2.383ln(x) + 60.772	712251.86	5	220	7.83E+08
3/13/2023	SB-13CNWX-5-T3_9	28.18	0.21	y = -2.383ln(x) + 60.772	871614.31	5	213	9.28E+08
3/13/2023	SB-13CNWX-5-T3_10	25.84	0.27	y = -2.383ln(x) + 60.772	2319875.90	5	223	2.59E+09
3/13/2023	SB-13CNWX-5-T3_11	24.89	0.29	y = -2.383ln(x) + 60.772	3463081.39	5	228	3.95E+09
3/13/2023	SB-13CNWX-5-T3_12	24.28	0.15	y = -2.383ln(x) + 60.772	4480907.35	5	227	5.09E+09
3/13/2023	SB-13CNWX-5-T3_13	24.44	0.37	y = -2.383ln(x) + 60.772	4174770.81	5	230	4.80E+09
3/13/2023	SB-13CNWX-5-T3_14	24.55	0.32	y = -2.383ln(x) + 60.772	3987219.14	5	225	4.49E+09
3/13/2023	SB-13CNWX-5-T3_15	26.12	0.19	y = -2.383ln(x) + 60.772	2067548.48	5	224	2.32E+09
3/13/2023	SB-13CNWX-5-T3_16	26.17	0.12	y = -2.383ln(x) + 60.772	2021537.36	5	228	2.30E+09
3/13/2023	SB-13CNWX-5-T3_17	27.42	0.51	y = -2.383ln(x) + 60.772	1197478.87	5	217	1.30E+09
3/13/2023	SB-13CNWX-5-T3_18	28.20	0.28	y = -2.383ln(x) + 60.772	865038.02	5	224	9.69E+08
3/13/2023	SB-13CNWX-5-T3_19	29.11	0.69	y = -2.383ln(x) + 60.772	589093.66	5	225	6.63E+08
3/13/2023	SB-13CNWX-5-T3_20	29.92	0.07	y = -2.383ln(x) + 60.772	419788.48	5	241	5.06E+08
3/13/2023	SB-13CNWX-5-T3_21	29.77	0.77	y = -2.383ln(x) + 60.772	446118.68	5	228	5.09E+08
3/13/2023	SB-13CNWX-5-T3_22	30.13	0.21	y = -2.383ln(x) + 60.772	383662.70	5	230	4.41E+08
3/13/2023	SB-13CNWX-5-T3_23	32.03	0.21	y = -2.383ln(x) + 60.772	173070.19	5	223	1.93E+08
3/13/2023	SB-13CNWX-5-T3_24	35.99	0.16	y = -2.383ln(x) + 60.772	32818.07	5	82	1.35E+07

Date	Sample	Cq_Av	Cq_SD	Equation	SQ	DF	Vol_frac_µL	Copies_frac
3/14/2023	SB-13CNWX-6-T3_2	31.08	0.29	y = -1.979ln(x) + 53.314	75917.36	5	230	8.73E+07
3/14/2023	SB-13CNWX-6-T3_3	29.90	0.15	y = -1.979ln(x) + 53.314	137371.25	5	247	1.70E+08
3/14/2023	SB-13CNWX-6-T3_4	30.53	0.14	y = -1.979ln(x) + 53.314	100018.66	5	246	1.23E+08
3/14/2023	SB-13CNWX-6-T3_5	30.85	0.19	y = -1.979ln(x) + 53.314	85053.85	5	240	1.02E+08
3/14/2023	SB-13CNWX-6-T3_6	29.96	0.08	y = -1.979ln(x) + 53.314	133622.18	5	232	1.55E+08
3/14/2023	SB-13CNWX-6-T3_7	31.28	0.09	y = -1.979ln(x) + 53.314	68537.47	5	237	8.12E+07
3/14/2023	SB-13CNWX-6-T3_8	28.68	0.08	y = -1.979ln(x) + 53.314	254057.46	5	226	2.87E+08
3/14/2023	SB-13CNWX-6-T3_9	26.89	0.07	y = -1.979ln(x) + 53.314	629411.28	5	239	7.52E+08
3/14/2023	SB-13CNWX-6-T3_10	26.50	0.29	y = -1.979ln(x) + 53.314	764928.35	5	229	8.76E+08
3/14/2023	SB-13CNWX-6-T3_11	25.18	0.23	y = -1.979ln(x) + 53.314	1493156.84	5	234	1.75E+09
3/14/2023	SB-13CNWX-6-T3_12	24.26	0.02	y = -1.979ln(x) + 53.314	2380343.14	5	231	2.75E+09
3/14/2023	SB-13CNWX-6-T3_13	24.39	0.13	y = -1.979ln(x) + 53.314	2229413.34	5	234	2.61E+09
3/14/2023	SB-13CNWX-6-T3_14	24.86	0.58	y = -1.979ln(x) + 53.314	1750755.08	5	227	1.99E+09
3/14/2023	SB-13CNWX-6-T3_15	25.77	0.16	y = -1.979ln(x) + 53.314	1108101.82	5	230	1.27E+09
3/14/2023	SB-13CNWX-6-T3_16	27.30	0.06	y = -1.979ln(x) + 53.314	511698.13	5	218	5.58E+08
3/14/2023	SB-13CNWX-6-T3_17	27.95	0.27	y = -1.979ln(x) + 53.314	368025.08	5	230	4.23E+08
3/14/2023	SB-13CNWX-6-T3_18	29.37	0.44	y = -1.979ln(x) + 53.314	179940.00	5	233	2.10E+08
3/14/2023	SB-13CNWX-6-T3_19	30.30	0.02	y = -1.979ln(x) + 53.314	112588.51	5	233	1.31E+08
3/14/2023	SB-13CNWX-6-T3_20	31.28	0.32	y = -1.979ln(x) + 53.314	68505.97	5	223	7.64E+07
3/14/2023	SB-13CNWX-6-T3_21	30.60	0.28	y = -1.979ln(x) + 53.314	96534.88	5	231	1.11E+08
3/14/2023	SB-13CNWX-6-T3_22	32.08	0.60	y = -1.979ln(x) + 53.314	45795.56	5	241	5.52E+07
3/14/2023	SB-13CNWX-6-T3_23	30.42	0.44	y = -1.979ln(x) + 53.314	105924.41	5	225	1.19E+08
3/14/2023	SB-13CNWX-6-T3_24	33.53	0.47	y = -1.979ln(x) + 53.314	22002.44	5	110	1.21E+07

CHAPTER FIVE: CONCLUSION

In conclusion, this thesis highlights the need to account for PyOM-C heterogeneity and ageing when estimating post-fire carbon stocks. Our study demonstrates that a small fraction of PyOM is highly mineralizable by microbes, and we found that lower temperature PyOM (350 °C) had higher mineralizability compared to PyOM produced at higher temperatures (550 °C). Moreover, ageing significantly increases the mineralization rate of 350 °C biochar C, implying that the carbon in lower temperature PyOM is more susceptible to microbial degradation in both the short and long term. This has important implications for estimating post-fire carbon stocks in soils that contain a higher proportion of low-temperature PyOM. The relationship between fire severity and PyOM characteristics is complex and can vary depending on multiple factors. Future studies could focus on characterizing and exploring this relationship to better understand PyOM-C stabilization and decomposition in post-fire soils.

Our study reveals that both time and PyOM temperature influence the rate of SOC mineralization in post-fire soils. In particular, the short-term changes in SOC dynamics were found to be strongly associated with the mineralizability of the water extractable PyOM fraction. Future investigations into the role of other PyOM structural and electrochemical properties are needed to better understand long-term C stabilization in PyOM containing soils, while considering soil properties such as texture and clay content that may affect these results.

This dissertation highlights the impact of low-temperature PyOM on microbial communities in the short term. Both 350 °C and 550 °C PyOM additions caused significant shifts in microbial communities, but more unique responsive taxa were identified with 350 °C PyOM addition compared to 550 °C PyOM. Moreover, only 350 °C PyOM addition resulted in a relative abundance increase at the genus level for several bacteria. Taken together, these findings

indicate that low temperature C is accessible to a wider range of bacteria. Interestingly, many of the responders to 350 °C PyOM in our study were also identified in other studies with different PyOM and soil characteristics, suggesting a unique response to PyOM-C. However, it has so far remained unclear whether the relative increase of these responders was due to their ability to degrade PyOM-C due to minimal evidence demonstrating active PyOM-C usage by bacteria. This dissertation provides evidence for active incorporation of relatively aromatic non-water-extractable 350 °C PyOM-C by bacteria, some of which were noted for their ability to degrade aromatic C. Furthermore, some of the incorporators were abundant in post-fire soils, confirming previous hypothesis that these bacteria dominate post-fire soils due to traits related to PyOM-C degradation.

Another important finding of this dissertation is that the incorporation of non-water-extractable 350 °C PyOM-C was not accompanied by an increase in relative abundance, indicating that uptake of the aromatic C structures in PyOM does not provide a competitive advantage to its degraders. This raises interesting questions about the metabolic pathways and functional roles of fire-responsive bacteria in PyOM-C cycling. Techniques like qSIP combined with metagenomics can provide more information on the functional changes that occur within the microbiome and shed light on these questions.

We observed no significant shifts in fungal community composition in response to PyOM addition. Furthermore, unlike bacteria, the responders to 350 °C PyOM were only detected at the OTU level, not at the genus level. The impact of PyOM addition on the fungal community in post-fire soils remains unclear, and it is uncertain whether these effects will become apparent over longer time scales. The use of qSIP to identify active fungal incorporators of PyOM-C can improve our understanding of the role of PyOM-C substrate availability for fungi in post-fire

soils. This approach can help distinguish fungal taxa that thrive in post-fire soils due to their ability to degrade PyOM-C from those that dominate due to traits of heat and stress tolerance.